THE GEOLOGY, GEOCHEMISTRY AND STRUCTURE OF THE MOOSHLA INTRUSION, BOUSQUET MINING CENTRE, QUEBEC.

ALEXANDER LANGSHUR

Thesis submitted to
the School of Graduate Studies and Research
in partial fulfillment of the requirements for the
degree of Master of Science in Geology

Ottawa-Carleton Geoscience Centre and
Université d'Ottawa/University of Ottawa

ISBN 0-315-68068-7

ABSTRACT

The Mooshla intrusion is located near the western limit of the Bousquet Mining Center (BMC) in the Abitibi greenstone belt of Northwestern Québec. It is spatially associated with five gold deposits, including Québec's largest gold producer, La Mine Doyon. The Mooshla intrusion is an elliptical body, 4.0 x 1.5 km and is hosted by the Blake River Group, a fault bounded sequence of bi-modal volcanic and volcaniclastic rocks. Contact metamorphic effects are negligible.

The intrusion is calc-alkaline in affinity and comprises four distinct units; 1) cumulate gabbros, 2) quartz diorites, 3) tonalites and 4) leucotonalites. The spatial distribution of these units reveals the reversely zoned nature of the intrusion which is consistent with emplacement from at least two magmatic pulses. Both pulses underwent *in situ* differentiation and do not appear to have mixed to any appreciable extent. The cumulate gabbros are composed of two textural facies; 1) mesocumulates and 2) a layered sequence. Excellent fine-scale rhythmic and cyclic layering of the layered gabbros indicate relatively stable conditions prevailed during evolution of the primary magma pulse. Textural and geochemical evidence suggests that the leucotonalite is the hydrothermally altered and sheared equivalent of the tonalite.

The intrusion records four generations of structures; D_1, D_2, D_3, and D_4. D_1 produced an E-W striking foliation, S_1, that dips moderately to the south and is localized to the core of the intrusion. It is not observed elsewhere in the BMC. D_2 represents a period of subhorizontal N-S compression and is the principal deformation event. It is responsible for an $\approx$E-W trending, regionally penetrative foliation, S_2, that dips steeply to the south and onto which most geological objects are flattened. S_2

contains stretching lineations L^s_2 and mineral lineations L^m_2, that plunge steeply to the west. Intersection lineation, L^i_2, is rarely observed and has an essentially subhorizontal plunge. S_2 correlates with the S_1 foliation documented elsewhere in the BMC by Tourigny *et al.*, (1988) and Marquis and Hubert (1989). Both D_3 and D_4 are reflected by predominantly brittle structures related to dominantly E-W directed horizontal shortening.

The Mooshla intrusion can be subdivided into three structural domains defined by which foliation they contain and the nature and frequency the high strain zones that they host. **Domain 1**, along the northern third of the intrusion, contains S_2 and narrow (<2.0 m), discreet zones of high strain. **Domain 2**, occupies the core of the intrusion. It contains S_1 and very few high strain zones. **Domain 3** forms the southern third of the intrusion and is classified as a lithotectonic Domain. It hosts S_{2S} and a wide zone of intense ductile deformation, the Southern Mooshla Shear Zone (SMSZ). Asymmetric Z-shaped intrafolial folds (F_2) and steeply west plunging stretching lineations suggest a reverse-oblique movement along the SMSZ.

The Mooshla intrusion is comagmatic with the host BRG. It is characterized by fractionated REE profiles with $[La/Yb]_N$ ratios ranging from 4.89 to 8.92 and generally flat HREE ($[Tb/Lu]_N \approx 1$-2). Major and trace element chemistry indicates that the primary magma pulse underwent fractional crystallization to produce tonalite and a sequence of cumulate rocks. Local water saturation was achieved within the tonalite. The second magma pulse remained in the axial region of the intrusion and evolved through equilibrium crystallization, eventually forming the quartz diorites. Geochemical evolutionary trends of the primary magma pulse suggest an initial composition similar to that of a quartz diorite. Trace element data are consistent with derivation of the parental magma from a subduction-modified garnet-free amphibolitic source.

SOMMAIRE

L'intrusion de Mooshla est située près de la limite occidentale du Centre Minier de Bousquet (CMB), à l'intérieur de la ceinture de roches vertes de l'Abitibi. Elle est géographiquement associée avec cinq gisements aurifères, incluant le plus grand producteur d'or du Québec, la Mine Doyon. L'intrusion de Mooshla est de forme éllipsoïdale (4,0 x 1,5 km) et est encaissée dans les roches volcaniques et volcaniclastiques du Groupe de Blake River. Les effets du métamorphisme de contact avec les roches encaissantes sont négligeables.

L'intrusion est d'affinité calco-alcalin et comprend quatre unités distinctes: cumulats gabbroiques, 2) diorites quartzifères, 3) tonalites et 4) leucotonalites. La distribution géographique de ces unités définit une zonation inverse, ce qui suggère deux événements d'injections magmatiques. Ces deux injections magmatiques se sont différenciées en place et ne semblent pas s'être mélangées. Les cumulats gabbroiques sont composés de deux faciès texturaux; 1) mésocumulat et 2) séquence litée. L'excellent litage rhythmique et cyclique des gabbros lités suggèrent que des conditions stables existaient lors de l'évolution de la première injection magmatique. Les évidences texturales et géochimiques suggèrent que la leucotonalite est l'équivalent altéré et déformé du tonalite.

L'intrusion démontre quatre générations de structures: D_1, D_2, D_3 et D_4. D_1 a produit une foliation, S_1, orientée E-W avec un faible pendage vers le sud. S_1 est localisée au coeur de l'intrusion et n'a pas été observée ailleurs dans le CMB. D_2 correspond à une période de compression sub-horizontale N-S, et représente l'événement principal de déformation. Elle se traduit par une foliation pénétrative régionale, S_2, sur laquelle la plupart des objets géologiques sont applatis. S_2 est d'orientation E-W

avec un fort pendage vers le sud et contient des linéations d'étirements, L^i_2, ainsi que des linéations minéralogiques, L^m_2, qui plongent abruptement vers l'ouest. Une linéation d'intersection, L^i_2, avec une plongée essentiellement sub-horizontale n'est que rarement observée. S_2 est l'équivalent de la foliation S_1 documentée ailleurs dans le CMB par Tourigny *et al.*, (1988) et Marquis et Hubert (1989). D_3 et D_4 sont représentées par des structures cassantes reliées à des périodes de compression horizontale E-W.

L'intrusion de Mooshla peut être subdivisée en trois domaines structuraux en termes de la foliation ainsi que la nature et fréquence des zones de cisaillements qu'ils contiennent. Le **Domaine 1**, situé le long de la partie nord de l'intrusion, contient S_2 et de nombreuses minces (<2,0 m) zones de cisaillements discrètes. Le **Domaine 2** occupe le coeur de l'intrusion. Il contient la foliation S_1 et seulement quelques zones de cisaillements. Le **Domaine 3** forme la partie sud de l'intrusion et est classifié comme étant un domaine lithotectonique. Il contient la foliation S_{2S} et une large zone de déformation ductile, la Zone de Cisaillement Sud du Mooshla (ZCSM). Des plis asymmétriques intrafoliaux (F_2) ainsi que des linéations d'étirements à forte plongée vers l'ouest suggèrent un mouvement oblique-inverse le long du ZCSM.

L'intrusion de Mooshla est co-magmatique avec les roches encaissantes du Groupe de Blake River. Elle est caractérisée par des profiles en ETR fractionnés (rapports $[La/Yb]_N$ de 4.89 à 8.92) et des profiles de ETR lourds généralement plat ($[Tb/Lu]_N \approx$ 1-2). La géochimie des élements majeurs et traces indique que la première injection magmatique s'est différenciée par cristallisation fractionnée, produisant les roches tonalitiques ainsi que les cumulats gabbroiques. La seconde injection magmatique s'est mise en place au coeur de l'intrusion et a évolué par processus de cristallisation

équilibrée. Celle-ci a produit les diorites quartzifères. Les tendances de l'évolution géochimique de la première injection magmatique suggèrent que la composition initiale du magma était similaire à celle des diorites quartzifères. Les données en éléments traces sont en accord avec une dérivation du magma parental par fusion partielle à partir d'une source amphibolitique dépourvue de grenat. De plus, ces données suggèrent que la fusion partielle à eu lieu dans une environnement tectonique s'apparentant à une zone de subduction.

ACKNOWLEDGEMENTS

This research would not have been possible without the financial, logistical and technical support of LAC Minerals Ltd. In particular, I would like to thank Dr. Bob Valliant, who encouraged me to undertake my research as soon as possible and secured initial funding for the project. M. Gilles Filion was instrumental in providing for my leave of absence from work to complete this research. The advice and help of mon ami et collègue, Harold Desbiens were always appreciated. Christian Massicotte, Robert Sansfacon, Yves Allaire, Carole Perry, Bill Cavalluzzo, Nan Boudreau and Daniel Beaudoin are all thanked for many stimulating discussions, technical support and morning doughnuts. Mmes. Marie France Bugnon and Nicole Giroux of Cambior Ltée graciously allowed me to map the Mouska property and gave freely of their time and data.

My supervisor, Dr. Keiko Hattori, generously provided funding, time and advice during the course of this research. Drs. André Lalonde, Francois Robert and Keith Benn are thanked for their comments and criticisms of earlier drafts of the thesis. Kudos are also due to my fellow graduate students for their helpful hints and scintillating scientific discussions.

During the roller-coaster ride that is a Masters, the encouragement and counsel of Brent McInnes, Noreen Evans, Caroline Duchesne and my family were invaluable. Their contributions, friendship and love are most warmly acknowledged. I shall always fondly remember our Thursday evenings.

Finally, this research was in part funded by a grant from les Fonds FCAR du Québec.

TABLE OF CONTENTS

PAGE

PAGE

LIST OF FIGURES

Chapter 1

Chapter 2

Chapter 3

Chapter 4

LIST OF FIGURES (cont'd.) **PAGE**

LIST OF FIGURES (cont'd) PAGE

LIST OF PLATES

PAGE

Chapter 2

Chapter 3

LIST OF PLATES (cont'd.)

PAGE

Chapter 4

LIST OF PLATES (cont'd) **PAGE**

Erosion

It took the sea a thousand years,
A thousand years to trace
The granite features of this cliff,
In crag and scarp and base.

It took the sea an hour one night,
An hour of storm to place
The sculpture of these granite seams
Upon a woman's face.

E.J. Pratt (1883-1964)

- in memory of my mother and Simon...

CHAPTER 1: INTRODUCTION

1.1 Statement of the problem and objectives

The spatial association of felsic intrusives to gold mineralization has been well documented throughout Archean greenstone belts (Hodgson and MacGeehan, 1982; Colvine *et al.*, 1989). Although a genetic link has been suggested between the two (Cameron and Hattori, 1987; Burrows and Spooner, 1989), evidence in support of such a link is equivocal (Kerrich, 1989). The Mooshla intrusion is a medium-sized felsic intrusive that is spatially associated with 3 gold deposits (the Mouska, MicMac and Doyon main zone) and is host to 3 others (Doyon west zone, Mooshla "A" and "B"). It is located near the western limit of the Bousquet Mining Center (BMC) in northwestern Québec. The BMC is one of the largest gold mining districts of the Abitibi greenstone belt with past production and present reserves totalling approximately 46 million tonnes at an average grade of 5.1 grams Au per tonne (Marquis, 1990). The economic importance of the BMC has spurred extensive research in the last decade in an effort to characterize the geology of the deposits and their host rocks, as well as to develop a coherent genetic framework for the district-scale mineralization (e.g. Valliant, 1981; Guha *et al.*, 1982; Tourigny *et al.*, 1989; Marquis, 1990; Stone, 1990). Despite this, comparatively little is known about the geology, the geochemistry and the structure of the Mooshla intrusion. Without such knowledge it is virtually impossible to evaluate the relationship between the intrusive and its associated deposits. As a result, this study was initiated to complement existing work in the eastern and central portions of the BMC and to provide a framework for future research by:

1) Documenting the petrology and geochemistry of the Mooshla intrusion lithologies

2) Examining the relationship between the intrusion and its host rocks,

3) Constraining the nature of its tectonic setting and the magma source for the intrusion,

4) Evaluating the evolution of the intrusion during and subsequent to emplacement, and finally 5) Documenting the strain fabrics recorded by the intrusion and integrating these results with those of the Bousquet Mining Center.

1.2 Location, access and physiography

The Mooshla intrusion is located in the northern half of Bousquet township and sits astride the north-south central township line (figure 1). It is approximately 40 km east of the town of Rouyn-Noranda and 80 km west of the town of Val d'Or. It is easily accessible by the chemin Cléricy (Parc Mont Brun) which branches north of highway 117. The chemin Cléricy road transects the eastern part of the intrusion. A gravel and dirt road branches south from the chemin Cléricy (between the abandoned MicMac mine and the Mouska project) and provides access to the western half of the intrusion. Numerous skidder roads, accessible by four wheel all-terrain vehicles, criss-cross the center of the intrusion. Access to the northcentral margin can be obtained from network of roads on the dried tailings behind the abandoned MicMac mine.

With the exception of two prominent knolls, the intrusion is covered largely by swampy lowlands typical of northern taiga. The two knolls correspond to areas of high outcrop density located in the southwestern (along the access road) and southcentral (just west of the diabase dyke) parts of the intrusion. The knolls are separated by a stream that runs north south and drains a large beaver-dammed pond in the geographic center of the intrusion. The intrusion is effectively divided into two for mapping purposes due to the difficulty in traversing either the pond or the stream.

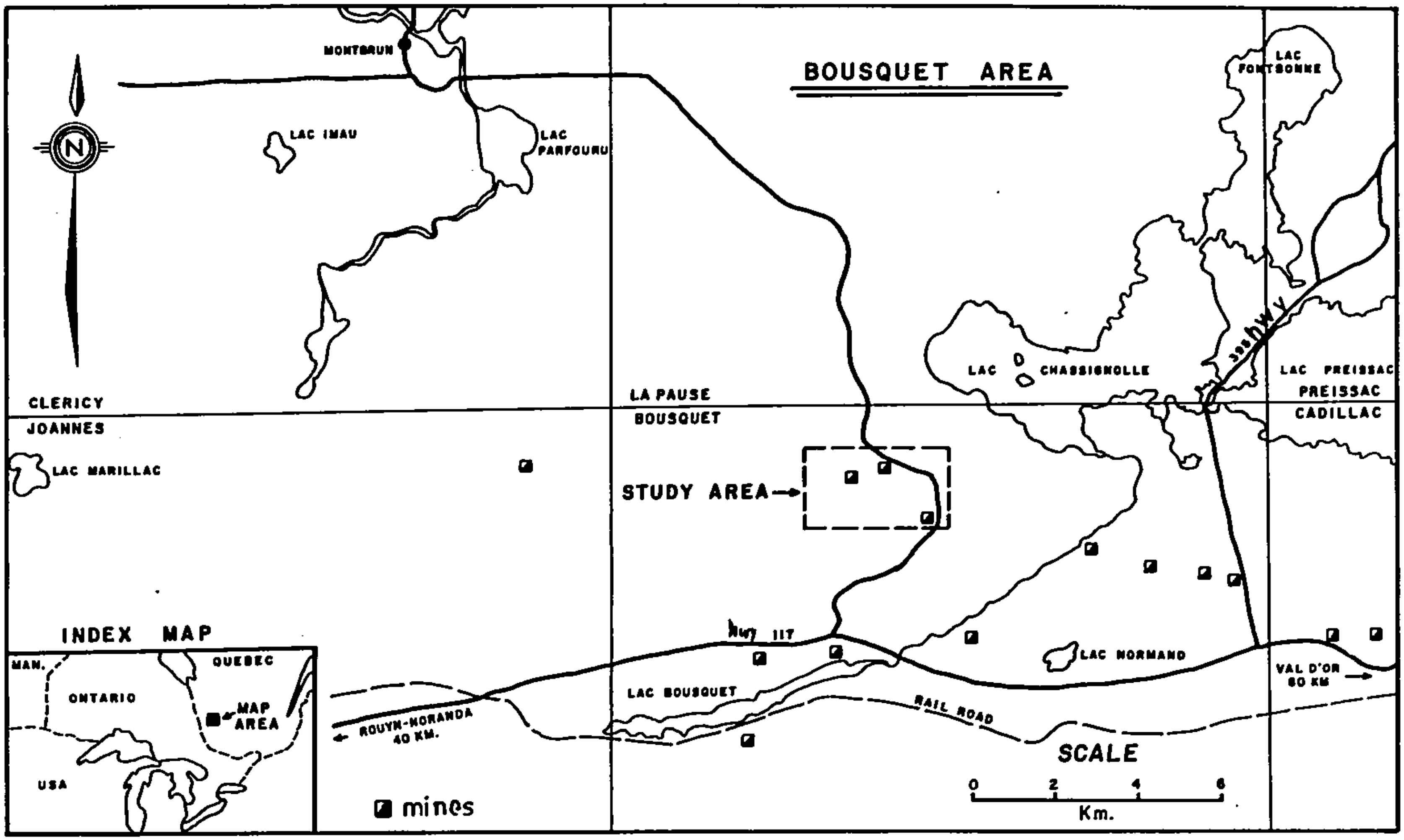

FIGURE I. : LOCATION AND ACCES TO STUDY AREA.

1.3 Method of study

The intrusion and periphery host rocks that outcrop within a perimeter of 500 metres were mapped at a 1:2500 scale during the summer of 1989. Minor verifications to the map were completed during September of 1990. Traverses were run along lines spaced 40 metres apart and outcrops tied into the Mouska property Cambior grid system. Outcrops outside the Mouska property were tied into the Cambior grid system by compass and pace. Additional data were collected from drill core examination and during a visit to the Doyon mine West Zone open pit. Most stripped areas were examined in detail except for the Mooshla "B" zone, which was washed subsequent to September 1990 and as such has only been perfunctorily examined. All geological data was digitized into an Autocad based databank for the BMC and appears on the 1:5000 scale map found in the back pocket. Air photos were used for additional outcrop control as well as for lineament interpretation. Lineaments were overlaid onto a magnetic susceptibility map for comparison (data from Cambior Ltée.). All the rocks within the area of the Mooshla intrusion have been metamorphosed (Stone, 1988). The term "meta" has therefore been omitted from all lithological descriptions in order to simplify the reading of the text.

Over 100 outcrop samples and 15 drill core samples were collected during the course of this study. Of these, approximately 52 representative samples were thin sectioned, 35 of which were polished. Geochemical analysis was completed on 47 samples with sample preparation done at the University of Ottawa. Major element and some trace element analyses were done using the X-ray fluorescence facilities of the University of Ottawa. Twenty-eight samples were analyzed for rare-earth elements by Activation Laboratories Ltd. of Ancaster Ontario. Nine additional rare-earth analyses including 4 comparison analyses were made at the Ecole Polytechnique, (Université de Montréal). Mineral compositions were determined by electron microprobe at McGill University. Details of all analytical methods employed are given in the Appendices.

1.4 Regional geology

The Mooshla intrusion is located near the southern limit of the Abitibi greenstone belt in the Superior Province of the Canadian Shield (figure 2). The supracrustal sequence of southern half of the Abitibi greenstone belt is dissected into a series of lozenge and arcuate-shaped blocks that are generally bounded by major structural discontinuities (figure 2; Ludden *et al.*, 1986; Hubert and Marquis, 1989). Each block is comprised of a volcano-sedimentary or volcanic-plutonic complex that may be dominantly ultramafic-mafic (e.g. sillon La Motte-Vassan; Imreh, 1984) or bimodal basaltic to rhyolitic (e.g. Rouyn-Noranda "caldera"; Rosen-Spence, 1976). Narrow sedimentary basins are sometimes localized along the structural discontinuities and may host Temiskaming-type sediments (e.g Kirkland Lake area; Hyde, 1980). Silica-undersaturated alkalic volcanics and intrusives form a small but significant component within these sedimentary basins (Cooke and Moorehouse, 1969).

The southern margin of the Abitibi greenstone belt roughly coincides with an east-west trending regional fault historically known as the Cadillac Break or the Larder Lake-Cadillac Break. South of the Cadillac Break lies the Pontiac metasedimentary subprovince (Card and Ciesielski, 1986). The Pontiac is an areally extensive sequence dominated by clastic sediments with minor intercalations of ultramafic to mafic igneous rocks and large gneissose intrusions (Dimroth *et al.*, 1982). In the vicinity of the BMC, the Blake River block (Hubert and Marquis, 1989) lies to the north of the Cadillac Break. The Blake River block comprises a central bimodal volcanic assemblage (the Blake River Group of Gélinas *et al.*, 1984) that is bounded to the north and south by sediments of the

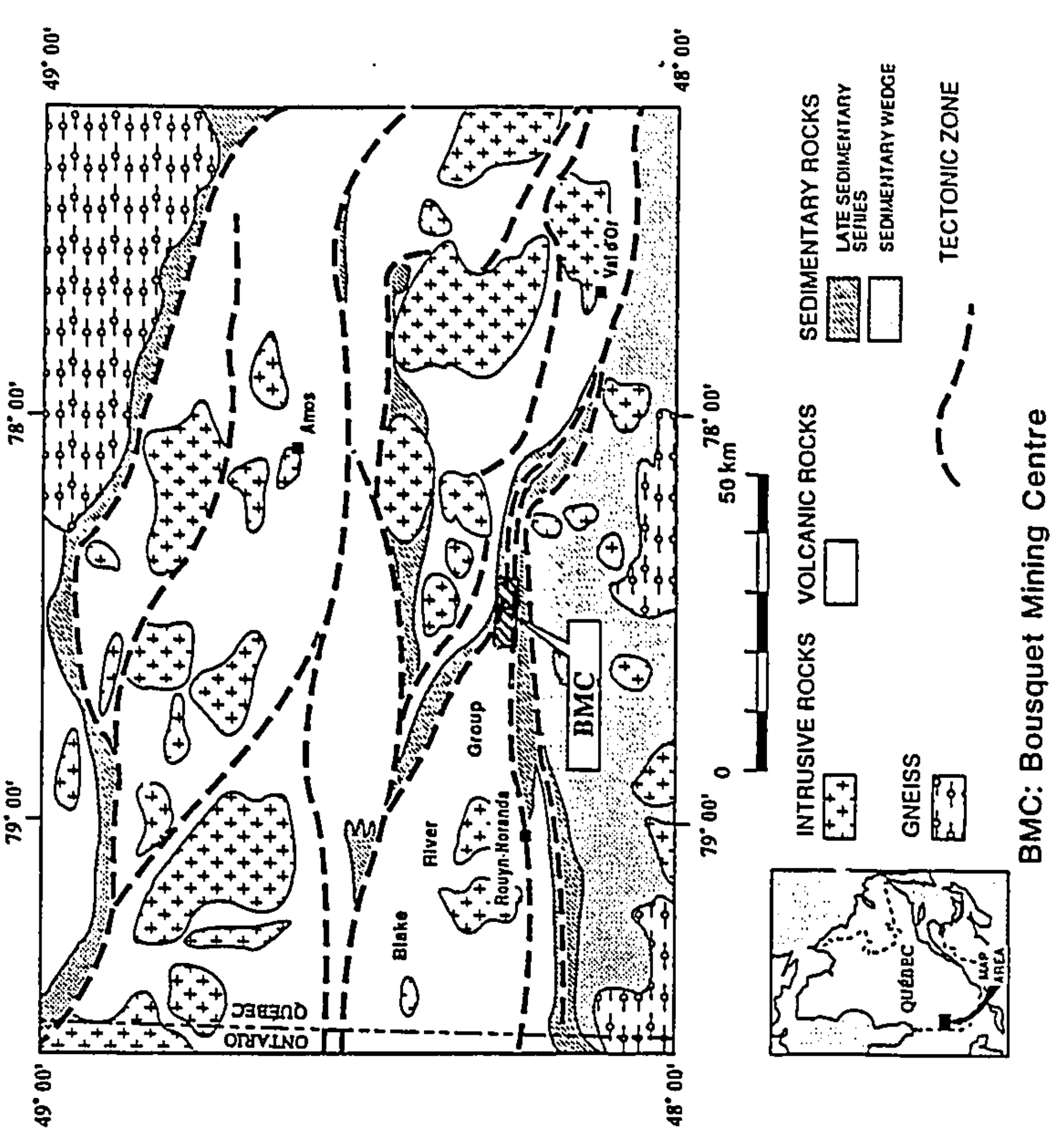

Figure 2: Regional geology. Modified from Ludden and Hubert (1986).

Kewagama and Cadillac Groups respectively (figure 3).

The region records two main periods of deformation (Ludden *et al.*, 1986). The first, D_1, produced NW-SE trending fold axes and a weak foliation related to wrench faulting. The second, D_2, was related to N-S directed compression and produced widespread E-W trending faults (dominantly thrust-faults), folds and foliations. The oldest recognized penetrative fabric within the BMC corresponds to the D_2 deformation and as such has been locally termed the S_1 fabric (Marquis *et al.*, 1990). D_1 structures are observed only in weakly strained areas. The entire region has undergone predominantly greenschist facies metamorphism except in the areas proximal to large post-tectonic intrusion where amphibolite grade is locally attained (Jolly, 1978).

1.5 Local geology

The Mooshla intrusion is hosted by the volcanic rocks of the Blake River Group (BRG). It is located at the point where the BRG undergoes a remarkable attenuation from > 6 km to < 2 km passing from west to east across the intrusion (figure 3). The BRG is a bimodal sequence; the lower BRG comprises tholeiitic basalts intercalated with minor andesites and rhyolites whereas the upper BRG consists of calc-alkaline andesites and voluminous rhyolites (Gélinas *et al.*, 1984). The Kewagama Group metasediments which lie to the north of the BRG are dominated by sandstones with lesser amounts of siltstone and mudstone (Stone, 1990). Abrupt reversals in facing directions and paleocurrent indicators on all scales suggest considerable folding within the sediments. The contact between the Kewagama and the BRG is marked by the Parfouru Lake Fault (PLF), a zone of localized intense strain and high permeability (Tourigny *et al.*, 1984). The Cadillac Group sediments south of the BRG are dominated by sandstones with intercalations of siltstone, mudstone,

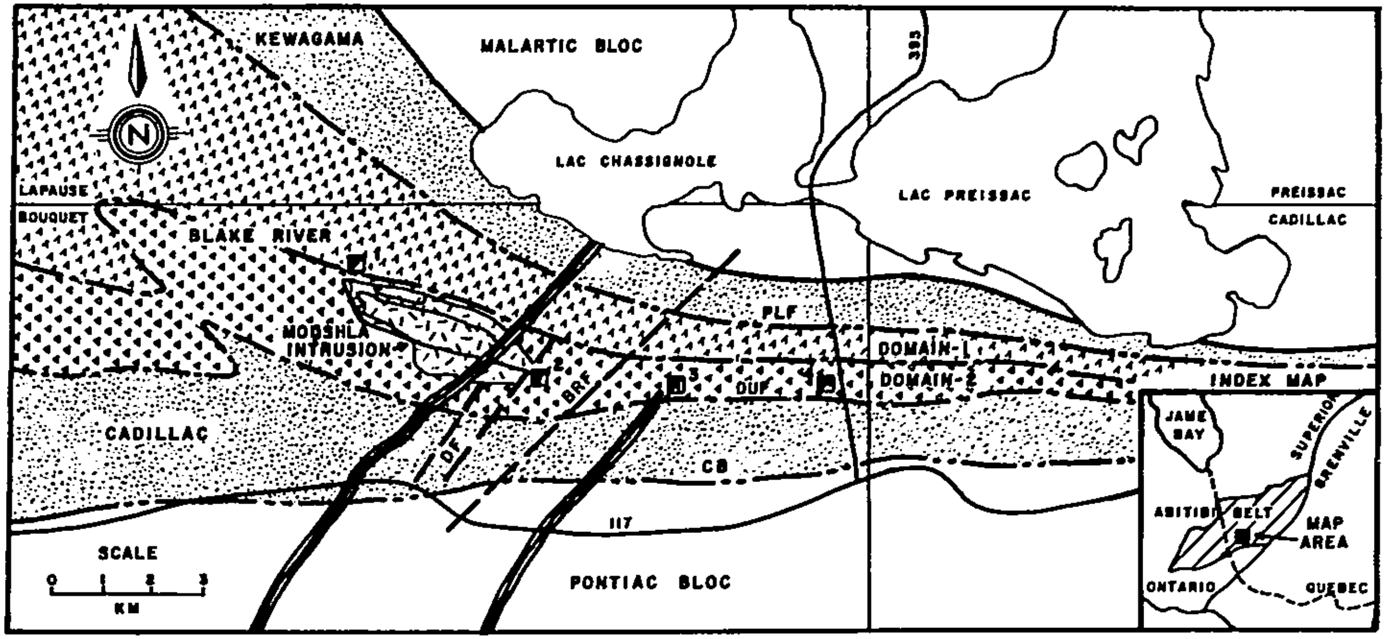

— LEGEND —

	Diabase dyke	▪	Mines under development/production	PLF	Parfouru lake fault
	Undifferentiated sediments	1	Mouska (Camblor)	DUF	Dumagami fault
	Intermediate to felsics volcanics, volcaniclastics	2	Doyon (Camblor / Lac Minerals)	CB	Cadillac break
	Mafic volcanics	3	Bousquet (Lac Minerals)	BRF	Bousquet river fault
	Mooshla Intrusion (undifferentiated)	4	Dumagami (Agnico Eagle)	DF	Doyon fault

DOMAIN 2 = Dumagami Structural Zone (DSZ)

FIGURE 3 : LOCAL GEOLOGY (Modified from Tourigny and al., 1988).

conglomerate and iron-formation (Gunning, 1941; J. Landry, pers. comm. 1989). The sediments are isoclinally folded about WNW-ESE axial surfaces (Gorman, 1986). The truncation of these folds at the contact with the BRG implies the existence of a fault, the Dumagami fault, along much of this contact (Tourigny *et al.*, 1988). The metamorphic grade in the vicinity of the BMC attained the greenschist-amphibolite transition (Stone, 1988).

The BRG has been divided into two lithotectonic Domains within the area of the BMC (Tourigny *et al.*, 1988). Domain 1, located in the northern part of the BRG, consists of a weakly sheared south-facing homoclinal succession approximately 900 metres in thickness. Rocks within Domain 1 are well preserved and comprise tholeiitic basalts (locally magnetic) that are intercalated with, and conformably overlain by, felsic volcaniclastic rocks (Tourigny *et al.*, 1988). The units strike E-W with steep dips to the south. The basalts contain hornblende, chlorite, oligoclase and clinozoisite with minor magnetite, ilmenite, biotite, quartz, pyrite and pyrrhotite (Stone, 1988). The excellent lateral continuity exhibited by some pillowed, massive and glomeroporphyritic flows enables them to be used as marker horizons (Savoie *et al.*, 1986).

Domain 2, otherwise known as the Dumagami Structural Zone (DSZ) forms the southern portion of the BRG (Marquis and Hubert, 1989). The DSZ is a $\approx$500 metre wide zone of intense ductile deformation that extends for some 10 km in an E-W direction and is host to the majority of gold deposits within the BMC. It comprises narrow anastamosing bands of schists, mylonites and phyllonites that outline lens-shaped blocks of transposed lithologies (Marquis and Hubert, 1989). The dominant fabric is a well-developed foliation that strikes E-W and dips to the south. Stretching lineations developed within the plane of this foliation typically plunge steeply westward. Kinematic indicators are consistent with reverse-oblique movement along the faults of the DSZ (Tourigny *et al.*, 1988). The least strained and altered rocks within the DSZ are represented by mafic and felsic metavolcanics. The mafic metavolcanic rocks contain andesine-chlorite with some muscovite, carbonate, quartz, biotite, epidote, titanite and pyrite whereas the felsic metavolcanic rocks contain quartz-plagioclase-muscovite with minor albite, chlorite, biotite, clinozoisite , pyrite, sphene and carbonates (Stone, 1988). The majority of the orebodies within the DSZ are hosted by a laterally continuous quartz-sericite schist (Marquis *et al.*, 1990).

1.6 Previous work

The entire Bousquet area was first described in the pioneering work of Gunning (1937 and 1941) and Gunning and Ambrose (1940). Gunning (1937) defined the general lithologic groups, established a stratigraphy and proposed the nomenclature that is still well accepted today. Virtually no research on the area was undertaken until the discovery of the Silverstack orebody in 1977. Subsequent to this discovery, Valliant (1981), Guha *et al.*, (1982), Savoie *et al.*, (1986), Stone (1988), Tourigny *et al.*, (1989), Marquis and Hubert (1989) and Marquis (1990) have done much to elucidate the nature and controls of the Au mineralization within this area. Regional studies by Dimroth *et al.*, (1982, 1983), Gélinas *et al.*, (1977, 1984) as well as Ludden and Hubert (1986b) have focussed on establishing the lithogeochmistry and structural framework of the BRG. Research specific to the Mooshla intrusion includes a discussion of its general geology and geochemistry by both Valliant (1981) and Stone (1988, 1990). Gaudreau (1986) mapped the intrusion and completed a cursory study of the geochemistry and petrography of intrusive units. The work presents a relatively detailed description of the alteration associated with the mineralized shear zones located along the northern margin of the intrusion.

The first recorded work on the Mooshla area dates back to the discovery of gold on the Mooshla "A" and "B" properties in 1933 (Giachino, 1936). Limited trenching and sampling were completed over the showing. This was followed in 1936 by the discovery of gold at the MicMac property (Mills, 1948). Mooshla "A" Mines eventually high-graded 4 400 tonnes of ore to produce 119.24 kg Au between 1939 and 1940 (Valiant and Hutchinson, 1982). The MicMac operated from 1942 to 1949 and produced 877 314 tonnes from which 3 948 kg of Au were recovered (Valliant and Hutchinson, 1982). More recently, Cousineau (1982) and Midra (1987) mapped the intrusion for SOQUEM and Cambior respectively. Savoie (1986) mapped a portion of the intrusion near its eastern limit for LAC Minerals from 1985 through to 1987. The discovery of the "Zone du Contact" by SOQUEM along the northern margin resulted in a stripping program and extensive diamond drilling to delineate the ore zones. Similarly, the discovery of the west zone at the Doyon mine by LAC Minerals in 1983 resulted in systematic drilling of much of the southeastern portion of the intrusion. In 1987, Cambior Ltée. announced the discovery of the Mouska deposit located within the volcanic rocks near the northern margin. This prompted renewed exploration over much of the intrusion which has continued essentially unabated to this day.

CHAPTER 2 GEOLOGY OF THE MOOSHLA INTRUSION AND HOST ROCKS

2.1 Introduction

The Mooshla intrusion is approximately tabular in form with dimensions of 4.0 x 1.5 km and a long axis oriented WNW. It consists of four mappable units and is bisected by a wide zone of high strain, the Southern Mooshla Shear Zone (SMSZ), that parallels its long axis. The units to the north of the SMSZ are weakly strained, hypidiomorphic and include: 1) cumulate gabbros, 2) quartz diorites and 3) (granophyric) tonalites. The fourth unit, the leucotonalite, forms the southern half of the intrusion and is host to the SMSZ. The leucotonalites are moderately to intensely sheared and exhibit varying degrees of hydrothermal alteration. The following chapter presents a description of the field units.

Historically, the number and nomenclature of these units have been quite variable. Published and unpublished research classify the intrusion into 3 to 4 units with names ranging from gabbros to trondhjemite (Table 2.1). The disparities in Table 2.1 are due largely to rock classifications based on calculated normative mineralogy (e.g. Stone, 1988). These classification schemes are considered unreliable due to the extensive alteration exhibited by the majority of mineral phases examined in thin section. As such, lithological names for the hypidiomorphic units are based on modal percentages of primary minerals that have been determined through point counting (see appendix C) and classified according to Streckeisen (1976; figure 4). With very few exceptions, all feldspars vary in composition from albite to oligoclase (Chapter 3). In addition, staining of thin-section slab cuts indicate very minor K-feldspar is present in the rocks. The variation in colour indices of the different units is graphically illustrated in figure 5.

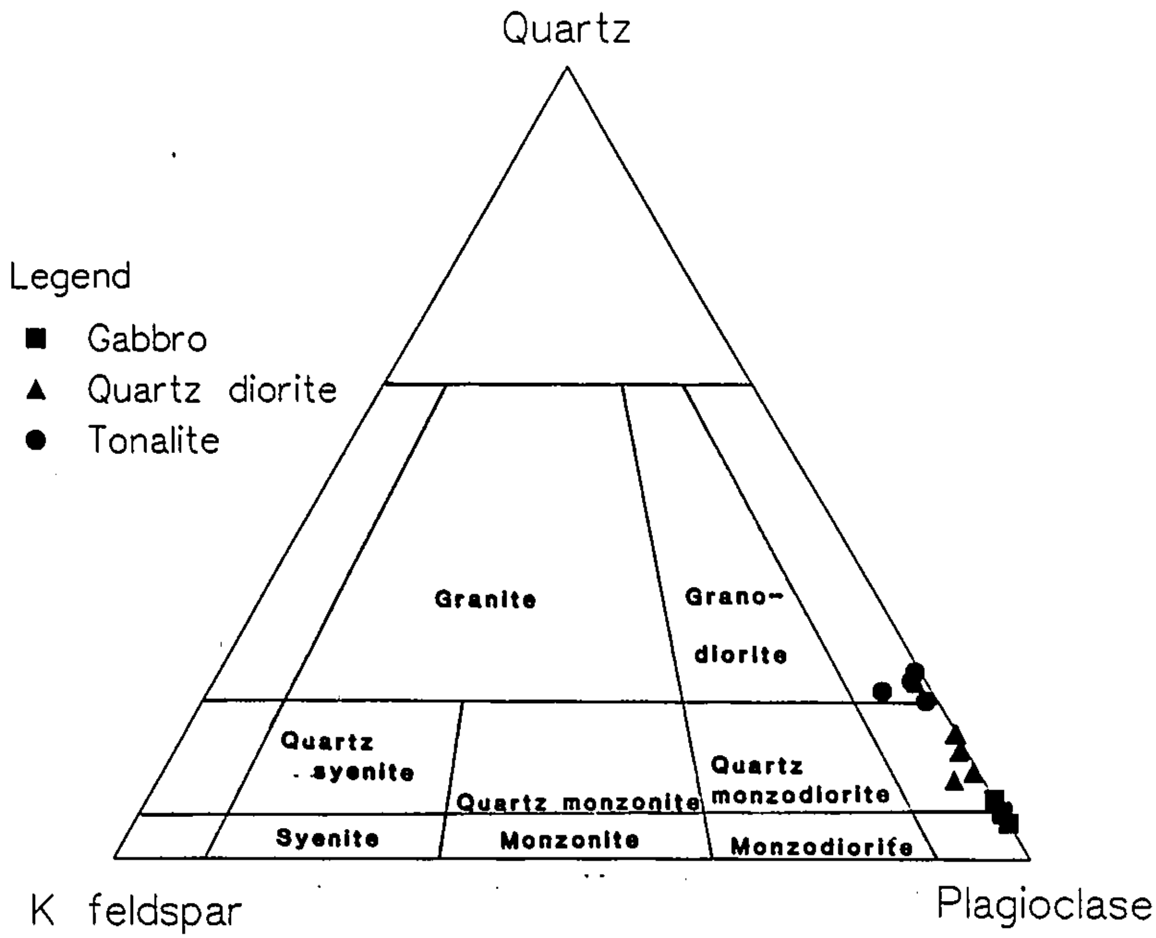

Figure 4: Modal classification for the rocks of the Mooshla intrusion. After Streckeisen (1976)

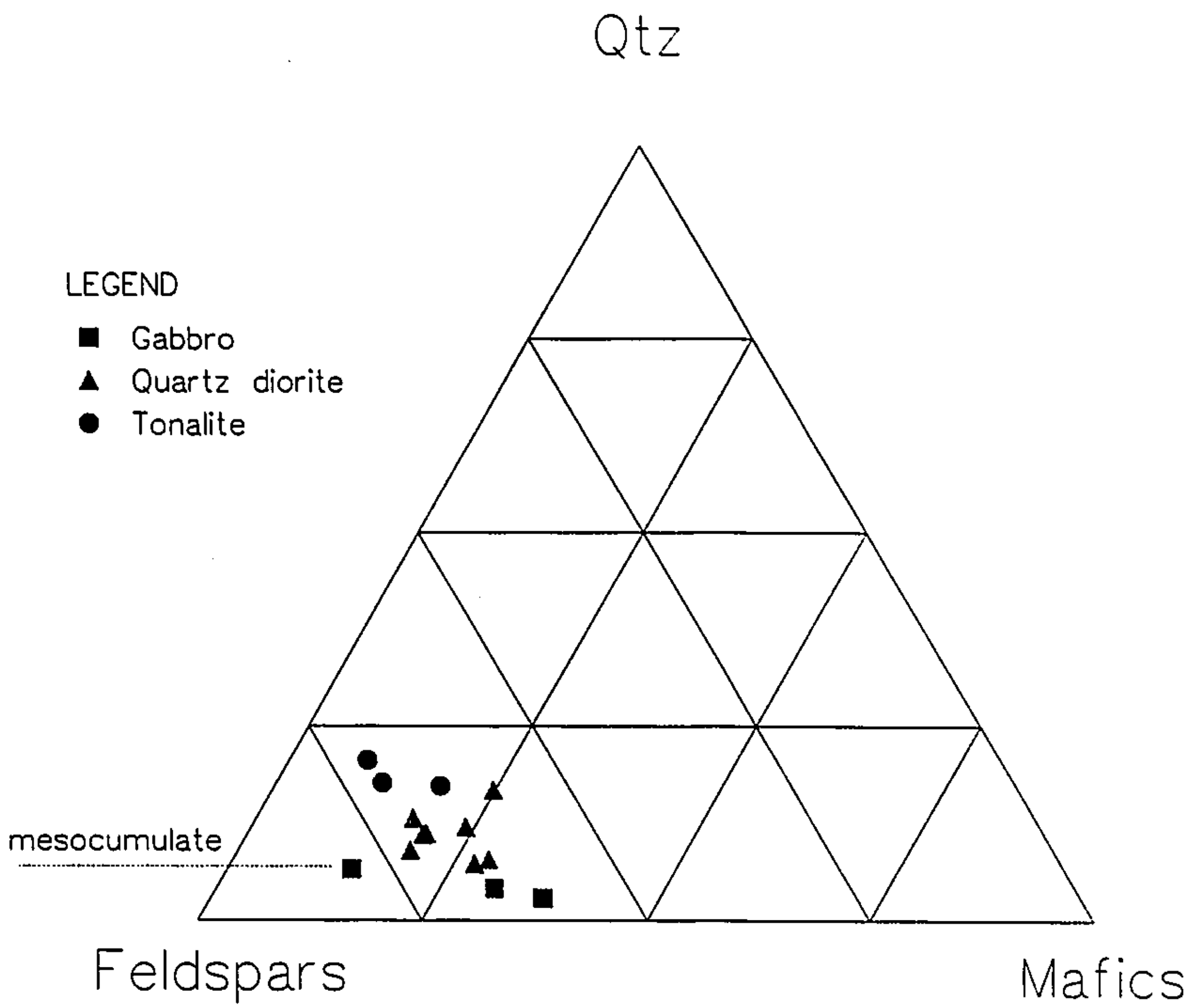

Figure 5: Modal analyses of Mooshla intrusion samples. Note location of mesocumulate gabbro

TABLE 1: Comparison of lithological nomenclature for units of the Mooshla intrusive among different authors.

This study	Stone (1988)	Gaudreau (1986)	Valliant (1981)
Cumulate gabbros	gabbro	gabbro-diorite	-
Quartz diorite	-	quartz-diorite	diorite
Tonalite	tonalite	tonalite	granodiorite
Leucotonalite	trondhjemite	granodiorite	Na-granite
Porphyritic leucotonalite	porphyritic tonalite	-	-

The sparse outcrop in the Mooshla intrusion is concentrated along its central and southeastern portions. The principal units, by surface area, are the leucotonalite and the quartz diorite, followed by the tonalite and finally, the cumulate gabbro (see map in back pocket).

2.2 Gabbros

The gabbros are the least mineralogically evolved unit within the intrusion and are composed of plagioclase and amphibole (± pyroxene) with accessory quartz. The major element chemistry of this unit (Chapter 5) is similar to that of typical gabbros (Le Maitre, 1976). The term gabbro is therefore more appropriate than diorite for this unit. Gabbro forms a narrow unit approximately 1.5 km long and 200 metres wide that is found along the northwestern periphery of the Mooshla intrusion. Outcropping in only a few places, they display textures typical of cumulate rocks (Jackson, 1967; Parsons, 1979) over a wide range of scales. There are two types of cumulates; to the west they are mesocumulates whereas to the east they are layered gabbros. The presence of such cumulates suggests that gravity induced crystal settling occurred during the post-emplacement evolution of the intrusion (Wager and Brown, 1968).

2.2.1 Mesocumulate gabbro

The mesocumulate gabbros form a narrow band near the extreme northwestern margin of the intrusion. In outcrop, they are greenish-grey, medium grained, massive and microfractured. Subhedral plagioclase phenocrysts 0.5 to 1 cm long are set in an actinolitic groundmass. No quartz is observed either on the fresh or the weathered surface. On a polished slab, the mesocumulate texture of the gabbros is evident (PLATE 1). It is composed of 80 vol.% subhedral plagioclase grains, the majority displaying overgrowths, set in a dark green intercumulus material.

2.2.2 Layered gabbro

The layered gabbros outcrop particularly well in the area just south of the MicMac Mine. They are dark green, medium grained, banded and equigranular. Dark green on fresh surface, they display blue quartz-eyes of less than 2 mm in size. Texturally, they are readily distinguished by a well developed rhythmic layering with amphibole and plagioclase as the principal cumulus phases. The layering is defined by changes in the proportion of two cumulus phases (ratio contacts; PLATE 2), abrupt changes in size or habit of a one or more cumulus phases (form contacts) or both (Jackson, 1967; Cox *et al.*, 1979; PLATE 3). Plagioclase laths show a preferential long dimension orientation parallel to the laminae. The laminae, or layers, are generally isomodal and fairly uniform in thickness ranging between 0.5 to 2.0 cm. They are laterally consistent over distances ranging from 3

A) PLATE 1: Polished slab of mesocumulate gabbro. Note the subhedral to euhedral forms of the plagioclase crystals and interstitial nature of the actinolite/chlorite matrix. Ruler for scale

B) PLATE 2: Centimetre-scale rhythmically banded gabbros. Hammer for scale (squares on hammer = 1 cm). L8+70E; 5+75N.

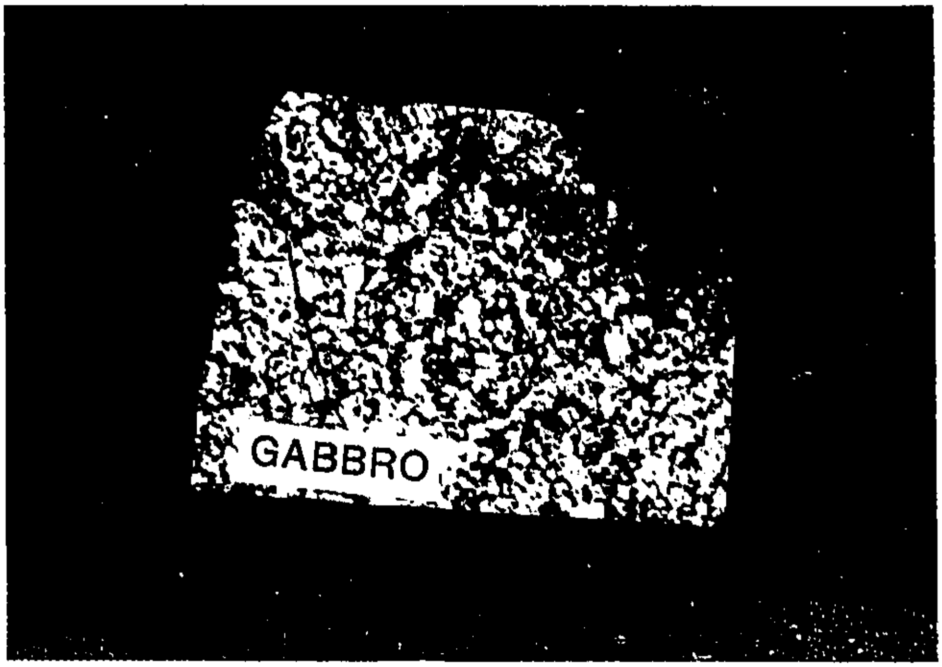

A

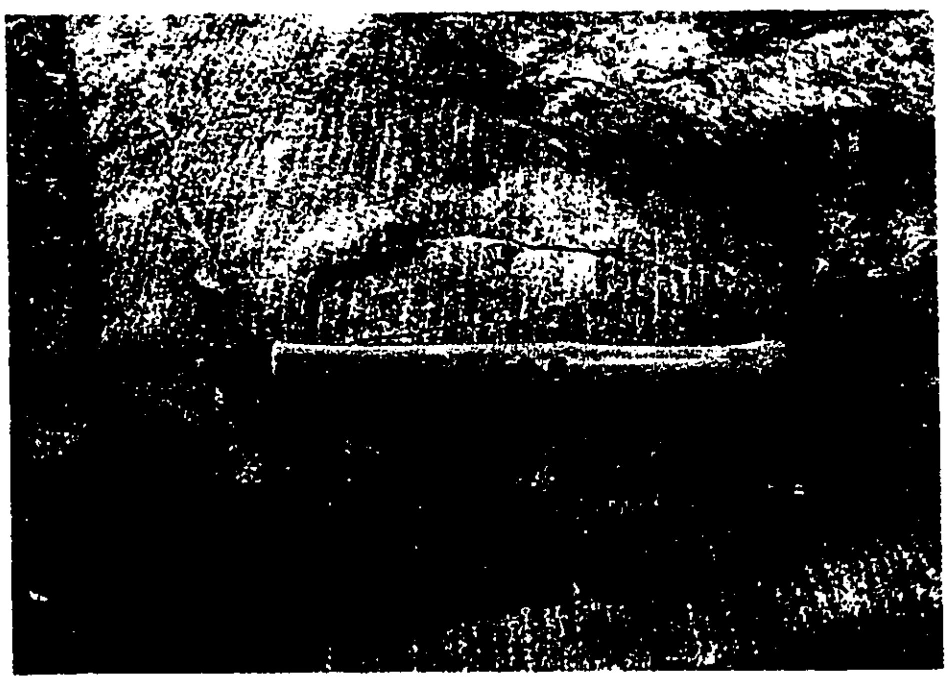

B

metres up to 15 metres (in cases of exceptionally good exposure). Mineral-graded or size-graded layers have not been observed during the course of this study. Channel structures or truncation surfaces are very rare and have been noted in only one locality. The strike of the layering is variable from 238° to 270° as one passes from west to east over the outcrop area. It dips consistently towards the north between 80 to 90°.

At least two cycles exist within the layered gabbro sequence. The lower of these two cycles, cycle 1, grades from an amphibole-rich mafic unit with very few of the plagioclase-rich layers into a transitional zone that is unevenly layered with a progressively greater proportion of plagioclase-rich layers. This transitional zone gives way to an extremely well layered sequence approximately 5 metres thick. The layering within this uppermost subunit is very even and continuous with a high proportion of plagioclase layers. This cycle is overlain by massive sequence, cycle 2, that is notable for its almost anorthositic character (plagioclase > 80 vol.% of rock). The minimum thickness of cycle 2 is 10 metres prior to being lost under the overburden. Weakly developed layering is noted approximately in the middle of cycle 2. The ratio contact between the two cycles follows the orientation of the layering and is both sharp and uniform (PLATE 4). Other cycles may very well exist within the layered gabbro sequence. These are difficult to distinguish and document given the lateral variability of layers as well as the quality and quantity of exposure.

The term schlieren has been previously assigned to the layering displayed by the cumulate gabbros (Gaudreau, 1986). However, schlieren represent mineral concentration through flowage (Davis, 1984; Hobbs *et al.*, 1976). Structures indicative of magmatic currents (e.g. washout channels) are rare within the layered gabbro sequence. Rather, the uniform and consistent nature of the layering coupled with the cyclicity of units, suggests that the cumulates developed through *in situ* bottom

A) PLATE 3: Close-up of excellent form and ratio contact for the layering within the layered gabbros. Loony for scale. L8+90E; 6+00N

B) PLATE 4: Contact between two cycles within the layered gabbro gabbros. Note well layered nature of lower cycle, the sharp uniform contact and the massive plagioclase rich nature of the overlying cycle. Contact is faulted along E-W trending 2nd order shears. Plan view. Hammer for scale. SOQUEM trench south of MicMac mine tailings.

A

B

accumulation of crystals in relatively quiescent conditions (Wager and Brown, 1968; Parsons, 1979).

2.3 Quartz diorite

The quartz diorites form a large portion of the intrusion and are confined to its core. They are mesocratic to melanocratic medium-grained equigranular rocks with a colour index of M=20-30 (PLATE 5). The quartz diorites are characterized by a speckled green-on-grey colour on the weathered surface caused by the subordinate nature of the ferromagnesian minerals within a plagioclase lath matrix. Outcrops are essentially massive and featureless with (rapid) local variations in the percentage of mafic minerals. Of note is the presence of two varieties of quartz; *i*) a grey vitreous quartz 1-2 mm in size present in virtually all outcrops and *ii*) 1 mm sky-blue quartz grains that are heterogeneously distributed throughout the unit. No systematic variation in one type of quartz with respect to the other was noted.

Fragments are common within the quartz diorites and are primarily found near the contact with the leucotonalite to the south. They are basaltic to quartz dioritic (?), angular to ovoid, of variable grain size and set in a typical medium grained equigranular quartz diorite matrix. The long axes of the more ovoid xenoliths are generally oriented parallel to the foliation. A characteristic outcrop texture of this unit are large (0.2-1.0 metre) fine-grained, epidote-green alteration patches. These are composed of epidote, albite, chlorite and calcite with milky-white quartz-rich cores (Gaudreau, 1986; Midra, 1988). They are easily distinguished by their prominent positive weathering profile and are concentrated in the area proximal to the contact with the leucotonalite in the south. The size and number of these epidote-green alteration patches are observed to generally increase from north to south across the unit. The transition from epidote-green alteration patch to unaltered rock is sharp.

A) PLATE 5: Polished slab of quartz diorite. Ruler for scale.

B) PLATE 6: Polished slab of tonalite. Ruler for scale.

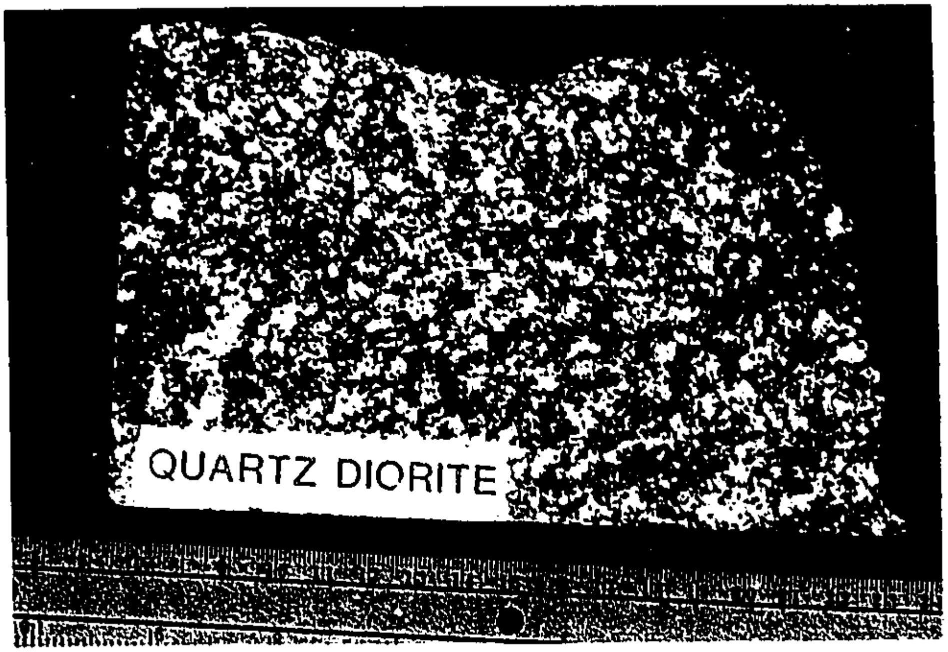

A

B

The textures and mineralogy of these patches resemble the "boules d'épidote" described by Imreh (1984) for the volcanic rocks of the Val d'Or area (La Motte-Vassan synclinorium).

2.4 Tonalite (micrographic)

Tonalite is found along the northcentral, northeastern, eastern and southwestern margins of the intrusion. With few exceptions it therefore rims the intrusion and, by extension, the quartz diorite. Tonalite represents the most mineralogically and texturally evolved unit within the Mooshla intrusion. Outcrops are scarce and occur in three broadly disparate regions of the Mooshla intrusion; *a*) along the southwestern edge and *b*) just south and to the southwest of the layered gabbros and 3) in a the vicinity of the Mooshla "B" shaft (see Map). They are mesocratic, medium grained, hypidiomorphic rocks with a colour index, M, of 10 to 20 (PLATE 6). Massive and featureless they are characterized in outcrop by their grey-white colour and rough texture caused by minute quartz grains in positive relief. The sky-blue variety of quartz is rarely found in this unit. In addition, small (1-3 mm) flakes of biotite and zoned plagioclase are conspicuous on the fresh surface.

2.5 Leucotonalite

The leucotonalite is a hydrothermally altered and variably deformed unit that forms the entire southern portion of the Mooshla intrusion. The term leucotonalite has been chosen in order to underscore the probable genetic relationship of this unit to the tonalite (section 3.4.3.7). Its width varies markedly; in the west it is less than 20 metres wide, whereas to the east it exceeds 400 metres in width. The Southern Mooshla Shear Zone (SMSZ), a wide zone of very high strain and associated alteration, occurs entirely within this unit. Shearing along the SMSZ has modified the initial texture of this unit; the leucotonalite is a fine to medium grained, beige-white to grey colored, well foliated porphyroclastic rock with a colour index, M, of 0 to 10 (visual estimate). It can be subdivided into two distinct facies defined on the basis of their mesoscopic and microscopic fabrics and textures. These are; *i*) a phyllonitic facies which forms the bulk of this unit and *ii*) a weakly sheared "porphyritic" facies that is restricted to the southeastern portion of the intrusion. Textural and mineralogical evidence (see below) suggests that the two leucotonalite facies were probably derived from a common protolith. Both exhibit similar bulk mineral assemblages and clear evidence of extensive dynamic recrystallization. However, they differ chiefly in the degree of penetrative fabric development. It is evident that the phyllonite was subjected to a higher strain than the porphyritic facies. In effect, the porphyritic leucotonalite may be viewed as a weakly-sheared megalithon within the highly-sheared phyllonite. The nature of the leucotonalite protolith is difficult to ascertain on the basis of mesoscopic observations. Note its spatial distribution as a unit that borders the intrusion margin is similar to the tonalite (which borders the intrusion to the north and east; see map).

2.5.1 Phyllonitic leucotonalite

The phyllonitic (Sibson, 1977) leucotonalite is a moderatly to intensly deformed sub-unit of igneous origin. In outcrop, the phyllonitic leucotonalite displays a prominent tectonic grain defined by the parallel alignment of micaceous minerals as well as quartz and feldspar porphyroclasts. Mafic minerals are virtually absent and pyrite, as anhedral to euhedral grains (0.5-10 mm large) is common. Carbonate is common in the groundmass and fizzes readily under dilute HCl. The primary groundmass minerals are largely destroyed and replaced by an alteration assemblage comprising varying proportions of sericite, quartz, carbonate and chlorite (PLATE 7). Angular quartz porphyroclasts less than 2 mm large comprise 15 to 25 vol.% of the rock and are of both sky-blue

A) PLATE 7: Leucotonalite enclosing basalt xenoliths; fragment zone behind old Doyon mine office building . Notebook for scale.

B) PLATE 8: Typical porphyritic leucotonalites. Note variations in colour and fabric. Samples from DDH's 82-1039, 1042, 1064 respectively. Ruler for scale.

A

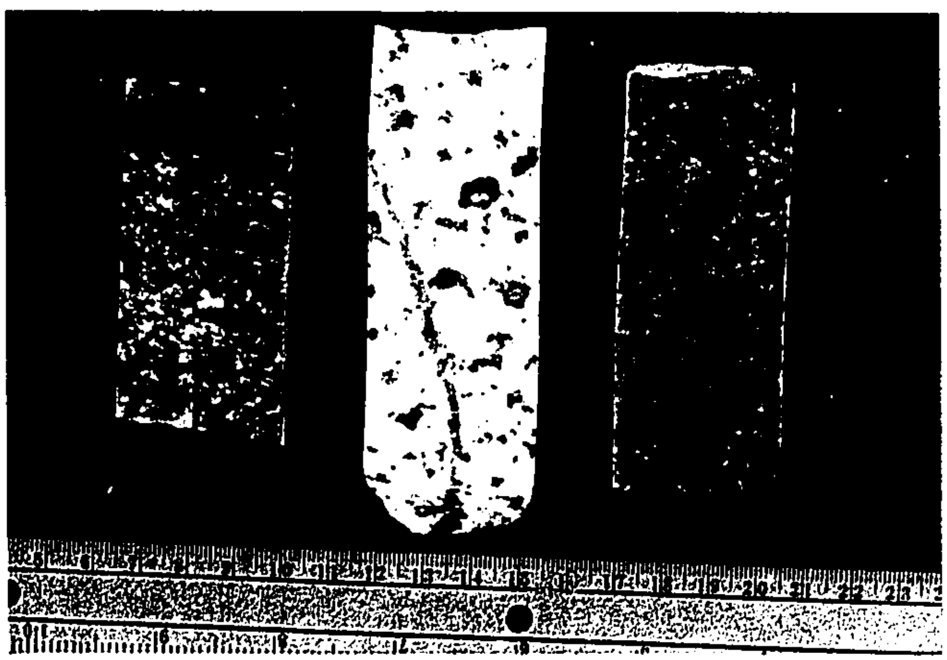

B

and grey-vitreous varieties. Feldspar porphyroclasts are very irregular in shape, comprise 5 to 10 vol.% of the rock and are less than 2 mm large. Compositional layering, defined by alternate chlorite and sericite-rich layers, is locally developed within the more highly strained portions of phyllonitic leucotonalite. Augen of either quartz or feldspar are very rare.

2.5.2 "Porphyritic" leucotonalite

The porphyritic leucotonalite is a narrow E-W trending texturally distinct facies which partially transects the phyllonitic leucotonalite. Its location and distribution is largely inferred from diamond drill hole data due to the paucity of outcrops. Although in its type location this sub-unit is characterized by a porphyritic texture, a random sampling of the first 45 metres of drill core culled from 15 widely spaced diamond drill holes reveals that the porphyritic leucotonalite is extremely heterogenous. A precise petrographic or textural description of this facies is impossible given the high degree of variability observed along the drill hole traverse as well as between individual drill holes. In effect, this sub-unit is more correctly characterized by its extreme mineralogical and textural heterogeneity accompanied by general lack of strong fabric development (PLATE 8).

Mesoscopic textures observed within this facies include: *i)* porphyritic; 15 to 25% euhedral extensively sausseritized relict plagioclase phenocrysts 1-5 mm large, and *ii)* megacrystic; large mafic clots, 0.4-1.2 cm across, cored by subhedral to euhedral pyrite. These features occur separately as well as together. Unlike the phyllonitic leucotonalite, a penetrative fabric is rarely observed on a hand sample scale.

2.6 Fragment zone

The fragment zone is a zone approximatly 100 m wide that comprises a series of en-echelon lenses containing 10-30% vol.% subangular to subrounded, green to grey, foliated, aphanitic to medium-grained fragments (PLATE 7). The term fragment zone is preferred because it has no genetic implications. The zone is located near, and trends subparallel to the northern contact of the phyllonitic leucotonalite (figure 6). Individual lenses vary greatly in dimension. Based on limited surface exposure, the lense widths range from 1-4 metres and lengths from 3-10 metres. In section the fragments may be attenuated, sometimes resembling a pancake. Fragments comprise both xenoliths of the host basalts as well as autoliths of the tonalite. Basalt xenoliths are dark to pale green, aphanitic, generally schistose and contain from 1-4 vol.% euhedral magnetite grains. Those that resemble autoliths of the quartz diorite are grey-green, fine grained, foliated and may contain up to 2 vol.% sky-blue quartz grains.

Basaltic to quartz dioritic fragments display systematic variations in amount, morphology and grain size. Both the abundance of fragments and their degree of angularity increase progressively from north to south across the intrusion, attaining a maximum (10-30 vol.%) within the fragment zone. South of this zone no fragments have been recognized within the sheared leucotonalite (figure 6). Conversely, the grain size of fragments decreases towards the south. Fragments (basalt xenoliths?; tonalite autoliths?) proximal to the northern contact are elliptical dark green equigranular patches consisting of a fine to medium grained mat of plagioclase feldspar and actinolitic hornblende. Their intermediate axes are parallel to subparallel with the regional foliation, S_2. Variations in grain size and change of colour from green to grey blurs the distinction between the xenolithic (volcanic) or autolithic (intrusive) nature of the fragments.

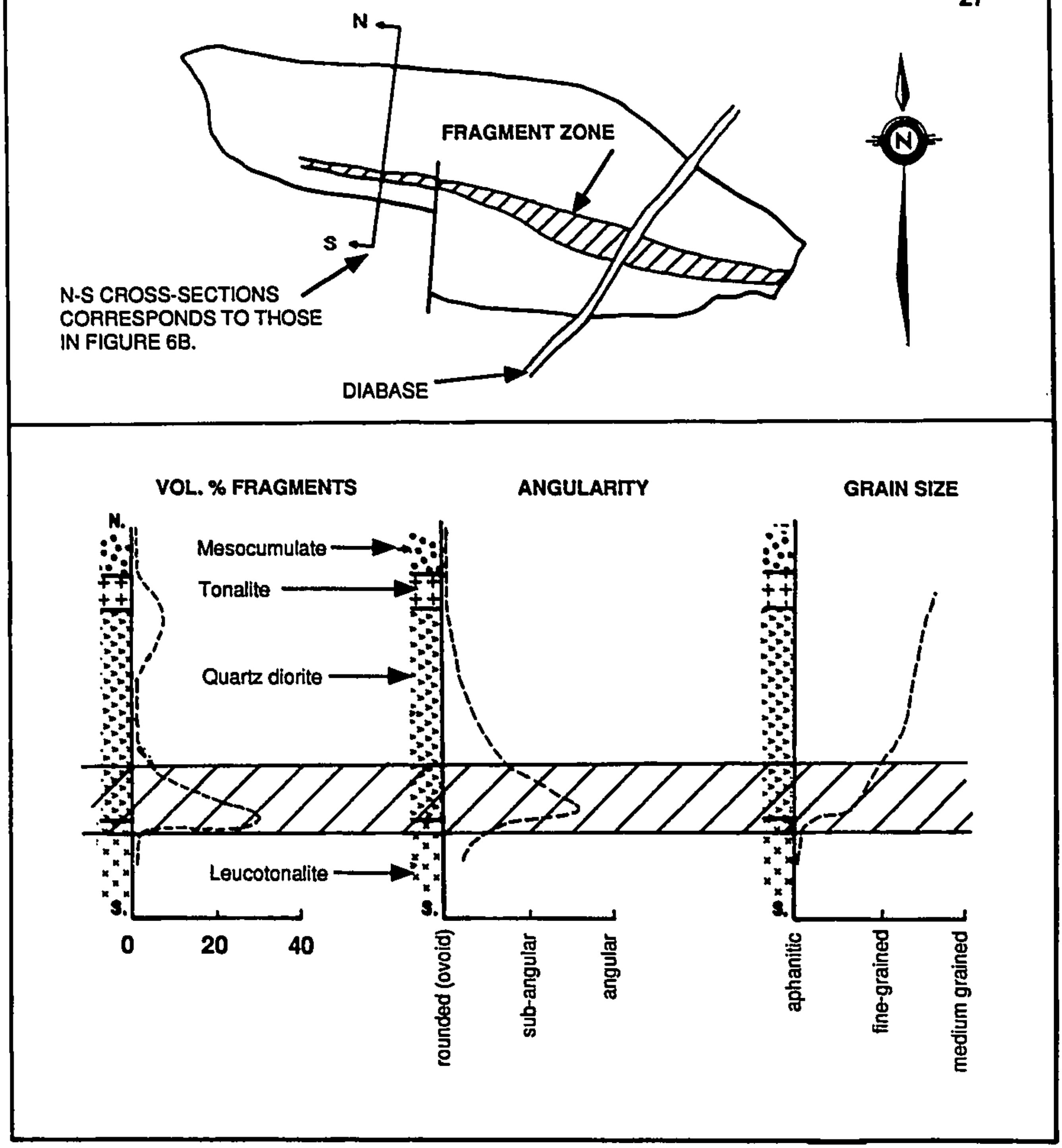

FIGURE 6: A) LOCATION OF FRAGMENT ZONE WITHIN THE MOOSHLA INTRUSION.

B) DIAGRAMMATIC CURVES SHOWING VARIATIONS NOTED IN Vol.% FRAGMENTS, THEIR ANGULARITY AND GRAIN SIZE (BASED ON VISUAL ESTIMATES

In contrast, the basalt xenoliths hosted by the leucotonalite to the south are dark to medium green, aphanitic with no macroscopic evidence of recrystallization. Some basalt xenoliths display narrow (1 - 2 mm) magnetite-rich reaction rims along the leucotontalite-basalt interface. Basalt xenoliths in the leucotonalite are sometimes flattened onto the plane of S_2 and are vertically stretched into a pancake shape. Where this occurs, their aspect ratios may vary from 5:1 to 15:1 in the horizontal plane and from 10:1 to 20:1 in cross-sectional plane. Basalt xenoliths in the quartz diorite immediately north of the leucotonalite - quartz diorite contact are relatively undeformed and show no preferred orientation. Savoie *et al.* (1989) note an abundance of these lenses in the area of the Doyon mine. The lenses are oriented parallel to the regional foliation (S_2), appear to be irregularly distributed and are possibly transposed equivalents of one another.

2.7 Quartz-phyric aplitic dykes

Narrow (0.1-0.5 m) leucocratic, aphanitic, porphyritic aplite dykes intrude the gabbro cumulates, quartz diorites and tonalites (PLATE 9). They contain 5-10 vol.% angular quartz and feldspar phenocrysts 1-2 mm large as well as 1-5 vol.% grains of biotite, 1-4 mm large, that give them a flecked-black appearance. In some cases, the cores of these dykes contain massive quartz as pods or lenses intergrown with the leucocratic matrix. Where this is observed, pods of tourmaline are also noted. Although the dykes display no preferred orientation, they are frequently associated with small shear zones and/or joint surfaces. Typically, dykes pinch out along strike and are displaced by the majority of fault surfaces. Trace disseminated magnetite lends the dykes a weak magnetism. They are interpreted as representing residual melts that were injected along fractures in the cooling Mooshla intrusion.

PLATE 9: Quartz phyric aplitic dyke cross-cutting tonalite and displaced by second order shear. Back-pack for scale.

2.8 Mafic dykes

Mafic dykes cross cut all other lithologies, including the quartz-phyric aplite dykes, and have only been observed in the area of the Mooshla "B" shaft. The mafic dykes are dark to medium green, massive, aphanitic and may contain from 1-10 vol.% euhedral plagioclase phenocrysts 5 - 15 mm long. They are 0.2 to 3 metres wide, with minimum lengths of 20 metres. The dykes typically exhibit a very strong foliation oriented subparallel to oblique with the contacts (see section 4.4.4.3). This foliation is sometimes crenulated. Mafic dykes are localized along shear structures and are associated with auriferous pod-like quartz veins that contain 1-3 vol.% disseminated pyrite. There is little to no wall-rock alteration associated with the dykes.

2.9 Host rocks

The Mooshla intrusion lies within a sequence of volcanic and volcaniclastic rocks. The primary host lithology is basalt which bound approximately 90% of the intrusion. The remaining 10%, located in the vicinity of the Doyon mine, is in contact with a sequence of mafic tuffs and blocky tuffs (A. Savoie, pers. comm. 1989).

2.9.1 Basalts

Subtle variations exist in the colours, morphologies, alteration and textures of the basalts around the intrusion. These variations may be used to define sectors within which the basalts are broadly similar. Three principal sectors have been identified; *i*) the north sector, *ii*) the west sector and *iii*) the south sector (figure 7).

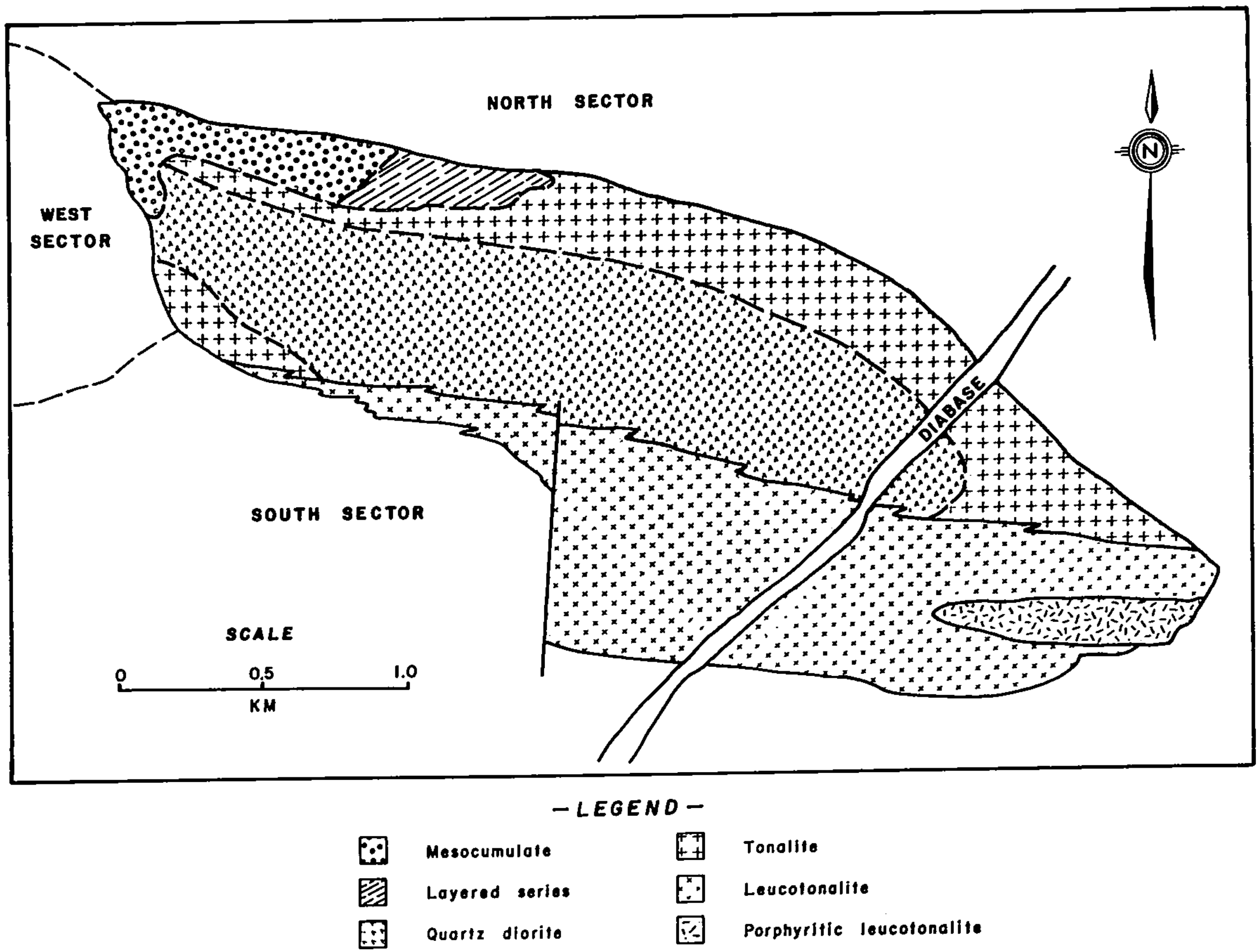

FIGURE 7 : LOCATION OF BASALT SECTORS AROUND THE MOOSHLA INTRUSION.

2.9.1.1 Northern sector

The basalts of the north sector are tholeiitic (Savoie *et al.*, 1986) grey-green, aphanitic to fine grained and are variably magnetic. They form a thick sequence of massive and pillowed flows that are sometimes porphyritic and vesicular. Thicknesses of these flows range from 2 to 50 metres with many displaying remarkable lateral continuity. In particular, a glomeroporphyritic (1-10 vol.% phenocrysts 0.5-3 cm large) flow and a pillowed flow have been identified as marker sub-units that may be traced over 2 km (Savoie, 1986). This sector is also noted for exceptionally well preserved pillowed facies. Pillows have thin rims (1-3 cm) that are recessive weathering and display poorly developed concentric cooling fractures. A thick flow breccia sequence is observed in the area just south of the MicMac mine. This is the only flow breccia noted around the entire intrusion.
The intensity of deformation and degree of alteration of the north sector basalts increases with proximity to the Mooshla intrusion. Anastamosing high strain zones are responsible for outcrop scale variations in the degree of attenuation of pillow facies. The number of these high strain zones reach their maximum in the immediate vicinity of the MicMac mine. In this area, pillows may be completely dismembered and a crude compositional layering is observed. Apple-green lenses of epidotization and elongate pods of magnetite 1-5 cm long are characteristic of this area. Relict plagioclase phenocrysts are also observed.

2.9.1.2 Western sector

Basalts within the west sector are dominated by fine to medium grained massive flows that are grey to green-grey in outcrop and moderately magnetic. These flows are rarely pillowed, porphyritic or vesicular. No flow breccias were observed. The development of a coarsening in the grain size within the thicker flows lends them an intrusive appearance. Of note is a subtle fabric that trends approximately 80° defined by thin (less than 2 mm) regularly spaced veinlets (?) of tourmaline (?). Quartz-phyric felsic dykes 5-20 cm wide are common in this sector. Smaller offshoots of these dykes form a stockwork pattern that isolates basalt fragments and partially recrystallizes their rims. Intercalations of intermediate to felsic volcanic rocks are observed within this sector.

Structure is dominated by a foliation, S_2 (section 4.4.1.2) and a prominent jointing that is ubiquitous throughout this sector. The joints are closely spaced, oriented roughly N-S and have an average frequency of 5/metre. A minimum apparent dextral displacement of 10 metres is documented along a N-S fracture in the southwestern portion of this sector (see Map). Irregular, heterogeneous beige to pale-green colored alteration is characteristic of this sector.

2.9.1.3 Southern sector

Basalts within the southern sector have a distinctly medium to pale bluish-green colour, are always aphanitic and are generally well fractured. Massive flows predominate, although pillowed facies and flow breccias are common. Most typical of this sector is the well developed penetrative fabric, S_2, that is observed in almost every outcrop. Magnetite, when present, occurs as disseminated euhedral grains 1-2 mm large. Intercalations of mafic lapilli tuffs and narrow porphyritic dacite intercalations are common. The porphyritic dacites weather a prominent beige-white and contain 10-20 vol.% subhedral to anhedral plagioclase phenocrysts 0.3-1.3 cm long set in a massive, aphanitic groundmass.

2.9.2 Blocky tuffs and mafic tuffs

The blocky tuffs are basaltic to andesitic in composition and consist of 1 to 40 cm sized polymictic fragments set in a fine grained chloritized matrix. Lapillis show flattening onto the foliation plane S_2 and define a pancake shape. The blocky tuffs are intercalated with thin, discontinuous fine grained tuffaceous horizons (Savoie, 1986). Magnetite is ubiquitous as 1-3 mm large subhedral to euhedral grains and may form up to 3 vol.% of the tuffs. Bedding is generally well defined whereas sorting is usually poor (Savoie, 1986).

2.10 Field relationships between lithologies

2.10.1 Mooshla intrusion

Gradational contacts have been observed between the tonalite and gabbro cumulates as well as between the tonalite and quartz diorite. These contacts are difficult to distinguish macroscopically (in drill core), are gradational over $\approx$30-50 m and are not associated with a reduction in grain size or strongly developed fabric. No outcrop contact has been observed between the quartz diorites and cumulate gabbros. In contrast to all other contacts, a tectonic contact marked by a zone of high strain exists between the phyllonitic leucotonalite and the quartz diorite. Transposition of the leucotonalite is a common feature along much of this contact.

The units of the Mooshla intrusion are arranged in a zonal manner with a core composed of quartz diorite (mafic) surrounded largely by a rim of tonalite (felsic). This arrangement, where a mafic core is surrounded by a felsic rim, is commonly referred to as reverse zoning and is thought to reflect multiple events of magma emplacement (Bourne and Danis, 1987). Note however that no textures typical of magma mixing such as dyke swarms, net-veined rocks, mafic enclaves, schlieren and skeletal or branching pyroxene/hornblende crystals (Goldie, 1978; Sutcliffe, 1989) were oberved for any unit within the intrusion.

The pegmatite-like nature of some of the quartz-phyric aplite dykes along with the frequent tourmaline pods suggest that these represent late stage volatile and incompatible element-rich internal dykes. Historically, the aplite dykes were interpreted as apophyses of the leucotonalite (Gunning, 1941). Their presence within all units *except* the leucotonalite was believed to indicate the relatively younger age of the leucotonalite compared to the remaining lithologies (Savoie *et al.*, 1986; Stone, 1988). However, the absence of aplite dykes in the leucotonalite may simply be due their obliteration during the period of high strain which affected much of this unit.

2.10.2 The Mooshla intrusion and its host rocks

Diamond drill hole data indicates that the northern margin of the Mooshla intrusive is a heterogenous zone of intermingled gabbro, quartz diorite and basalts that varies substantially in width from 50-200 metres. This sequence of rocks resembles a dyke/sill swarm and defines the border zone. The location of the contact drawn on the map (see back pocket) represents the point at which volcanic rocks form less than 5 vol.% of the drill core traverse within the border zone. No peripheral cataclasis zone or contact breccia were observed. In addition, the preservation of much of the original rock fabric as well as the lack of porphyroblasts and high temperature minerals (e.g. garnet), suggest that no contact metamorphic aureole occurs within the host volcanics.

The southern margin of the intrusion has undergone significant post-emplacement shearing. The contact between the phyllonitic leucotonalite and the host volcanics is sharp and transposed. Transposition occurs within a 5-50 metre wide zone of high strain. Mineral and stretching lineations on and within the plane of foliation in this high strain zone plunge steeply westward and indicate that the final strain increment involved subvertical movement along this contact (see section 4.4.4.1). As noted on the map, the leucotonalite is offset by a fault with a N-S orientation (inferred from geophysics and air photo lineaments). A similar displacement of the northern intrusion contact by this fault is not observed.

2.11 Summary

The Mooshla intrusion is a reversely zoned composite body. It comprises 4 distinct units that define a petrologic spectrum from gabbro (cumulates) through quartz diorite, tonalite, and leucotonalite. No textural evidences of magma mixing were observed and contacts between these units, with the exception of the leucotonalite, are apparently gradational. The elongate nature of both the intrusion and its units suggest that it was emplaced as a sill-like body. The intricate rhythmic layering exhibited by the mafic cumulate sequence is consistent with *in situ* differentiation. The cumulates appear to only be in contact with the tonalites. This suggests that the two may be genetically related.

The intrusion is bisected by the SMSZ. Rocks within the SMSZ (leucotonalite) exhibit a heterogeneously developed compositional layering, numerous porphyroclasts and few mafic minerals. Quartz veining, abundant sericite and disseminated pyrite suggest extensive hydrothermal alteration of the leucotonalite may have accompanied deformation.

CHAPTER 3: PETROGRAPHY AND MINERALOGY OF THE MOOSHLA LITHOLOGIES

3.1 Introduction

The following presents the results of petrographic descriptions of both the Mooshla lithologies and their host rocks. Almost all primary phases within the Mooshla intrusion have been subjected to alteration. However, the intensity of the alteration is heterogenous over the unit scale. As a result, the primary mineral assemblage can be fairly well constrained through comparison of many thin sections. North of the SMSZ, the primary mineral assemblage comprised; plagioclase, amphibole ± pyroxene and quartz with accessory apatite, titanite, zircon and opaques (ilmenite, magnetite, hematite, Fe-sulphides, chalcopyrite and sphalerite). Secondary phases include albite, quartz, amphiboles, chlorite, biotite, epidote, sericite, calcite, pyrite, rutile and titanite. Within the SMSZ, the tectono-metamorphic assemblage comprises quartz, albite, sericite, epidote, chlorite, calcite and pyrite.

3.2 Gabbro

3.2.1 Mesocumulates

Large plagioclase phenocrysts (0.2-2.0 cm) within the gabbro mesocumulates are completely altered to a fine grained felty aggregate of albite, epidote and white mica (sericite/paragonite). Textures, however, are preserved. Many of the plagioclase phenocrysts display a ghost euhedral shape in the core defined by a relatively clear and coarse-grained alteration assemblage. These ghost cores are mantled by a darker, fine-grained overgrowth. This may represent a relict adcumulus texture.

In the best preserved sections, a single, large, optically continuous grain of fibrous amphibole fills the interstices between adjacent plagioclase crystals. These amphiboles range in size from 1.0 to 7.0 mm, are pale green to colorless and exhibit alteration along their cleavages to chlorite and quartz (PLATE 10). They are marked by a highly variable birefringence and generally sharp plagioclase/amphibole interfaces defined by a thin rim of finely recrystallized quartz.

Mesocumulate amphiboles range in composition from actinolitic-hornblende to actinolite (figure 8). In many of the thin sections studied, the primary ferromagnesian minerals within plagioclase interstices are completely altered to a fine grained aggregate of quartz and chlorite with accessory epidote. The quartz is finely recrystallized (in part polygonatized). Biotite is not observed within this unit. Opaque minerals are very rare within the mesocumulate gabbros. They occur only as small (less than 0.5 mm long) anhedral grains of ilmenite and rutile that may represent remnants from titanomagnetite (?).

3.2.2 Layered gabbro

In thin section the layered gabbros exhibit large subhedral to anhedral plagioclase that are entirely recrystallized to a fine-grained grey-brown mat of albite, epidote and quartz with minor white mica (sericite/paragonite). Relict twinning is rarely observed. The plagioclase range in composition from An_{0-5} and partially to fully enclose the ferromagnesian minerals. The coarse grained plagioclase cores noted in the mesocumulate gabbros are not as prominent within this sub-unit. Amphibole constitutes the principal ferromagnesian mineral. It occurs as both coarse and fibrous grains. The coarse amphiboles are all magnesio-hornblendes (figure 8). They are characterized by an even pleochroism

A) PLATE 10: Photomicrograph of large, optically continuous (actinolitic) amphibole (outlined in blue) filling interstices between plagioclase grains. Gabbro mesocumulate. Darker material may represent adcumulus overgrowth. p = plagioclase; o = overgrowth of plagioclase; a = amphibole. Plane light. Width of field = 4.6 mm.

B) PLATE 11: Photomicrograph of well preserved amphibole within the layered gabbro sequence. a = amphibole; p = plagioclase. Crossed polars. Width of field = 0.46 cm.

A

B

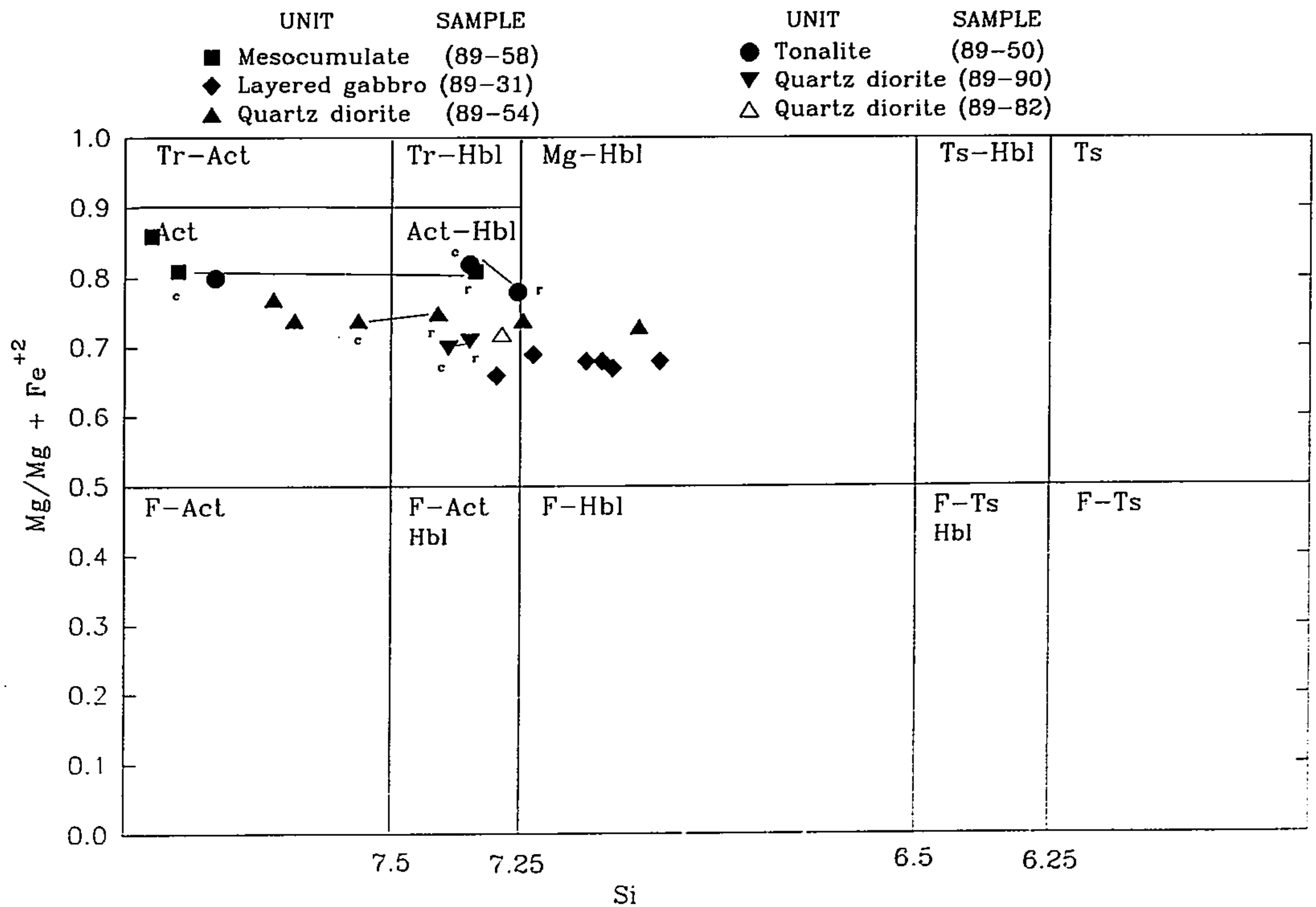

Figure 8. Compositions of the calcic amphiboles of the Mooshla intrusion. Nomenclature after Leake (1978). Abbreviations: Tr= tremolite; Tr Hbl= tremolitic-hornblende; Act= actinolite; Act-Hbl= actinolitic-hornblende; Hbl= magnesio-hornblende; Ts= tschermakite Ts-Hbl= tschermakitic-hornblende; F= ferro. Lines join analyses on the same grain; c= core of grain, r= rim of grain.

from yellow-brown to dark green, good excellent cleavages and a paucity of primary mineral inclusions (PLATE 11). The magnesio-hornblendes display remarkably uniform compositions and have the highest A site occupancy of all analyzed amphiboles (appendix B.2). Small domains of alteration and subhedral pale green chlorite-rich patches are common within the coarse amphibole. Plagioclase/amphibole interfaces are sharp and exhibit no amphibole overgrowth, plagioclase replacement or quartz rim (see above). Fibrous amphibole is actinolitic in composition, It is usually pale coloured, marked by uneven and patchy pleochroism and occurs as elongate crystals (figure 8).

As is frequently the case, amphiboles are replaced by 'clots' comprising a fine-grained irregular aggregate of chlorite, quartz, sericite and epidote with variable quantities of minor biotite, carbonate and opaque minerals. Chlorite proximal to the opaque minerals display anomalous brown birefringence. No relict pyroxenes have been noted in any of the samples examined during this study, although Gaudreau (1986) and Stone (1988) record their presence in this unit.

A characteristic microtexture of the layered gabbros are layer-parallel bands of euhedral apatite crystals 0.4 to 1.6 mm long (PLATE 12). In some cases, apatite may comprise up to 3 vol.% of the rock (MS-89-47) and is generally very well preserved. The anomalous concentration of apatite in layer-parallel bands reflects its high relative density and early crystallized nature. In addition, it further suggests that crystal settling was a factor in layered gabbro development. Quartz is a minor phase comprising less than 5 vol.% of this unit. It occurs as small interstial fillings in and around apatite and plagioclase and is rarely recrystallized into smaller grains.

Opaque minerals form between 2 and 5 vol.% of the layered gabbros. Ilmenite is the dominant phase and occurs in two textural forms; 1) as anhedral blebs that typically display exsolution lamellae and

PLATE 12: Photomicrograph of lamination-parallel concentration of euhedral apatite crystals within the layered gabbros. a = apatite. Plane light. Width of field = 0.46 cm

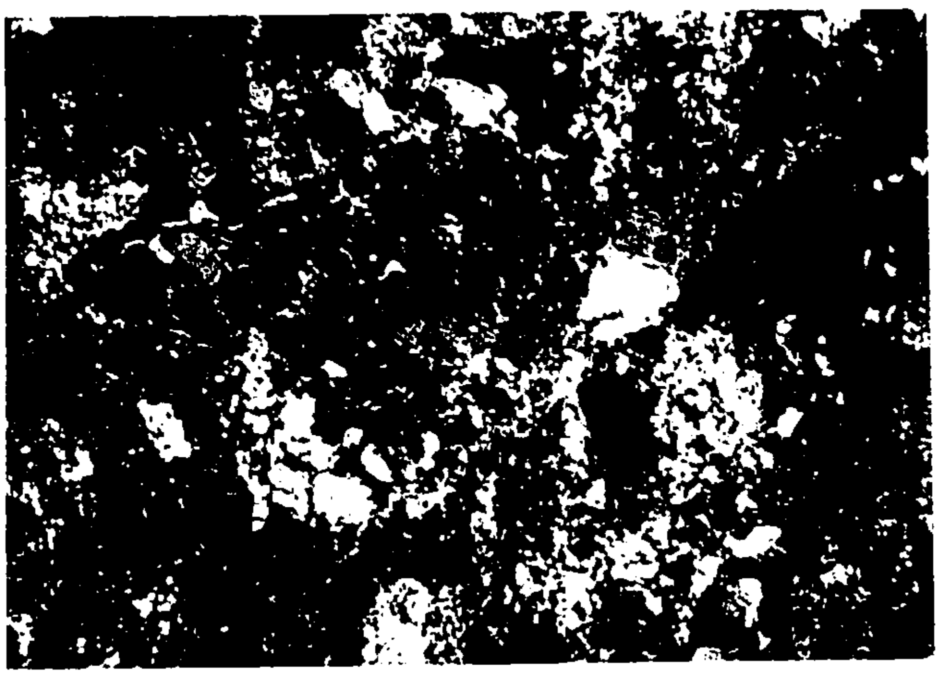

2) as oriented trellis networks. The trellis networks are the less common of the two types and consist of ilmenite and rutile lamellae 0.5 to 1.5 mm long. The lamellae form a regular array with intersection angles ranging from approximately 30° to 85° with respect to one another. They are typically set within a fine grained groundmass of chlorite and quartz and usually are associated with a larger grain of ilmenite. Trellis networks are interpreted to develop through oxy-exsolution of primary titanomagnetite (Haggerty, 1976; MacFie, 1989). Magnetite, rutile and hematite are present in significantly lesser quantities. Very small, discreet blebs of pyrite and chalcopyrite, generally less than 0.5 mm in diameter are ubiquitous throughout the layered gabbros. Sulphide blebs such as these form less than 10 vol.% of all opaque minerals within this sub-unit.

3.3 Quartz diorite

Relative to the gabbro cumulates, the quartz diorites contain a greater number of mineral phases and are thus mineralogically more evolved. Their primary mineral assemblage comprised plagioclase, amphibole (± pyroxene ?), quartz, apatite, titanite, zircon, ilmenite and magnetite. Plagioclase is the dominant phase (55 to 65 vol.%) and occurs as euhedral to subhedral sausseritized crystals 1-6 mm in size, that display prominent albite twinning. Carlsbad twinning is also relatively common within this unit, whereas pericline twinning is quite rare. The sausseritized plagioclase are dominantly albitic, but exhibit a wide range of An content from An_5 up to oligoclase, An_{16} (see microprobe analyses, Appendix B). Relict unaltered plagioclase occurs as small (< 1 mm) non-turbid, well twinned patches within larger sausseritized grains. Analysis of one of these relict plagioclases yielded an oligoclase composition (An_{26}). This may reflect the initial composition of the majority of the plagioclase feldspars prior to alteration. Sausseritization of plagioclase is widespread and is characterized by grains that are invariably altered to a fine-grained aggregate of epidote, sericite and chlorite. A thin,

A) PLATE 13: Photomicrograph of interstitial quartz within an interlocking matrix of euhedral plagioclase crystals. Note undulouse extinction of quartz. High-birefringent mineral in lower-right is actinolite. p = plagioclase; q = quartz. Crossed-polars. Width of field = 0.46 cm.

B) PLATE 14: Photomicrograph of actinolitic-hornblende in quartz diorite displaying patchy reen pleochroism with apatite and magnetite inclusions. a = actinolitic-hornblende. Plane light. Width of field = 0.46 cm

A

B

irregular, clear albite overgrowth mantles some plagioclase. The most characteristic microtexture of this unit is the interstitial nature of the quartz that fills the angular gaps between interlocking plagioclase laths (PLATE 13). The quartz forms 8 - 16 vol.% of the unit, displays undulose extinction and is only rarely recrystallized into smaller grains.

Unlike the gabbros, amphiboles within the quartz diorites are, for the most part, poorly preserved. Large (1-5 mm) well formed amphiboles with prominent cleavages comprise only $\approx 15\%$ of the ferromagnesian phases. These are characterized by an uneven green to yellow-brown pleochroism dotted by patches that are pleochroic pale green to pale brown. Inclusions of apatite, epidote and opaque phases are common (PLATE 14). The rims of these better preserved grains are usually pseudomorphed by fibrous pale green-blue actinolite producing 'feathery' textured edges. In the majority of thin sections examined the primary ferromagnesian minerals are completely altered to irregular aggregates of chlorite with minor quartz, calcite, epidote and opaque minerals. The pale green chlorite and numerous opaque minerals lends these aggregates a distinctive appearance. The chlorite sometimes exhibits anomalous violet to brown birefringence. Biotite is ubiquitous within these aggregates. It generally occurs as tan-brown euhedral to anhedral flakes 0.2 to 0.8 mm long that overprint the chlorite and/or the amphibole.

Results of microprobe analyses on the best formed amphibole crystals in several samples show compositional variation at unit, sample and grain scales (figure 8). These range from actinolitic hornblende to magnesio-hornblende. A persistent feature is the overall low A site occupancy. This probably reflects the low alkali content of the host rock.

Accessory phases include apatite, titanite, zircon and opaques. Apatite is the dominant accessory phase and occurs as stubby blade-like crystals usually less than 0.5 mm in length. It comprises less than 1 vol.% of the unit. Ilmenite occurs as anhedral blebs up to 6 mm large that frequently contain fine 'blebs' of rutile or magnetite. Electron microprobe analyses of 4 ilmenite grains yields an average composition of $Fe_{0.99}Ti_{0.95}Mn_{0.6}O_3$. Magnetite also occurs as discreet anhedral grains 0.5 to 2 mm large. Both trellis networks and sulphides are rarely observed within the quartz diorites. Secondary titanite occurs as rims and blebs associated with ilmenite.

3.4 Tonalite (micrographic)

The original tonalite mineral assemblage comprised plagioclase, amphibole (pyroxene ?), quartz, apatite, titanite, zircon and opaques. Plagioclase forms 55 to 66 vol.% of the unit and occurs as 1-5 mm long, euhedral crystals that are, for the most part, well preserved. The majority display a characteristic relict oscillatory zoning defined by symmetric variations in the concentration of alteration minerals (e.g. epidote, sericite, quartz; PLATE 15). Normal zoning is predominant, although reverse zoning has been noted. Pericline twinning occurs in minute patches generally near the periphery of the larger plagioclase grains. Albite twinning, although present, is not as widespread as it is in the plagioclase of the quartz diorite. Thin, irregular albite overgrowths mantle most of the grains. The plagioclase An content varies widely; a) twinned relict (fresh) plagioclase yields An_{38-39}, b) zoned plagioclase ranges from An_{14-26} in the core to An_{3-8} along the rims, and c) albite overgrowths are generally less than An_5 (see Microprobe data, Appendix B).

Quartz constitutes 16-20 vol.% of the unit, occurs as 1-4 mm large anhedral grains and is no longer a purely interstitial phase. Mutually embaying grain boundaries with plagioclase indicate that both crystallized simultaneously. It displays undulose extinction and is rarely recrystallized into polygonal

A) PLATE 15: Photomicrograph of zoned plagioclase in tonalite. Note the anhedral nature of the quartz. p = plagioclase, q = quartz; h = amphibole; t = titanite. Crossed polars; width of field = 0.46 cm.

B) PLATE 16: Photograph of micrographic and/or vermicular intergrowths within the mesostasis between plagioclase and quartz grains in the tonalite. Crossed polars; width of field = 0.23 cm.

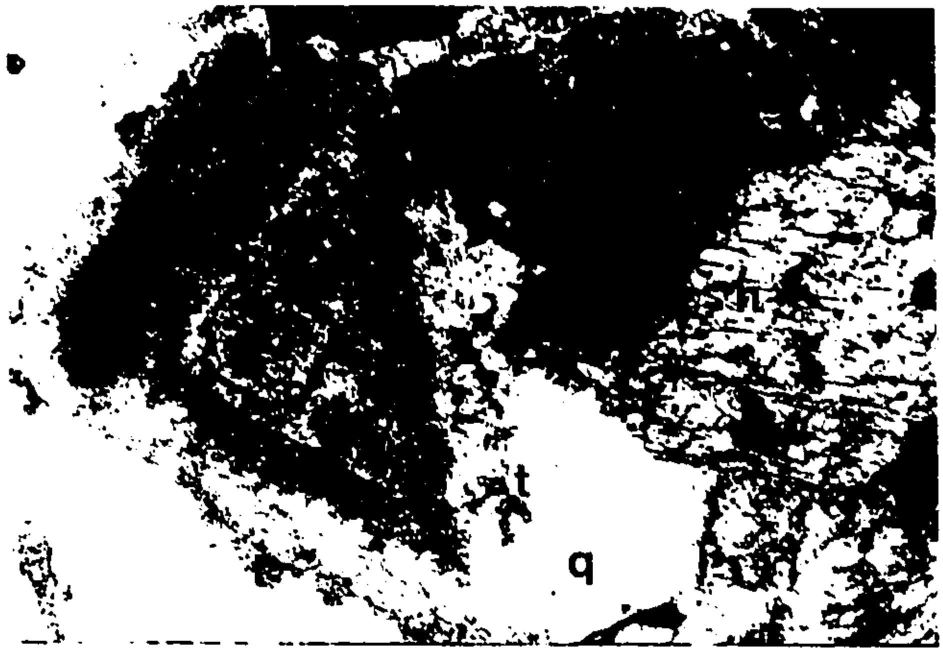

A

B

grains. Another characteristic microtexture of this unit are micrographic and vermicular intergrowths in the mesostasis between euhedral plagioclase grains (PLATE 16). Quartz grains in micrographic growths have triangular terminations whereas vermicular intergrowths display more worm-like forms. The quartz blebs typically exhibit optically continuity with one another. Microprobe analyses of adjacent pods from several locations indicate that the intergrowths in the tonalites consist of quartz and albite (An_{08}). Coleman and Donato (1979) noted similar plagioclase-quartz intergrowths in oceanic plagiogranites. They ascribe an igneous origin to the intergrowths and attribute the lack of potassium feldspar due to insufficient K_2O in the melt (Coleman and Donato, 1979). Although these textures are not widespread, they are found throughout the tonalite and indicate that local water saturation was achieved within this unit.

Ferromagnesian minerals account for 8-18 vol.% of the tonalite. Amphibole, which may represent the original ferromagnesian phase, is generally poorly preserved. Where present, it is mostly actinolitic and displays fibrous to elongate crystals that exhibit pale green patchy pleochroism. The high birefringent needles are up to 5 mm in long dimension and are commonly cut by sinuous calcite veinlets. Inclusions of magnetite and apatite, relicts from the original amphibole are frequently observed. Microprobe analyses reveal that they range in composition from actinolitic-hornblende to actinolite. As in many of the amphiboles within the intrusion, A site occupancy is low. By far the majority of the amphiboles are completely replaced by fine grained aggregates of chlorite + quartz + opaques. The chlorite is in turn overprinted by stubby biotite flakes.

Micas exhibit morphological and compositional variations from north to south across this unit. Biotite is found in tonalites that outcrop in the north. It occurs as stubby anhedral to subhedral flakes (5 mm long) that exhibit a dark-brown to tan-yellow pleochroism and a mottled extinction. Pleochroic haloes around mineral inclusions are not observed. Biotite Mg/(Mg+Fe) ratios range from 0.44 to 0.46 and TiO_2 contents from 1.68 to 1.88 wt.%. Phlogopite is the dominant mica in tonalites that outcrop proximal to the leucotonalite contact. It typically pseudomorphs amphiboles and exhibits an even light-brown to yellow-tan pleochroism with a less pronounced mottled extinction relative to the biotite. Small (<0.1 mm) isotropic mineral inclusions (allanite?, monazite?, zircon?) that exhibit pleochroic haloes are common. Phlogopite Mg/(Mg+Fe) ratios range from 0.71 to 0.73 with TiO_2 contents of ≈ 0.9 wt.% (appendix B.5).

Titanite, apatite and zircon are ubiquitous in all sections examined and, with the exception of apatite, are at their highest abundance within this unit (apatite is anomalously concentrated within the layered gabbros possibly as a result of crystal settling). Titanite occurs as stubby anhedral grains 0.2-0.8 mm long that are in high relief and weakly pleochroic tan to clear-tan. Comprising up to 3 vol.% of the unit, titanite generally occurs in association with quartz, frequently lodged between two quartz grains (PLATE 15). The mode of occurrence of titanite suggests that it was a late crystallizing phase. As in the quartz diorites, titanite is also found as blebs surrounding ilmenite. Similarly, apatite occurs as stubby euhedral inclusion rich grains that are 0.1-0.4 mm long. Principally associated with clots of mafic minerals, apatite content ranges from 0.5-2 vol.%. Zircon forms clear to light brown grains, 0.5-1.0 mm long that are evenly disseminated throughout the intrusion. Their stubby euhedral to subhedral form reflects their magmatic origin. They do not display any preferred mode of occurrence and comprise less than 1 vol.% of the rock.

Opaques are composed primarily of ilmenite with minor rutile, magnetite and hematite. Trellis networks of ilmenite and rutile were not observed within this unit. Ilmenite occurs as small (less than 3 mm) anhedral grains that commonly display exsolution blebs and lamellae of magnetite ± rutile.

Of note is the presence of very small (less than 1 mm) sulphide blebs. The blebs consist of an anhedral pyrite core (± chalcopyrite) that is rimmed by thin layer of sphalerite. The sphalerite rim displays extremely fine banding that mimics the shape of the pyrite core.

3.5 Leucotonalite

3.5.1 Phyllonitic leucotonalite

Microstructures and textures indicative of grain-size reduction and recrystallization are abundant within the quartzo-feldspathic assemblage of the phyllonites. Notably, porphyroclasts of quartz and feldspar display pressure solution overgrowths, serrated edges and grain-to-grain suturing (Ramsay and Huber, 1987). They comprise 20-50 vol.% of the rock and are hosted by a fine-grained dynamically recrystallized matrix. Feldspar porphyroclasts range in composition from albite (An_7) to oligoclase (An_{12-16}) and sometimes exhibit relict albite twinning. The undulose extinction exhibited by all porphyroclasts is indicative of their high degree of internal strain. Pull-apart fractures, mircofractures and dislocation fractures within feldspar porhyroclasts are lined with polygonal quartz grains (PLATE 17). In addition, these porphyroclasts are frequently surrounded by coronas of recrystallized quartz. O-structures, defined by the form of the dynamically recrystallized pressure shadow tail around porphyroclasts (Passchier and Simpson, 1986), are commonly observed. The lack of a consistent shear sense defined by these structures probably reflects the variability of the primary attitudes of the feldspar crystals with respect to the developing fabric.

The phyllonite matrix mineral assemblage consists of quartz, feldspar, sericite, carbonate, variable crudely segregated into bands that define a compositional layering (PLATE 18). In addition, they

A) PLATE 17: Photomicrograph of dislocation fractures, polygonal quartz and quartz coronas developed around plagioclase porphyroclasts in the phyllonitic leucotonalite. Trend of foliation crosses plate from upper left to lower right. p = plagioclase. Crossed polars; width of field = 0.46 cm.

B) PLATE 18: Photomicrograph of compositional layering comprised of quartz-rich (q), carbonate-rich (c) and chlorite-rich (cl) bands within highly strained portion of the phyllonitic leucotonalite. Note folded quartz in center of plate. Crossed polars; width of field = 0.46 cm.

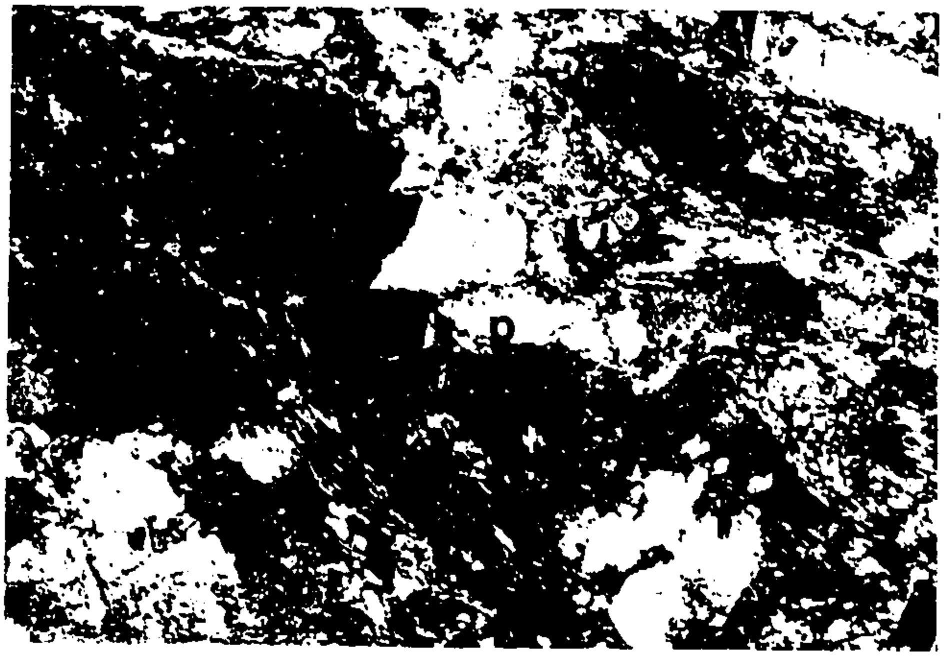

A

B

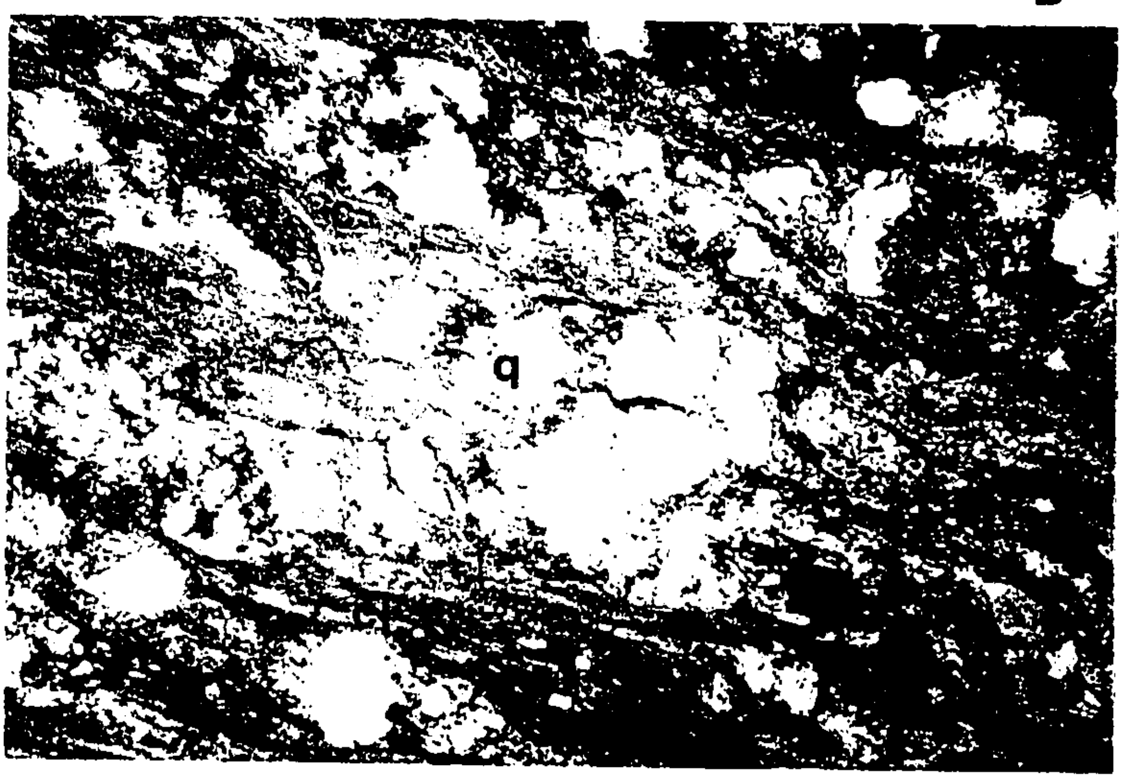

show a strong preferred orientation parallel to the foliation direction. In all cases, mosaic quartz displays clear polygonization. Spaced surfaces marked by thin opaque films resembling pressure solution features (stylolites), run parallel to and enhance the foliation. Pyrite forms 3 to 5 vol.% of the rock and has two distinct morphologies; *i*) as large euhedral crystals (1-3 mm) with prominent pressure shadows infilled exclusively with chlorite and *ii*) as small (less than 1 mm) anhedral grains and grain aggregates aligned parallel to and enhancing the dominant foliation. The large euhedral grains are sometimes embayed and rarely microfractured. Rutile is a very minor phase and occurs as very small (less than 0.2 mm) laths randomly disseminated throughout the leucotonalite groundmass.

3.5.2 "Porphyritic" leucotonalite

The matrix in which the megacrysts and relict plagioclase phenocrysts are hosted comprises a fine grained assemblage of quartz, sericite, feldspar, carbonate with minor epidote, pyrite, magnetite, biotite, chlorite and zircon. This mineral assemblage forms an interlocking tectonogranular mosaic. With the exception of the phyllosilicates, the matrix grains are commonly serrated and display undulose extinction. Both quartz and feldspar porphyroclasts show extensive pressure solution overgrowths and grain-to-grain suturing. White mica (sericite) flakes with their long axes oriented perpendicular to the margin of quartz grains produce a distinctive corona texture (PLATE 19). Mineral segregation, compositional layering and pressure solution residues were not observed. Preferred orientation or parallel alignment of mica flakes although present, are not a dominant feature of this facies.

Due to the lack of a strong penetrative fabric, a primary granophyric microtexture is locally preserved within the porphyritic facies. Subhedral to euhedral altered plagioclase feldspar phenocrysts 1-4 mm

A) PLATE 19: Photomicrograph of corona texture around quartz porphyroclast, porphyritic leucotonalite. s = sericite. Crossed polars; width of field = 0.16 cm.

B) PLATE 20: Photomicrograph of relict granophyric texture within porphyritic leucotonalite. Crossed polars; width of field = 0.23 cm.

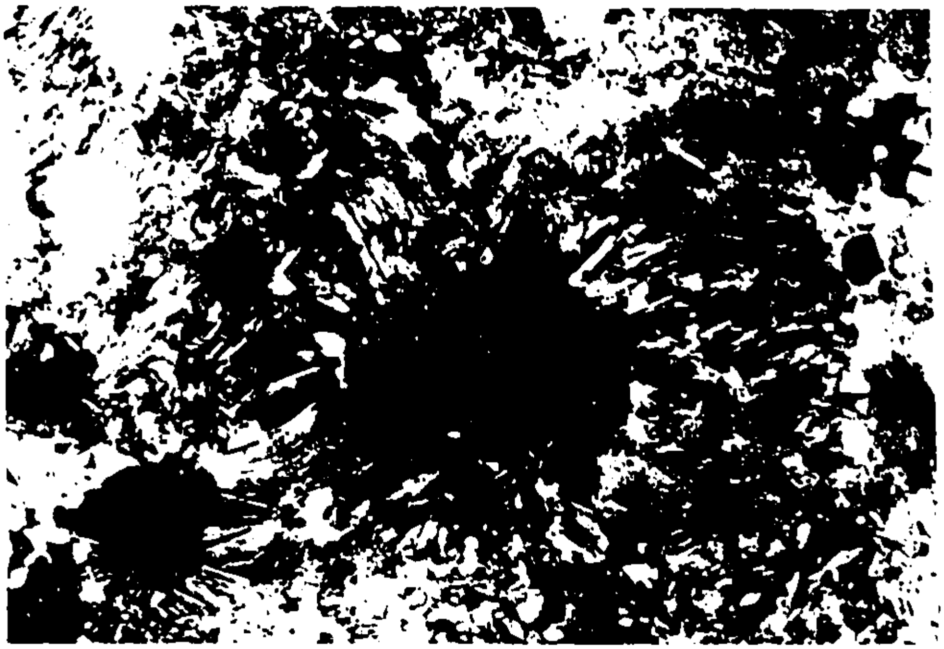

A

B

long are surrounded by a granophyric intergrowth of quartz and feldspar (PLATE 20). A similar granophyric texture is locally present in sections of the phyllonitic leucotonalite examined by Savoie (1989). In addition, Savoie (1989) also noted the presence of interstitial and anhedral quartz grains within a relict primary igneous fabric.

3.6 Quartz-phyric aplitic dykes

The aplitic dykes are composed of quartz, plagioclase, epidote and sericite with accessory chlorite, titanite and zircon. Quartz grains are subangular, 0.2-1.0 mm large and exhibit sutured grain-to-grain contacts and minor polygonal contacts. A fine grained assemblage of epidote + sericite is often observed to rim the grains. Recrystallization of quartz into small equant polygonal grains is not observed. The plagioclase are euhedral, generally twinned randomly oriented and 0.5-4.0 mm large. They are sausseritized to varying degrees displaying a fine-grained felty mat of albite + epidote + sericite. There is no strong fabric development within the rock.

3.7 Host rocks

3.7.1 North sector basalts

In thin section the least deformed pillowed facies display excellently preserved intergranular fabric formed by interlocking plagioclase microlites and fibrous uralite (PLATE 21). Small circular features that resemble vesicles less than 2 mm large dot the slide. They are infilled with subhedral

A) PLATE 21: Photomicrograph of well preserved microlites and mat texture within northern sector basalts. pl = plagioclase; ur = uralite. Crossed polars; width of field = 0.46 cm

B) PLATE 22: Photomicrograph of highly altered and recrystallized southern sector basalt proximal to contact with the leucotonalite. Note the quartz as anhedral grey patches. Crossed polars; width of field = 0.46 cm

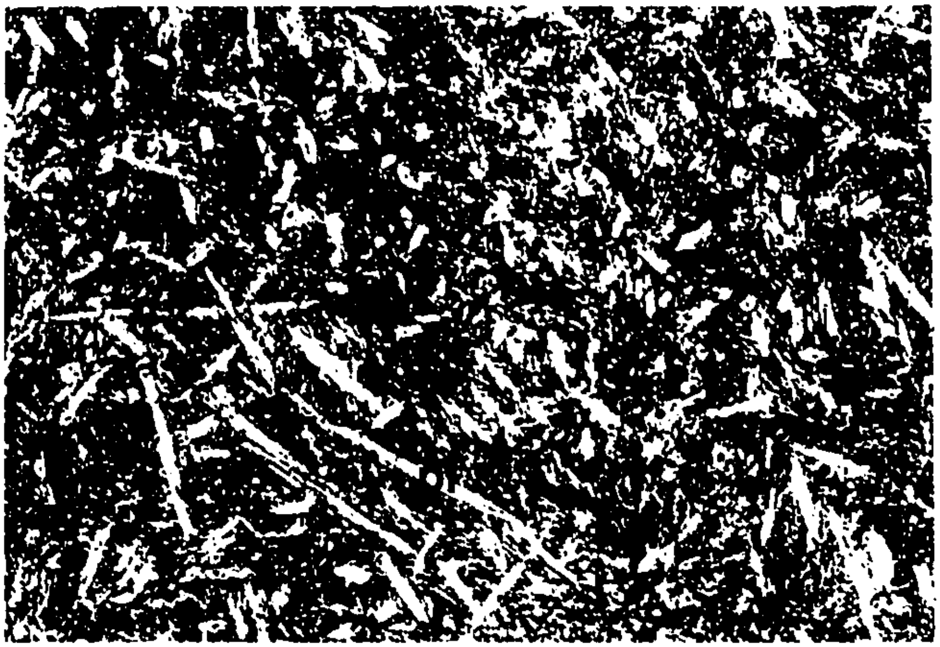

A

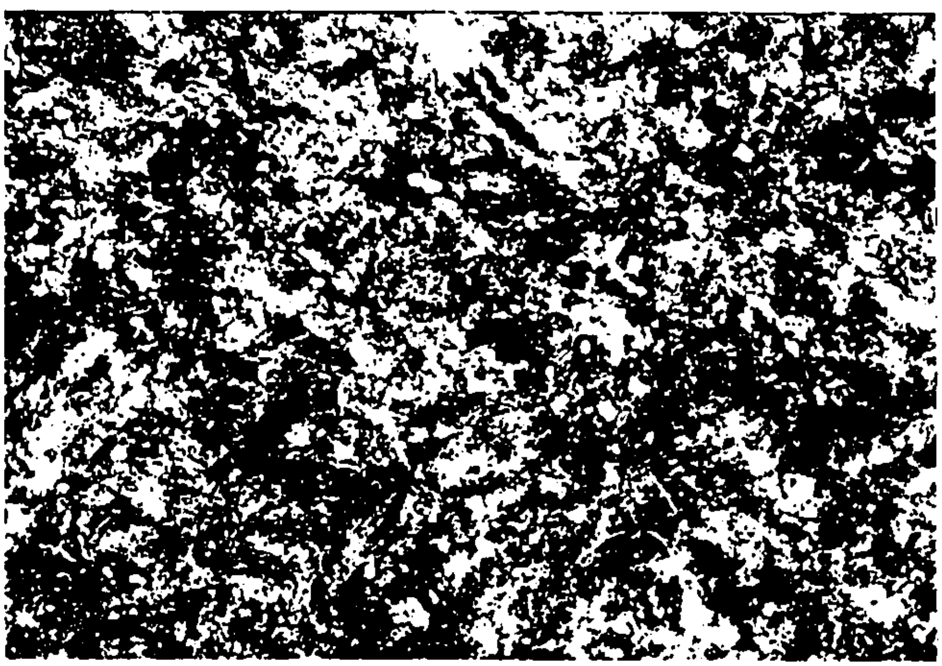

B

amphibole, feldspar, quartz, carbonate, epidote and magnetite. The magnetite is always found in the core of the vesicle as large anhedral blebs that tend to be bounded by the amphibole. Epidote and chlorite are the most easily distinguishable alteration minerals.

3.7.2 West sector basalts

West sector basalts are composed of a felty mat of interwoven plagioclase microlites now largely altered to a fine grained assemblage of chlorite, epidote and albite. Fibrous pale green, weakly pleochroic actinolite replaces ferromagnesian phenocrysts. Basalts that are altered exhibit a an increase in groundmass epidote, additive quartz and a destruction of the skeletal plagioclase microlites. Fractures within the altered basalts are lined by quartz.

3.7.3 South sector basalts

Microscopic textures within the basalts are indicative of extensive hydrothermal alteration and recrystallization. Relict plagioclase microlites are up to 0.5 mm long and are frequently twinned. Many display serrated edges and grain-to-grain suturing. The majority of the groundmass is composed of a mass of small inequant grains of anhedral plagioclase with extensive quartz, chlorite and epidote (PLATE 22). Carbonate is a common groundmass constituent as well. The intensity of alteration is observed to increase with proximity to the phyllonitic leucotonalite.

3.8 Nature of the amphiboles

The morphologies of the amphiboles within the Mooshla intrusion vary from grains that are well preserved to extensively altered. Well preserved grains exhibit an even pleochroism, excellent cleavages, sharp interfaces with surrounding grains, negligible alteration and generally lack secondary mineral inclusions. Such grains are interpreted as being unaltered, or "fresh" and are found exclusively within the layered gabbros. Extensively altered amphiboles are usually found as relict grains within a fine-grained aggregate composed of chlorite, sericite, quartz, epidote, opaques ± calcite. These aggregates, or ferromagnesian clots, represent the end result of amphibole alteration. Stages of amphibole alteration intermediary between "fresh" grains and ferromagnesian clots are the dominant morphology within the intrusion. Such amphiboles are typically subhedral, 2-5 mm large, exhibit uneven pleochroism, numerous inclusions, irregular grain interfaces and incipient alteration along either cleavage planes or within the core.

Electron microprobe data of amphibole chemistry for the hypidiomorphic units of the Mooshla intrusion are listed in appendix B. A $Fe^{3+}/(Fe^{3+}+Fe^{2+})$ ratio of 0.21 was selected from the literature (MacFie, 1989) and used to calculate Fe^{3+} contents from microprobe analyses. The $Fe^{3+}/(Fe^{3+}+Fe^{2+})$ chosen was determined through wet chemical analysis of amphiboles from a gabbro-anorthosite intrusion (MacFie, 1989). The essential and accessory mineralogy of this intrusion resembles that of the layered gabbros in which the "fresh" amphiboles are found. A comparison based ratio is felt to be more realistic than stoichiometric calculations in evaluating the relative Fe^{2+} and Fe^{3+} abundances since stoichiometric calculations inevitably introduce a large degree of uncertainty (Hawthorne, 1983).

Following the classification of Leake (1978), all amphiboles within the Mooshla intrusion are calcic. They are magnesian ($Mg/[Mg+Fe^{2+}] > 0.50$), have $(Na+K)_A < 0.50$; $Ti < 0.50$ and range in compositions from actinolite to magnesio-hornblende (figure 8). They define a rough trend that shows increases of $Mg^{2+}/(Mg^{2+}+Fe^{2+})$ with increasing Si for all units. $Mg^{2+}/(Mg^{2+}+Fe^{2+})$ and Si vary widely for the altered amphiboles of the mesocumulates, quartz diorites and tonalites. In contrast, the $Mg^{2+}/(Mg^{2+}+Fe^{2+})$ ratios and Si contents of layered gabbro texturally "fresh" amphiboles are fairly restricted and are the lowest values relative to all other lithologies. Individual grains reveal very slight decreases in $Mg^{2+}/(Mg^{2+}+Fe^{2+})$ with increasing Si from the core to the rim for amphiboles of the quartz diorites. The opposite trend is noted for those of the tonalites. On a plot of Ti (atoms per unit formula) versus tetrahedral Al^{3+} (Al^{iv}), the amphiboles of the intrusion do not define a uniform linear trend. Instead, a least two, and possibly three trends may be defined (figure 9); 1) texturally "fresh" amphiboles of the layered gabbros (89-31) have a steep slope and high Al^{iv} 2) moderately altered amphiboles (89-54, 82) display a shallow slope and low overall Al^{iv} and 3) weakly altered amphiboles are intermediate between the two with moderate slope and Al^{iv} concentrations (89-90). Mesocumulate amphiboles are completly lacking in Ti.

Based on textural and chemical evidence, it is clear that the amphiboles of the mesocumulate gabbros, quartz diorites and tonalites are variably altered and therefore cannot be considered as primary phases. These may have replaced a primary pyroxene or another amphibole. Constraining the nature of this original ferromagnesian phase is difficult due to the lack of any relict textures and/or grains. Indirect evidence may be provided by the amphiboles of the layered gabbros. These amphiboles appear texturally "fresh" and display coherent mineral chemistry that is atypical of those found in other lithologies. Their overall higher Ti and Al contents are similar to those found in igneous amphiboles (Helz, 1973) and may indicate a primary nature for these amphiboles. Based on the

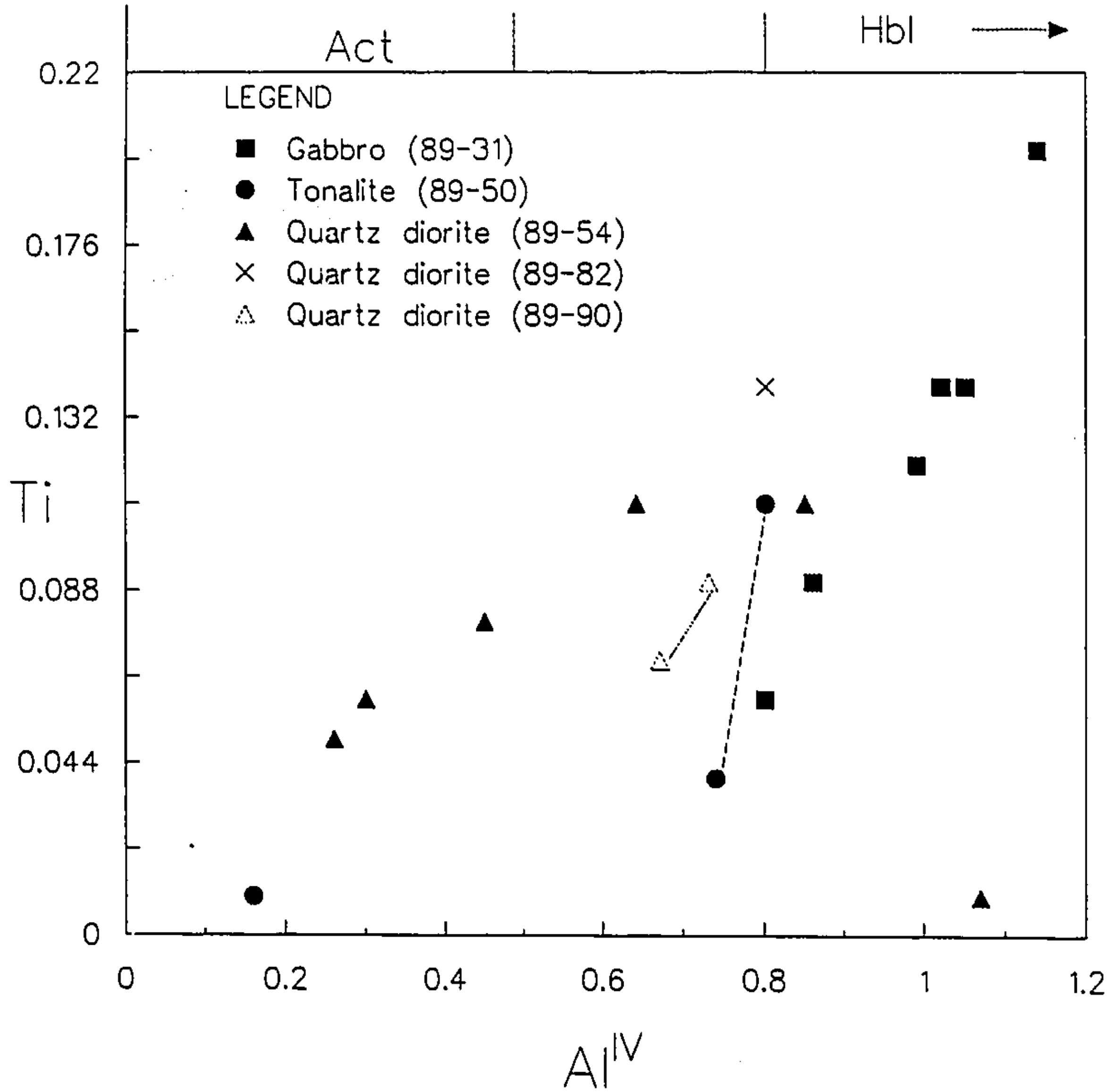

Figure 9: Ti (atoms per formula unit) versus tetrahedral Al^{+3} for amphiboles of the Mooshla intrusion. Lines join analyses on the same grain. Act=actinolite; Hbl=hornblende

above evidence, the "fresh" amphiboles of the layered gabbros are interpreted as being, for the most part, primary. It is therefore probable that some of the altered amphiboles of the remaining units are secondary after primary amphibole, whereas others may be secondary after pyroxene. Mesocumulate amphiboles are distinguished from all others within the intrusion by their low values of Ti, Al^{iv} and high $Mg^{2+}/(Mg^{2+}+Fe^{2+})$ ratios. This distinct composition is likely inherited from the precursor mineral and may reflect the presence of pyroxene. Note that although none was observed during this study, both Gaudreau (1986) and Stone (1988) report the presence pyroxenes within the gabbros.

3.9 Summary

The lithologies of the Mooshla intrusion are characterized by the following petrographic textures and, with the exception of the leucotonalites, primary modal mineralogy:

Mesocumulate gabbros: (80 vol.% plagioclase, 14 vol.% amphiboles (± pyroxene), 6 vol.% quartz). Large plagioclase phenocrysts displaying some overgrowths. Interstices filled with optically continuous actinolite-actinolitic hornblende. Lack of oxides or accessory phases.

Layered gabbros: (proportions of minerals vary widely, in general 55 vol.% plagioclase, 35 vol.% magnesio-hornblende, 5 vol.% quartz, 2 vol.% apatite, 3 vol.% opaques [ilmenite, magnetite, Fe-sulphide]). Elongate plagioclase laths poikilitically encloses "fresh" hornblende. Euhedral apatite form some layer-parallel bands. Quartz fills interstices. Oxides exhibit trellis textures.

Quartz diorites: (63 vol.% plagioclase, 12 vol.% quartz, 22 vol.% amphiboles , apatite 1 vol.%, opaques 2 vol.% [ilmenite, magnetite]). Plagioclase laths exhibiting albite and Carlsbad twinning form an interlocking framework. Interstices filled by quartz. Amphiboles vary from actinolite to magnesio-hornblende. Apatite, zircon and titanite are rare.

Tonalites: (62 vol.% plagioclase, 18 vol.% quartz, 13 vol.% amphiboles, 2 vol.% titanite, 2 vol.% apatite, 1 vol.% zircon, 2 vol.% opaques [ilmenite, minor magnetite, Fe-sulphide]). Plagioclase exhibit oscillatory zoning, may display albite and Carlsbad twinning. Quartz no longer purely an interstitial phase. Micrographic and vermicular intergrowths of quartz and albite observed in the mesostasis. Titanite and apatite common accessory phases. Titanite frequently observed lodged between quartz grains or rimming ilmenite. No trellis textures.

Phyllonitic leucotonalites: 20 to 50 vol.% porphyroclasts set in a fine grained, dynamically recrystallized matrix composed of quartz, sericite, chlorite, calcite and plagioclase. Compositional layering, grain-to-grain suturing and polygonatization are common within the matrix mineral assemblage. Opaques consists almost exclusively of pyrite.

"Porphyritic" leucotonalite: Megracrysts and phenocrysts set in a fine-grained tectonogranular mosaic of quartz, sericite, feldspar, carbonate with minor epidote, pyrite, magnetite, biotite, chlorite and zircon. Penetrative fabric development is weak to absent. Relict granophyric microtexture locally observed. Unit is characterized by heterogenous mineral assemblage and textures. Pyrite is dominant opaque phase.

The holocrystalline units of the intrusion exhibit a progressive evolution in modal mineralogy and textures from cumulates through to micrographic tonalite. A general increase in the vol.% of accessory phases, notably titanite is similarly noted. The majority of amphiboles in the holocrystalline units appear to be secondary. These possibly replace a primary amphibole, although some evidence suggests that pyroxene may have been present within the mesocumulate gabbros. Amphibole alteration produces ferromagnesian clots comprising chlorite, sericite, quartz, epidote, opaques ± calcite. Biotite is always observed as a late-stage mineral which overprints these clots, or more rarely, pseudomorphs amphibole.

The leucotonalites have undergone extensive hydrothermal alteration characterized by the destruction of all amphibole, and a significant increase in modal quartz, sericite, pyrite and carbonate. The similarity of some of the relict textures within the leucotonalites to those of the tonalites suggests that the two may be related.

CHAPTER 4 STRUCTURAL GEOLOGY

4.1 Introduction

This chapter presents the results of a structural survey of the mesoscopic fabrics and macroscopic structures of the Mooshla intrusion. The aim of this study is to document the structural framework of the Mooshla intrusion and integrate this with results of Marquis and Hubert (1989), Savoie (1989) and Tourigny *et al.* (1989, 1988) for the central portion of the Bousquet Mining Center.

4.2 Primary structures

Primary structures are found both within the Mooshla intrusion and in the host volcanic rocks.

4.2.1. Volcanic textures

The volcanic rocks display two principal primary textures; pillows and flow breccias. The pillow facies are developed within the basalts north of the intrusion. They are typically 0.5 to 1.0 m wide with thin (2 to 5 cm) selvages that are in positive relief. Drain-away cavities (Dimroth *et al.*, 1979) filled with coarse milky quartz and tourmaline are sometimes noted in the cores of the pillows as are large irregular patches of epidote and quartz. Pillow morphology, amygdule concentration and the half-moon shape of drain-away cavities indicate tops towards the south (PLATE 23). Flow breccias comprise brown-black sub-angular fragments 2 to 20 cm large in positive relief that are set in an aphanitic chloritic matrix. No complete section of massive basalt grading into pillowed and brecciated flows was observed.

PLATE 23: Pillows basalts north of Mooshla intrusion. Note well preserved half-moon shaped drain-away cavities filled with quartz. Facing direction toward south (top of picture). Hammer for scale. L6+00E; 1+40N.

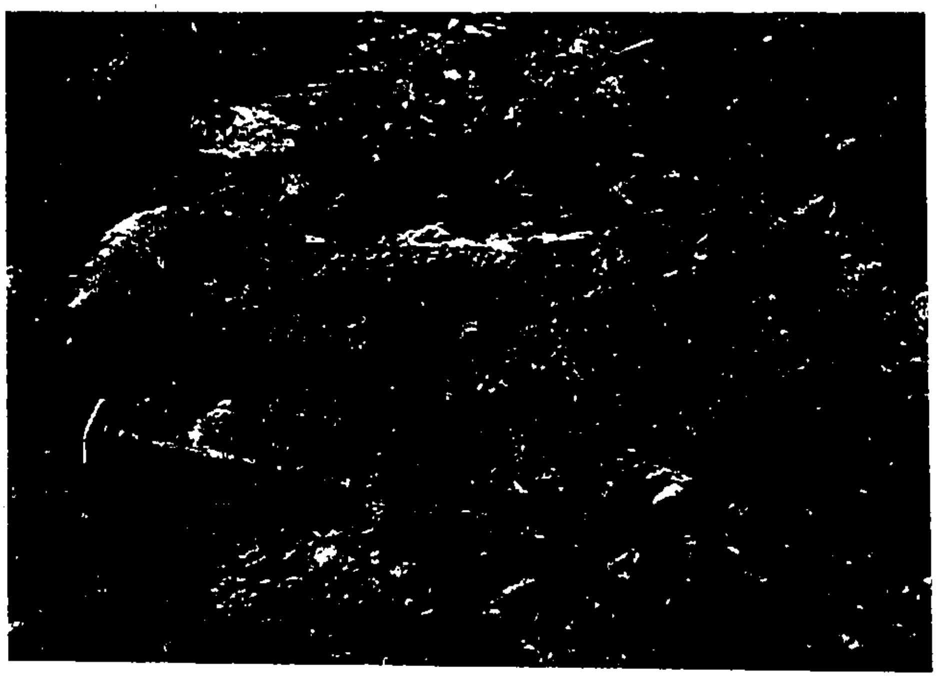

4.2.2. Cumulates

The cumulates provide two independent lines of evidence as to their facing direction. Following the criteria of Cox *et al.*, (1979), the asymmetric distribution of cumulate facies (mesocumulates outcrop in the west; the layered sequence outcrops to the east) is consistent with an overall easterly facing direction to this unit. Similarly, modal variations as well as repetition of cycles in the layered series (see 2.2.2) suggests that their base lies towards the northwest and their stratigraphic top is to the south, southeast. The orientation of the layering within the layered gabbros changes progressively from 238/70° to 270/90° from west to east across the series. The layering thus appears to be overturned. However, note that igneous layering does not necessarily define a paleohorizontal (Cox *et al.*, 1979)

4.2.3 Occurrence of Fragments

Stoping of wall-rock fragments above a magma during emplacement is a feature common to many intrusions. The skewed distribution of xenoliths along the southern intrusion margin (within the fragment zone) may therefore indicate the overall facing direction of the intrusion was to the south. Settling of these xenoliths through the magma may, in part, account for the observed coarsening in grain size and greater degree of "rounding" to the north.

4.3 Deformation and related structures

Structures formed in four deformational events, termed D_1, D_2, D_3 and D_4 occur in the Mooshla intrusion. D_1 and D_2 are two deformation events that were largely ductile in nature. D_1 imparted a localized foliation that is only observed within the intrusive rocks. D_2 represents the principal strain event and is responsible for the majority of fabrics observed in the area. D_3 structures comprise a series of N-S brittle fractures and joints, a spaced cleavage and locally, a crenulation cleavage. It is not clear whether D_3 represents a distinctly later event or simply a third increment of the progressive deformation that may include D_1 and D_2. Finally, D_4 structures are represented by a conjugate set of kink bands and brittle faults.

4.4 Structural domains

The Mooshla intrusion can be subdivided into three structural domains based on the attitude of their planar structural fabric and the nature and frequency of the high strain zones that they host (figure 10). *Domain 1*, along the northern third of the intrusion, contains a steeply dipping planar fabric (S_2) and narrow discrete high strain zones. The high strain zones are discontinuous along strike and have a frequency of between 2 and 5 per decametre. They are notable for both their consistent parallelism and brownish coloration. *Domain 2* occupies the core or middle third of the intrusion. It contains a moderately to shallowly dipping planar fabric (S_1) and remarkably few narrow zones of high strain. Where observed, the high strain zones are discrete and lack the brownish colour typical of those found in Domain 1. A N-S oriented fracture cleavage (S_3) characterizes the southern limit of this Domain. *Domain 3* forms the final southern third of the intrusion and may be classified as a lithotectonic domain. It comprises a single unit, the leucotonalite, that is host to a zone of intense ductile deformation, the Southern Mooshla Shear Zone (SMSZ). This deformation zone contains a steeply dipping planar fabric (S_{2S}). N-S and NW-SE brittle faults are common within this lithotectonic domain.

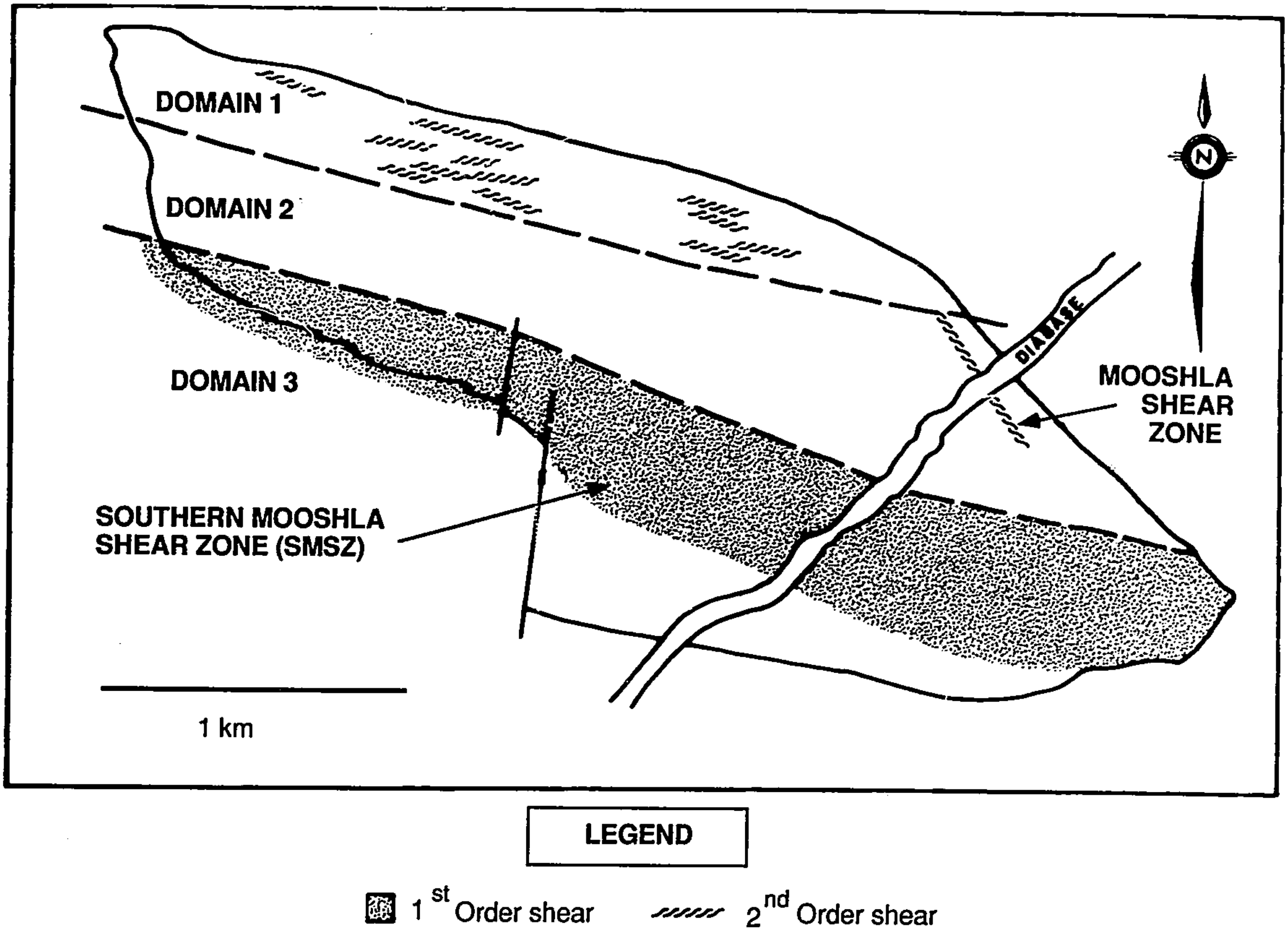

FIGURE 10: STRUCTURAL DOMAINS WITHIN THE MOOSHLA INTRUSION

4.4.1 Foliations

Three foliations, S_1, S_2 and S_3 have been noted in the Mooshla intrusion and immediate vicinity. The two principal foliations, S_1 and S_2 formed during D_1 and D_2 respectively. Shear zones parallel to S_2 cross-cut the S_1 foliation within Domain 1 and form the basis on which the chronological order between these two fabrics has been established. The third foliation, S_3, is only locally developed and reflects the D_3 event.

4.4.1.1 S_1

S_1 is a weakly developed, penetrative foliation that is only observed within Domain 2 and is entirely absent from the host volcanic rocks. It occurs in outcrop as a moderatly developed cleavage that trends between 85 and 115° and dips from 30 to 70° towards the south (figure 11). Xenoliths and groundmass minerals do not display a preferred dimensionality parallel to this foliation. S_1 is not readily observed in thin section.

4.4.1.2 S_2, S_{2S}

The S_2 foliation is found in Domain 1 and the host volcanic rocks. When observed in the volcanic rocks S_2 is a strongly developed penetrative cleavage that strikes ESE-WNW with steep southerly dips. Primary igneous features such as phenocrysts, lapillis, pillows, amygdules etc. show a strong preferred orientation parallel to this foliation. It is therefore the prinicpal plane of flattening and as such, may be correlated with the S_1 defined by Tourigny *et al.*(1988) for the rest of the Bousquet mining centre. In thin sections of the volcanic rocks, S_2 is defined by chlorite and thin films of opaque minerals (pyrite+rutile) as pressure-solution residue (PLATE 24). In Domain 1 S_2 is an anastamosed foliation that trends from 095 to 120° and dips towards the south at 65 to 90° (figure 12). It is a moderately penetrative fabric that is most easily observed proximal to the narrow zones of high strain that characterize this Domain.

Partioning of strain to lithotectonic domain 3 during the D_2 event is reflected by the development of a wide zone of ductile deformation. This zone is characterized by a penetrative foliation designated as S_2 shear, or S_{2S}. S_{2S} is ubiquitous throughout lithotectonic Domain 3 and is defined by a schistosity best developed within bands of phyllonite and mylonite. Although the trend of S_{2S} is the same as S_2, the dips are somewhat steeper, ranging from 70 to 90° (figure 13). Due to the variable nature of the alteration in the leucotonalite, S_{2S} is defined by various mineral assemblages across this lithotectonic Domain. Generally speaking, where the K_2O content exceeds 2.0 wt.%, sericite, partially recrystallized quartz, feldspar, chlorite and lepidoblastic carbonate define the foliation (PLATE 18). When the K_2O content is less than 1.0 wt.% S_{2S} is defined by chlorite, subgrain quartz and feldspar with minor carbonate and sericite. Anhedral pyrite is frequently aligned along S_{2S} within the phyllonitic leucotonalite.

4.4.1.3 S_3, S_{3c}

S_3 is observed primarily in the volcanic rocks and quartz diorite in Domain 2 and locally in a sheared mafic dyke of Domain 1. S_3 is a spaced cleavage that is oriented NNE-SSW and NNW-SSE with steep dips to the west. It is best observed along the southern poriton of Domain 2 and in the volcanic rocks immediatly west of the intrusion where it resembles very closely spaced, planar, parallel jointing. In both these areas the cleavage planes exceed roughly 10 per metre and may be described

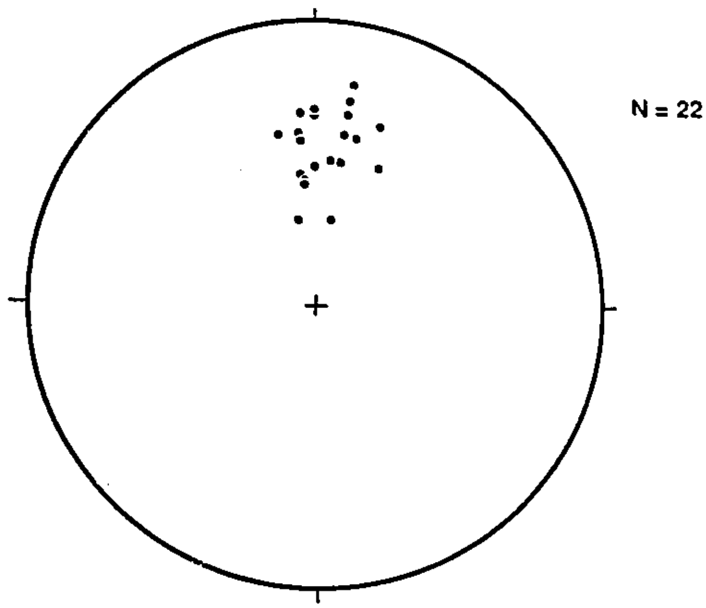

Figure 11: Equal-area stereographic projections of poles to S_1, Domain 2 of the Mooshia Intrusion area.

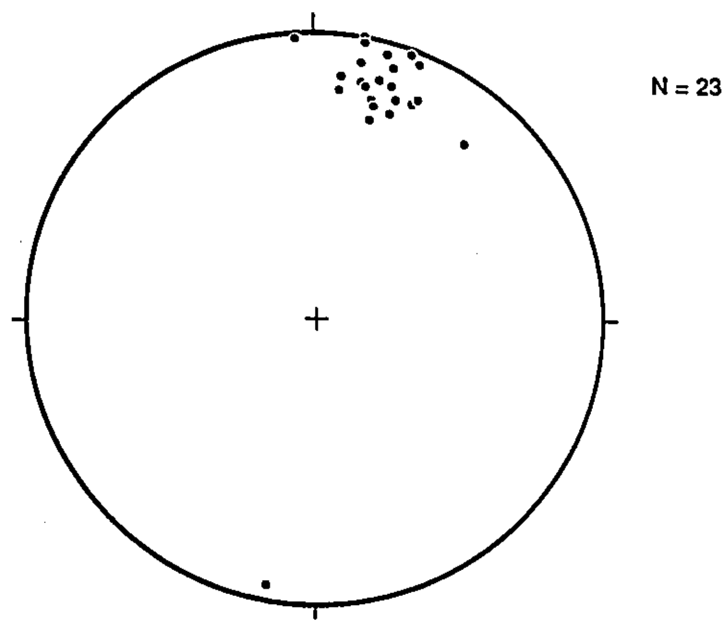

Figure 12: Equal-area stereographic projection of poles to S_2, Domain 1 of the Mooshia Intrusion area.

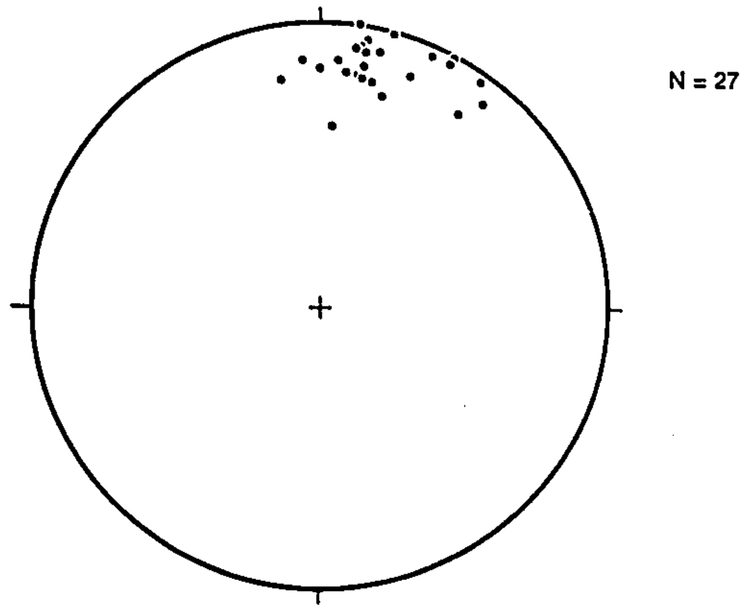

Figure 13: Equal-area stereographic projection of poles to S_{2s}, lithotectonic Domain 3 of the Mooshla intrusion area.

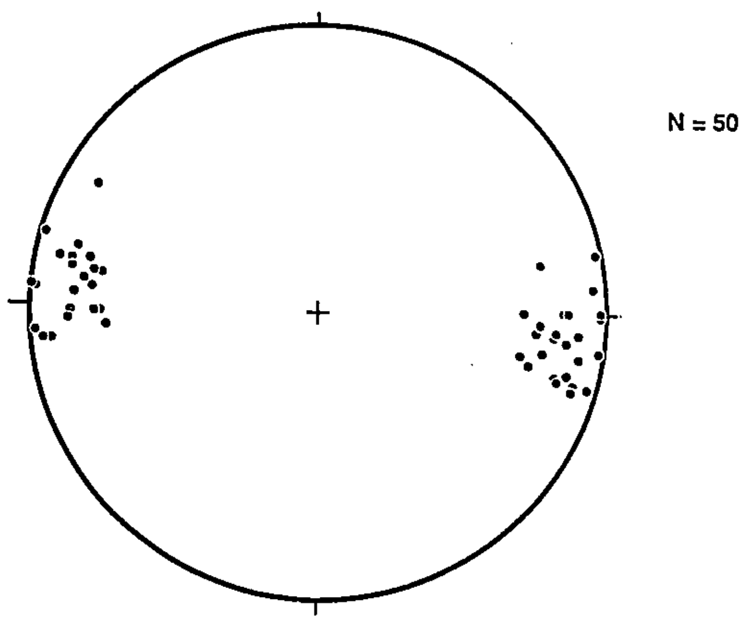

Figure 14: Equal-area stereographic projection of poles to S_3, Domains 1, 2 & 3 of the Mooshla intrusion area.

A) PLATE 24: Photomicrograph of thin ..... of chlorite and opaque mineral film defining S_2 fabric in basalts south of the Mooshla intrusion ($S=S_2$). Note plagioclase microlites throughout plate. Plane light. Field of view = 4.5mm

B) PLATE 25: Plan view outcrop photograph of S_{3c} cleavage crenulating mafic schist of the Mooshla shear zone ($S=S_{3c}$). Hammer for scale. Mooshla "B" showing

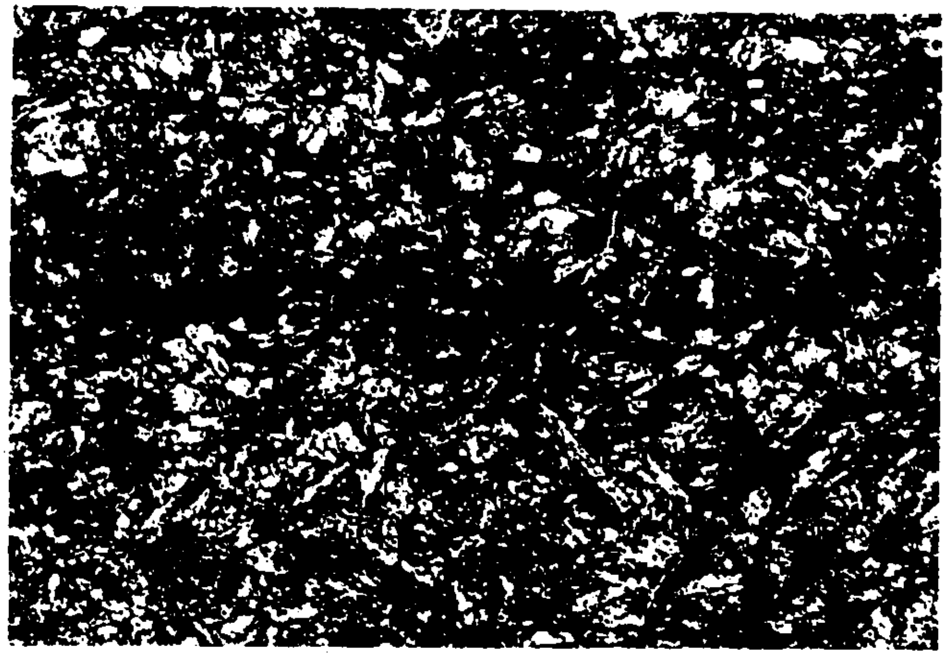

A

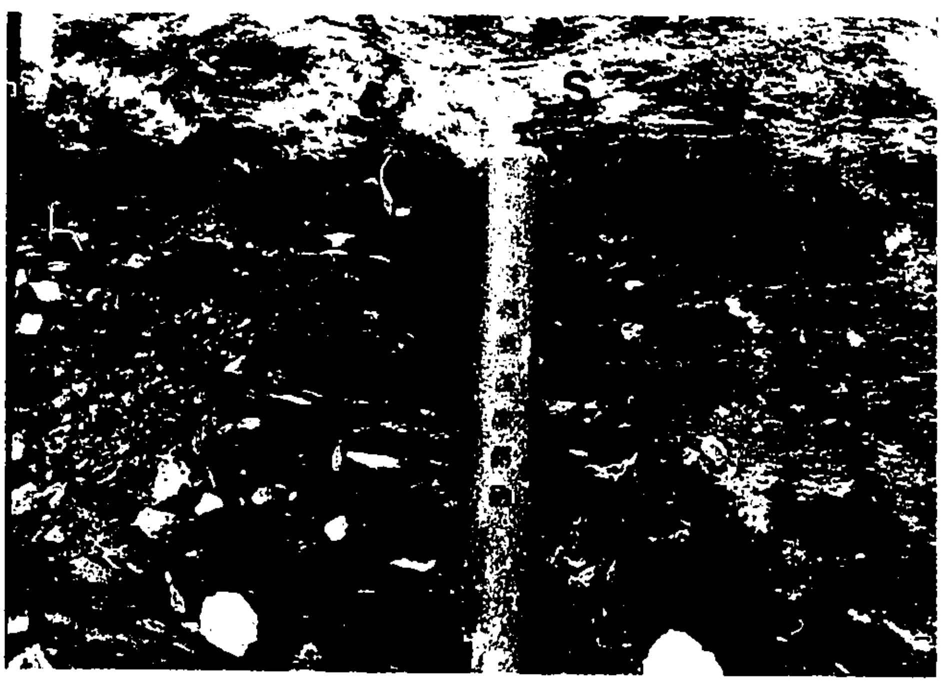

B

as weak to moderate (Davis, 1984; figure 14). As a note of interest, a prominent magnetic susceptibility anomaly coincides with the well developed S_3 fabric.

S_{3c} is a crenulation cleavage and has been observed only within the Mooshla shear zone (4.4.4.3). The Mooshla shear zone is located near the eastern limit of the intrusion in Domain 1 (see map). It was recently uncovered during stripping in the summer of 1990. The shear is developed within a highly strained mafic dyke that displays a strong penetrative schistosity oriented at 325°/80° and is crenulated by S_{3c}. S_{3c} dips subvertically and strikes NNE-SSW (PLATE 25). The nature of the fabrics associated with D_3 suggest that these may have been developed transitional between the brittle and brittle-ductile regime.

4.4.2 Lineations

Three classes of lineations are observed within the area of the Mooshla intrusion. These include; 1) stretching lineations, L^s_2, 2) mineral lineations, L^m_2, and 3) intersection lineations, L^i_2. Mineral lineations are by far the most commonly observed, whereas intersection lineations are quite rare.

4.4.2.1 Stretching lineations, L^s_2

The stretching lineations are preferentially located within or proximal to high strain zones. They plunge steeply to the west within the S_2 fabric (PLATE 26). Cumulate gabbro L^s_2 (Domain 1) lineations are defined by elongate chlorite aggregates that anastomose around plagioclase porphyroclasts and/or megacrysts that display grain-to-grain contact suturing, grain serration and brecciation. The leucotonalite L^s_2 lineations (Lithotectonic Domain 3) are defined by elongate ribbon-like aggregates of phyllosilicates (muscovite ± sericite ± chlorite), partially recrystallized quartz and carbonate. Abundant plagioclase porphyroclasts separate these ribbon aggregates. In the host volcanic rocks, pillows within areas of high strain are attenuated (length to width ratios approaching 7:1) onto S_2 and display symmetric terminations. It was not possible to measure the *X* plane of these pillows as no adequate cross-sections were found.

The stretching lineations define a unimodal distribution whose mean vector orientation is 254/74° (figure 15). This correlates well with the orientation of elongation lineations measured in other parts of the Bousquet Mining Centre by Savoie et al. (1989), Tourigny et al. (1988) and Marquis and Hubert (1989). Therefore, the relative displacement along the S_2 surface in the area of the Mooshla intrusion is dominantly subvertical.

4.4.2.2 Mineral lineations, L^m_2

Mineral lineations are found exclusively along S_2 as film-like black to dark-green blade-like needles of actinolite/chlorite (PLATE 27). These have a general orientation that is subparallel to the L^s_2 lineation, i.e. steep to the west.

4.4.2.2 Intersection Lineations, L^i_2

The intersection lineation L^i_2 is found principally in shear zones of Domain 1 and lithotectonic Domain 3. It has also been observed in the highly strained andesites along the southern contact of the intrusion. L^i_2 is defined by a very fine crenulation cleavage that plunges shallowly to the WSW and WNW between 0 and 5° within the plane of S_2 (PLATE 28; figure 17). The significance of L^i_2 is not

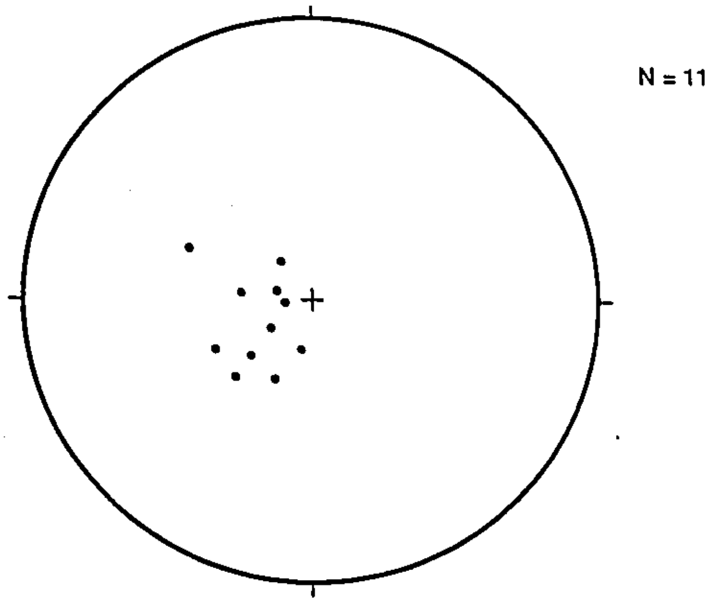

Figure 15: Equal area stereographic projection of stretching lineations, L_2^s, for Domains 1 and 3 of the Mooshla Intrusion.

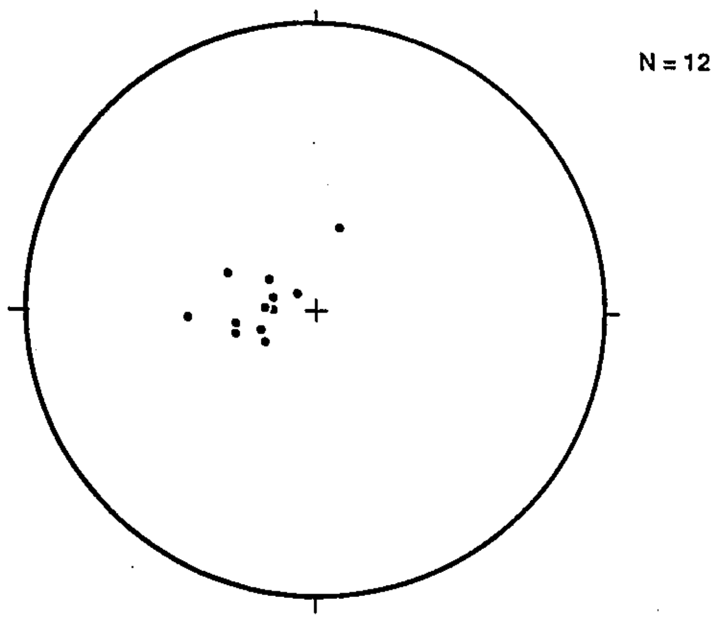

Figure 16: Equal area stereographic projection of mineral lineations L_2^m, for structural Domains 1, 2 and 3 of the Mooshla Intrusion.

A) PLATE 26: Section view ouctrop photograph of steeply west plunging stretching lineations, L^{s}_{2}, on S_{2S} within leucotonalite. Looking north. Quarter for scale.

B) PLATE 27: Section view outcrop photograph of steeply west plunging mineral lineation L^{m}_{2} defined by chlorite and actinolite needles on S_2 parallel plane. Looking south. Dollar coin for scale.

A

B

yet clear and no mesoscopic fabric has as yet been associated with it. However, as noted by Poulsen and Robert (1989), such crenulations are fairly common in schistose rocks and therefore may be of little tectonic importance.

4.4.3 Folds, F_2, F_{3a} & F_{3b}

Folds are rarely observed in the Mooshla area. F_2 folds are asymmetric upright intrafolial folds (rarely tight) of the S_{2S} surface that range in size from mm to cm scales (PLATE 29). They have only been observed in cross-section within the highly strained leucotonalite of lithotectonic domain 3. Measurement of their axes is therefore difficult, however, they appear to have either a very shallow plunge to the west or are essentially horizontal. This may explain their scarcity on the large expanses of horizontal outcrop that characterize the eastern portion of the leucotonalite. F_2 folds display a constant vergence in section that suggests a reverse movement, south side up along the S_2 surface.

Folds developed on the S_2 surface that are not intrafolial in nature are classified as F_3 folds. F_{3a} folds are broad, low amplitude (10 cm) open folds with a wavelength of approximatly 1 m. Their axial surfaces trend 015 to 020° and are steeply dipping. Fold axes plunge vertically to steeply north. They are well developed proximal to the quartz diorite-leucotonalite contact. Recumbant low amplitude folds were observed at one locality within the stripped area surrounding the old Mooshla A prospect. The folds are developed on the S_2 surface and have an axial plane that trends E-W and is inclined to the north. The fold axes plunge 0-15° to the west and no axial planar cleavage was noted.

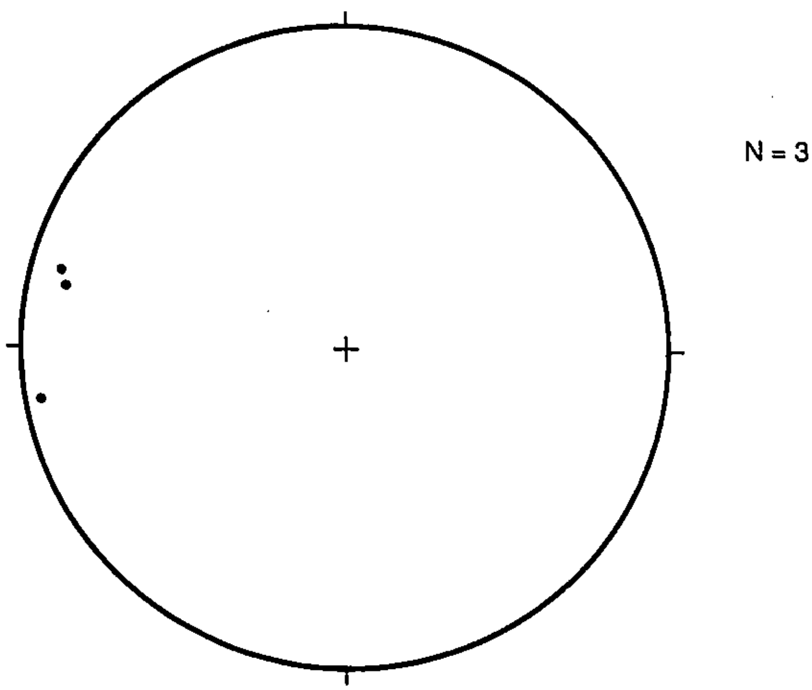

Figure 17: Equal area stereographic projection of intersection lineation, L^{i}_{2} . Domain 3 of the Mooshla intrusion.

A) PLATE 28: Outcrop section view of very fine-scale sub-horizontal intersection lineations, L^i_2 (L^i on plate), in basalts south of the Mooshla intrusion. Loony for scale.

B) PLATE 29: Cross-sectional outcrop photograph of F_2 intrafolial fold developed on S_{2S} surface within highly strained leucotonalite. Looking downplunge. Note asymmetry indicative of reverse movement. Loony for scale. Stripped outcrop along southern access road, Minnova Tie-line 30+00; 7+40mE

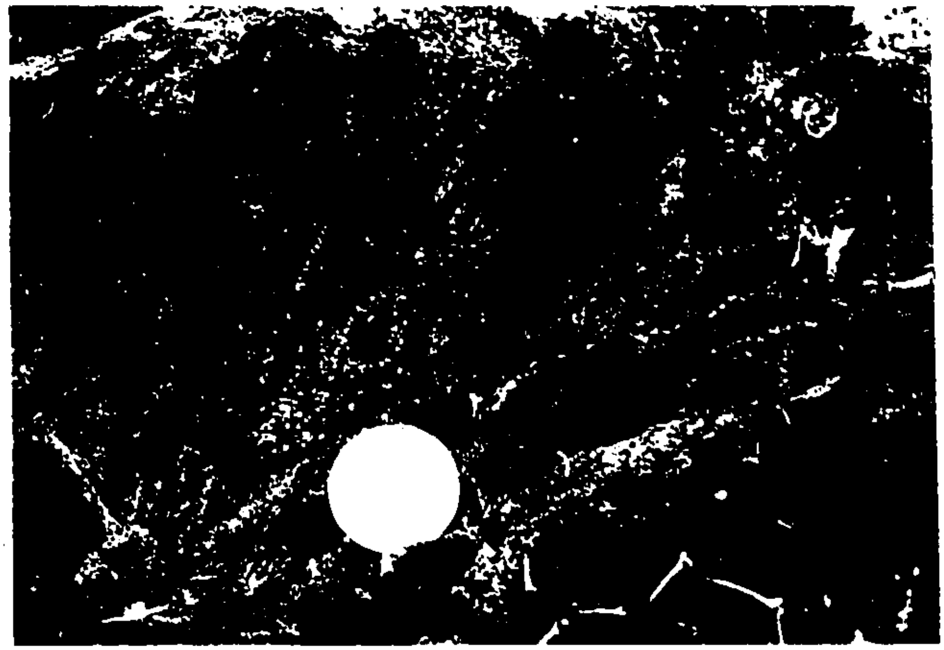

A

B

4.4.4 Shear Zones and Faults

The structural architecture and economic geology of the Mooshla intrusion and immediate vicinity are largely dominated by shear zones and faults. Two main classes of shear zones are distinguished; *i)* brittle-ductile shear zones and *ii)* brittle faults. The brittle-ductile shear zones can be further subdivided into 1st order, 2nd order and transitional shears based on their dimensions and associated alteration. There appear to be two generations of brittle faults; pre to syn-mineralization and post-mineralization.

A 1st order shear is defined as having an average width greater than 50 m, a strike length of at least 500 m and one that contains bands of phyllonites and/or mylonites. Second order shears are less than 2 m wide with strike lengths of (on average) less than 100 m. Shears that are 2-50 m wide and 100 to 500 m long are orders are classed as transitional. Fault sets host to sulphide bearing quartz veins that exhibit wall-rock alteration are classified as pre to syn-mineralization. Those faults that displace all pre-existing structures are post-mineralization. Mineralization refers to the gold deposits of the Doyon, Mooshla and MicMac mines.

4.4.4.1 1st Order Shear - The Southern Mooshla Shear Zone (SMSZ)

The only 1st order shear identified in the Mooshla intrusion is the Southern Mooshla Shear Zone (SMSZ). The SMSZ is bounded to the north by the quartz-diorite and to the south by the host basalts. It occupies the entire surface area of the leucotonalite and their dimensions vary sympathetically; in the west it is 20 m wide whereas to the east it exceeds 400 m in width (figure 10). It strikes ESE-WNW with steep dips to the south and strikes parallel to the Dumagami Structural Zone

(Marquis *et al.*, 1989). To the east, it appears that the SMSZ exits the leucotonalite and manifests itself as the sericite schist of the Doyon main zone (A. Savoie, pers. comm., 1989). Although no outcrop occurs to the west, it is probable that the SMSZ extends into the volcanic rocks.

The SMSZ is a zone of high strain characterized by S_{2S}, a strongly developed, penetrative schistosity (PLATE 30). S_{2S} is generally parallel to subparallel with the boundaries of the SMSZ and contains stretching and mineral lineations with steep westerly plunges. Similarily, the long axes of boudinaged quartz veins exhibit subvertical plunges along S_{2S}. The direction of slip is therefore well constrained as being subvertical. The sense of shear is less well constrained due to the paucity of asymmetric structures. However, rare F_2 folds suggest a reverse movement along the SMSZ. The SMSZ is therefore a reverse-oblique shear zone, consistent with the nature of the major shears within the Dumagami Structural Zone (Marquis and Hubert, 1989). The rocks of the SMSZ are essentially Ls-tectonites within which bands of phyllonite and mylonite form anastomosing patterns that outline large, less strained lithons. Blue quartz grains and primary textures (e.g. porphyritic and granophyric) are sometimes observed within these lithons. Mylonites are best developed proximal to the quartz-diorite contact and display a well developed foliation-parallel millimetric to centimetric compositional layering.

A pervasive alteration characterizes much of the SMSZ. The key aspects of this alteration are a marked increase of selected lithophile elements (K, Rb, Ba, Th, Zr, Si), and carbonate accompanied by a destruction of ferromagnesian minerals (relative to the tonalite protolith). The intensity of alteration is variable; it appears to be greatest in the vicinity of the weakly strained porphyritic leucotonalite to the east. Alteration intensity can therefore not be easily correlated with the intensity of the penetrative fabric. Of note is that the alteration envelope is almost exclusively confined to the SMSZ.

A) PLATE 30: Southern Mooshla Shear Zone, proximal to the quartz diorite contact. Note dextral offset along brittle faults oriented at 345°. Hammer for scale. Minnova Tie-line 30+00; 7+40mE

B) PLATE 31: Plan view outcrop photograph of typical 2nd order shears in Domain 1 displaying regular spacing, parallel alignment and brownish discolouration. Note lack of penetrative fabric in tonalite between shears. Hammer for scale. L10+30E; 6+50S

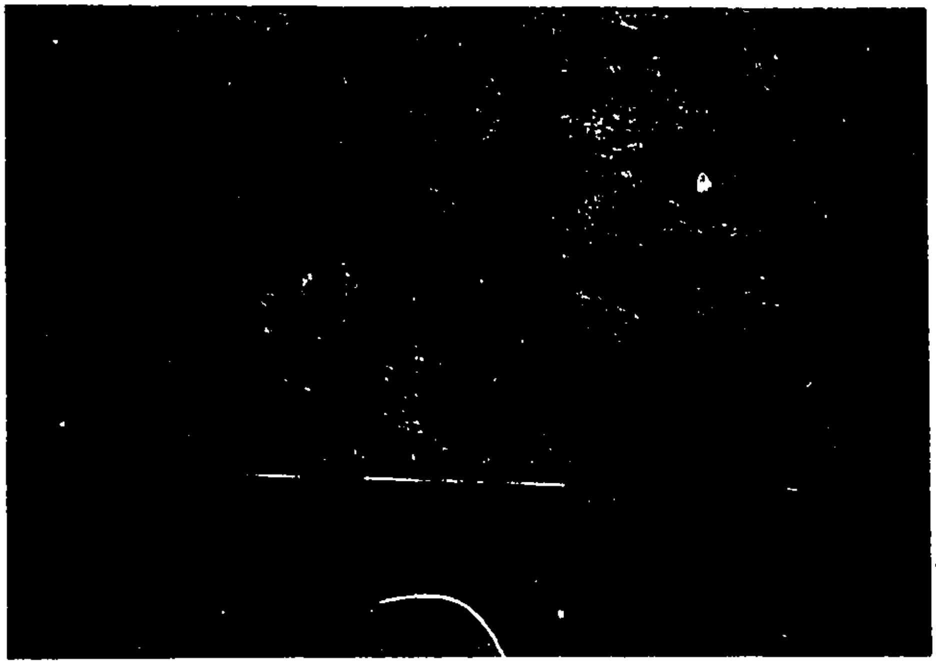

A

B

Collectively these features suggest that the SMSZ was a zone of structurally controlled high permeability.

4.4.4.2 Second order shears

Second order shears are abundant in the area of the Mooshla intrusion. Their greatest apparent concentration is in the immediate vicinity of the northern intrusion contact, south of the MicMac mine. Many of these are auriferous and form a distinct metallotect known as the "Zone de Contact". Second order shears have trends that range from 100-130° with steep dips to the south. They are distinguished by their remarkable parallelism and discontinuous nature (PLATE 31).

Two types of second order shears have been identified on the basis of their internal fabric; 1) plan view oblique shears (PVO) and 2) plan view parallel shears (PVP). When viewed in *plan*, PVO shears have an internal foliation which displays a slight *obliquity* to the shear zone boundaries on the order of 10-40° (PLATE 32). In contrast, the internal foliation of PVP shears is parallel to the shear zone boundary in plan and *oblique* to the shear zone boundary in *section*, subtending an angle from 10 to 20° (PLATE 33). Both types of shears have mineral lineations which plunge steeply to the west on the plane of the internal foliation. Steeply west-plunging stretching lineations were observed only within the PVO shears. A few subhorizontal mineral lineations have been noted within the foliation plane of sulphide-bearing PVO shears. The internal foliation of PVP shears is axial planar to small scale asymmetric quartz vein folds. The fold axes of these quartz veins plunge steeply to the west within the plane of the PVP foliation. Collectively, these internal structures can constrain the direction and sense of shear along these shear zones.

A) PLATE 32: Plan view of a PVO shear displaying oblique foliation with respect to the shear zone boundary. Angle of obliquity varies from 10 to 40°. Flagging tape for scale. L10+60E; 6+00S

B) PLATE 33: Section view of a PVP shear displaying oblique foliation with respect to the shear zone boundary. Note the parallelism of the internal fabric in plan view in the foreground. Quarter for scale. L11+50E; 6+30S.

A

b

For the PVP shears, the slip direction can be reasonably inferred from the mineral lineation, the plunge of the fold axes and the intersection between the oblique foliation and shear zone boundary (B-axis). These direction criteria suggest a dip-slip movement for this type of shear. The sense of shear, as suggested by the obliquity of the internal foliation to the shear zone boundary, is normal. PVP shears dextrally offset the layered gabbros (PLATE 4). The vertical dip of the layering proximal to the shears indicates that the offset is real and not apparent. Dextral offset along these shears is consistent with the asymmetry observed in the quartz vein folds internal to the shear zone (P. Marquis, pers. comm. 1990). These features, assuming that they formed contemporaneously with the shear zones, provide independent criteria which supports a normal dip-slip movement for the PVP shears of the northern Mooshla margin.

Stretching lineations within the foliation plane of PVO shears uniquely determine the slip direction subvertical to the west. This is consistent with the direction and plunge of measured mineral lineations and the slip direction of PVP shears. The plan view angular relationship between the shear zone boundary and the internal foliation repeatedly indicates a dextral shear sense (PLATE 32). However, this presents a paradox; the intersection of the oblique foliation with the shear zone is not perpendicular to the slip direction indicated by the strectching and mineral lineations. Similar contradictory internal fabrics have been noted throughout the southern Abitibi greenstone belt; in the Bousquet mining center (P. Marquis, pers. comm. 1990), the Val d'Or area (Robert, 1989) and the Kirkland Lake-Larder Lake gold camps (Toogood and Hodgson, 1985; 1986). Two tectonic models may account for these observations; (*i*) dextral transpression related to a single progressive deformation event that evolved from a shortening component into a transcurrent shear component or (*ii*) two superimposed deformation events.

In the first case, dextral transpression, it is possible to develop a subvertical maximum stretching elongation during a period of significant shortening across a zone of transcurrent shear (Robert, 1989; Sanderson and Marchini, 1984). Zones of transpression are characterized by the presence of a discontinuity surface parallel to the shear zone boundaries. This surface develops in order to preserve strain compatibility with the surrounding rocks (Sanderson and Marchini, 1984). However, the PVO shears of the Mooshla intrusion rarely display this discontinuity surface along their margins. Furthermore, applicability of dextral transpression at the scale of the small PVO shears is debatable. The second model implies a strike-slip event superimposed on a dip-slip event. The observed subvertical elongation lineation records thrusting or normal faulting during the first deformation event. Subsequent dextral strike-slip movement would produce the oblique foliation and is consistent with the dextral offset noted in the layered gabbros along the PVP shears. However, it may also result in a horizontal mineral lineation and X direction to the finite strain ellipsoid (Huddleston *et al.*, 1988). Subhorizontal mineral lineations are only observed within a few mineralized shears. Note that Marquis and Hubert (1989) record evidence of a D_3 event related to dextral shear.

Typical second order shears exhibit an alteration envelope that is crudely zoned and extends symmetrically 0.1 to 0.5 m into the wallrock. The idealized alteration assemblage is characterized by a steady increase in the percentage of sulphides (pyrite, ± pyrrhotite, ± chalcopyrite), biotite and carbonate towards the shear center (Gaudreau, 1986). A chloritic envelope generally surrounds the shear and biotite is not always present towards the shear center. This mineralogical assemblage is similar to that found underground at Cambior's Mouska deposit (A. Belkabir, pers. comm. 1990). Progressive penetrative fabric development is responsible for destruction of the hypidiomorphic-granular nature of the host rock. In thin section this is observed through progressive increase in recrystallized quartz, plagioclase porphyroclasts, lepidoblastic biotite, chlorite, sericite and carbonate including both Fe and Mg-rich varieties (Gaudreau, 1986). Pyrite is present as two morphologically distinct populations. The first comprises anhedral grains that are generally embayed, sometimes poikiloblastic and typically less than 1 mm in size. The second comprises larger grains (greater than 1 mm) that are euhedral, sometimes with a long axis parallel to the foliation and typically with pressure shadows infilled with large chlorite flakes. The brownish discolouration observed on outcrop is due in large part to weathering of both the disseminated sulphides and minor Fe-carbonate.

4.4.4.3 The Mooshla Shear Zone

The Mooshla Shear Zone (MSZ)is located in the NE sector of the intrusion. It was named subsequent to the discovery of a mineralized quartz vein-hosting shear zone in 1933 by Mooshla Gold Mines Ltd. The MSZ is developed within a dark-green schistose mafic dyke and trends 330-335° with steep dips to the NE (PLATE 35). It is exposed over approximatly 100 m with a uniform width of just under 1 metre. It pinches out abruptly to the NW, terminating in a finger-like transposition of dyke-schist into the wall rock. To the southeast it is cross-cut by a diabase dyke and is lost under the Quaternary cover. The Mooshla shear is a PVO shear with an internal foliation that makes an angle of 5-10° with the shear zone boundaries. The shear sense is poorly constrained due to the lack of stretching or mineral lineations within or on the plane of the internal foliation. However, the obliquity of the foliation with respect to the shear zone boundaries suggests a dextral component of shear. Shear zone boundaries are very sharp and display only localized evidence of a penetrative foliation. When observed, this boundary foliation is parallel to the shear envelope. The very strong anisotropic fabric of the mafic schist is crenulated along a 015-020° trending cleavage (S_{3c}). The fold axes of the crenulations plunge very steeply to the NNE. No stretching lineations were noted. Mineralization consists of 2-4 vol.% disseminated pyrite that is slightly concentrated proximal to the shear boundaries. Quartz-

A) PLATE 34: Outcrop photograph of the Mooshla shear zone looking NW towards Mooshla "B" exploration shaft. The shear dips steeply to the NE and has a remarkably uniform thickness. Backpack for scale.

veining is restricted to the NE end of the shear and is composed of massive to brecciated honey-brown to grey-white quartz. Mesoscopic wall rock alteration is minor to absent and, where observed, is confined to within 15 cm from the shear. It consists predominantly of silicification. No thin sections were studied.

4.4.4.4 Transitional shears

Proximal to the southern limit of Domain 2, shear zones have been observed that share similarities with both 1st and 2nd order shears. These are termed transitional shears. They occur as 3 to 6 metre wide zones of alteration, sulphide mineralization (pyrite) and variable fabric development. Their internal foliation strikes 100°-115° with steep southerly dips. On a mesoscopic level, shears with a moderately developed fabric are bleached white to pale grey in colour with prominent rusty spots due to the weathering of 3 - 5 vol.% disseminated pyrite. In thin section they display large (0.5 to 3.0 mm) laths of plagioclase with extensively sutured grain boundaries, veinlet carbonate and large (0.2 to 0.5mm) euhedral zircons. These shears share mesoscopic affinities to 2nd order shears and differ mostly in the degree of development of microscopic metasomatic textures.

Mesoscopically, those shears with a well developed fabric are leucocratic with 4 - 8 vol.% disseminated pyrite that weathers as large rusty spots with small stain haloes. Microscopically, they have extensive recrystallized quartz, plagioclase porphyroclasts and a foliation defined by anastamosing phyllosilicates. Pressure shadows around large euhedral pyrite grains are infilled with subgrain quartz and/or chlorite flakes. Shears with well developed fabric are closer in both meso and microscopic features to 1st order shears.

4.4.5 Discussion of S_1 foliation

For the purposes of discussion, several models are presented below which may account for the present attitude of S_1. However, it is not within the scope of this study to present an exhaustive analysis of each model. S_1 may reflect 1) rotation, or 2) incipient folding. A satisfactory model must be able to reconcile both the shallow dip of the S_1 surface *and* its restricted development to Domain 2, the core of the intrusion.

The first model assumes that initially S_1 had a steeper dip, perhaps similar to S_2. Thrusting along the SMSZ caused rotation of the intrusion. In response, the dip of S_1 shallowed. Synthetic shears (second order shears) oriented parallel to the SMSZ developed along the northern margin in response to rotation. The second model is somewhat analogous to the first and implies that the foliations S_1 and S_2 are essentially the same. N-S directed horizontal compression produced one foliation, S_2 throughout the Mooshla area. Partioning of dip-slip shear within the SMSZ produced a large-scale asymmetric structure that may approximate a fold. The dip of the S_2 foliation within the asymmetric structure would therefore be shallower. Shearing along the northern margin is simply a response to rheological contrasts. Both models can explain many of the features associated with S_1 and are therefore equally valid. However, the tectonic implications of each model are quite different. The data is, at present, insufficient to conclude which model is more likely correct.

4.4.6 The finite strain ellipsoid

The orientation of the D_2 finite strain ellipsoid can be well constrained. The X-Y plane of the ellipsoid is defined by both S_2 and the orientation of the stretching lineations that it contains and therefore has an attitude of approximatly 110°/80°. The X axis follows the stretching lineation, L'_2, and plunges steeply to the west. The Y axis, perpendicular to the X axis, plunges shallowly to the east at 0-15°. The pancake shape of many geological objects indicates that shortening was significant. The shape of the resulting ellipsoid is therefore somewhere between oblate and prolate. This compares favourably with the shape of the finite strain ellipsoid defined by Tourigny *et al.*, (1988) for the rest of the Bousquet area.

4.4.7 Brittle faults; pre to syn-mineralization

A set of subvertical faults that range in trend from NNW-SSE to NNE-SSW cut both the S_1 and S_2 fabrics. These faults have roughly the same orientation as the S_3 spaced cleavage. Characteristic of this fault system are the presence of sulphide-bearing quartz veins (described more fully in section 6.6.3). The attitude of these vein-bearing faults is similar to that of the Mooshla mine vein system (Valliant and Hutchinson, 1982), the Doyon mine West zone (Savoie *et al.*, 1986) and the Cambior trench showing. The obvious focussing of auriferous fluids along this structural trend classifies them as pre to syn-mineralization faults. Generally, they are less than 10 cm in thickness and exhibit a dominantly dextral sense of offset as indicated by geologic markers. The magnitude of this displacement varies greatly; observed slips generally range from a few mm to 1 metre. An extraordinary displacement of approximatly 150 m is inferred for the central offset in the leuctonalite (see Map in back pocket). The trend and displacement along this fault are reasonably well constrained from drill hole data (LAC Minerals; Orion B-6, B-7 properties) and from interpretation of both air photos and magnetic susceptibility lineaments. Steeply plunging mineral lineations have been observed in only one location and suggest local subvertical movement may occur on some fault surfaces.

4.4.8 Brittle faults; post-mineralization

A younger conjugate set of strike-slip faults occur throughout the district. These trend NW-SE (dextral) and NE-SW (sinistral) and are subvertical. The fault planes are typically less than 1 cmetre wide and displacements are generally less than 1 metre. However, exceptions do occur as is the case for the Bousquet and Doyon Faults where wide zones of graphitic fault gauge are associated with lateral displacements of 200 and 75 m respectively (Savoie *et al.*, 1989).

4.4.9 Kinks

Kink bands overprint the S_2 and S_3 foliations and represent the final deformation episode. They are absent within the intrusion and are only observed in well foliated volcanic rocks. The sinistral and dextral kink bands are developed on the S_2 foliation and trend 045° and 330° respectively. Kink planes have a subvertical dip. Kink bands such as these result through layer-parallel shortening (Davis, 1984) and are ubidquitous throughout the Abitibi greenstone belt. They are interpreted as representing a late stage east-west directed stress system (Dimroth *et al.*, 1982; Ludden and Hubert, 1986a; Tourigny *et al.*, 1988; Marquis and Hubert, 1989)

4.4.10 Veins

There are several generations of veins and vein bearing structures in the area of the Mooshla intrusion. For purposes of presentation, all veins are classified into two categories; (*a*) barren veins and (*b*) mineralized veins. Mineralized veins are defined as pyrite-bearing and may also be auriferous. Following Marquis and Hubert (1989) and Tourigny *et al.* (1989) two vein types are defined for each category based on their geometric relationship to the S_2 foliation, (*i*) foliation-oblique veins, and (*ii*) foliation parallel veins.

4.4.10.1 Barren foliation-oblique veins

Barren foliation-oblique veins generally occur as fracture fillings along NNE-SSE, NNW-SSE and E-W directed joints. They are rarely observed outside the quartz diorite phase of the intrusion. The veins have vertical, northerly and southerly dips. They range in width from 1 to 12 cm and extend laterally up to 30 m. Mesoscopic alteration of the wallrock is not observed. The vein mineralogy is consistently dominated by milky white quartz with accessory chlorite, carbonate and sericite.

Similar veins sets exist in the volcanic rocks east of the intrusion and are described by Marquis and Hubert (1989). They note a strong host rock control on the vein mineralogy and suggest that the vein forming solutions were in equilibrium with the host rocks. Fluid inclusion studies by Savoie *et al.* (1989) indicate systematic variation between the composition of quartz-forming fluid and the host lithologies. The fluids for these barren foliation-oblique veins are therefore interpreted as having been derived from the surrounding country rocks (Savoie *et al.*, 1989).

4.4.10.2 Barren foliation-parallel veins

This class of vein is most frequently hosted by second order shear zones within North and West sector basalts. They are tightly folded and are transposed parallel with the regional schistosity. They are therefore pre to syn-S_2. These veins are generally comprised of honey-brown saccharoidal quartz. Mesoscopic alteration of the wallrock is not observed. They range in width from millimetric to centimetric and extend laterally for up to 1 m.

4.4.10.3 Mineralized foliation-oblique veins

Within the Mooshla intrusion, mineralized foliation oblique veins are fracture controlled and are oriented NNE-SSW to NNW-SSE with steep dips generally to the west. In general, their width ranges from 1 to 20 cm with lateral extensions up to 5 m. Notable exceptions do occur, however, as in the case of the Doyon mine West zone where the veins are approximatly 0.2 to 1 metre thick and extend laterally up to 30 m (Savoie *et al.*, 1986). The veins are composed of ribboned quartz to creamy white quartz with less than 3 vol.% disseminated pyrite. Wall-rock alteration is frequently observed extending up to 5 cm on either side of these veins. The alteration mineralogy consists of sericite, quartz, carbonate with minor epidote, chlorite and up to 5 vol.% disseminated sulphides. The majority of these mineralized foliation-oblique veins are undeformed and occur in the area near the leucotonalite-quartz diorite contact (see Map in pocket).

By far the most important mineralization hosted by this class of quartz veins is in the West Zone of the Doyon mine (Savoie *et al.*, 1989). Located entirely within the leucotonalite, the veins within the West Zone display a slight buckling or large wavelength, low amplitude open folding. This suggests some component of N-S shortening occurred subsequent to auriferous mineralization in the West Zone (F. Robert, pers. comm., 1990). East of the Mooshla intrusion, the bulk of the Au mineralization at the Doyon mine occurs in the slightly S_2 discordant foliation-oblique veins of the No. 2 zone (Savoie *et al.*, 1989; Marquis and Hubert, 1989).

4.4.10.4 Mineralized foliation-parallel veins

Mineralized foliation-parallel veins in the vicinity of the Mooshla intrusion occur within, or adjacent to, shear zones. Three types of veins can be recognized on the basis of their morphology and the order of the shear zone with which they are associated. The first type of vein, V_1, occurs only in 2^{nd} order shears and as such are found mostly within Domain 1. They are irregular, massive veins whose width ranges from 0.5 cm to 20 cm and may extend up to a few m in length. Their mineralogy comprises saccharoidal quartz, ankerite, tourmaline and pyrite. Wall rock inclusions or scepta are rare. Native gold occurs as 10 to 50 um sized grains that are spatially associated with disseminated sulphides within the quartz (Gaudreau, 1986).

The other two foliation-parallel vein types, V_2 and V_3, are found exclusively within the SMSZ of lithotectonic Domain 3. They strike roughly east-west with steep dips to the south. Thicknesses of both types of vein range from a few mm up to 15 cm with lateral extension rarely exceeding 1.5 m. V_2 veins are beige to buff-white in colour and are boudinaged along a vertical axis. Quartz within individual boudins displays a long crystallographic axis perpendicular to the wall-rock. Such relationships suggest that V_2 veins formed as early dilation veins of the S_2 foliation and were subsequently boudinaged.

V_3 veins contain abundant, parallel wall-rock scepta which lends them a laminated or ribboned appearance (Hodgson, 1989). This morphology is indicative of crack-seal processes and is caused by fluid pressure cycling; fluid pressure repeatedly exceeds the lithostatic pressure (Sibson *et al.*, 1988). They display no evidence of boudinage and are mineralized with 2-3 vol.% disseminated pyrite and pyrrhotite. In contrast, the foliation-parallel veins of the Doyon mine No. 1 zone are laminated *and* boudinaged (Savoie *et al.*, 1989; Marquis and Hubert, 1989). They are interpreted to have formed as dilations of the regionally developed S_2 foliation (Tourigny *et al.*, 1989).

4.5 Discussion and Summary

The Mooshla intrusion has an southerly to southeasterly facing direction that is subconcordant with the southerly facing direction established for the host volcanic rocks. It is located entirely within the Dumagami Structural Zone of Marquis and Hubert (1989) and records four generations of deformation related structures. The first-generation structures, D_1, are represented by a weakly penetrative foliation, S_1, that is localized to Domain 2. It may represent a period of N-S compression. The S_1 foliation is unique to the Mooshla intrusion and has not been documented elsewhere in the Bousquet Mining Centre.

Second-generation structures correspond to a moderatly penetrative foliation, S_2, some minor folds and to a several orders of shear zones. The S_2 foliation is the principal plane of flattening in the Mooshla area and therefore correlates with the S_1 foliation described by Tourigny *et al.*, (1988) and Marquis and Hubert (1989) for the Bousquet Mining Centre. Dip-slip shear zones that accomodated horizontal shortening and vertical extension bound the intrusion to the north and south. Both the shear zones and the S_2 foliations were produced during the principal compressive regime D_2, a period of subhorizontal N-S compression.

The Ls-tectonites of the SMSZ record one principal event dominated by reverse-oblique movement. Similar movement is well documented for the many shear zones of the Dumagami Structural Zone by Tourigny *et al.* (1988), Marquis and Hubert (1989) and Marquis (1990). In contrast, the second order shears in Domain 1 display independent evidence of reverse oblique faulting, normal oblique faulting and dextral shear. The variability in displacement vectors from shear to shear suggests complex movement histories marked by shear zone reactivation. The development of a superposed dextral shear foliation on many second order shears (PVO shears) reflects a transcurrent shear component that was late to post D_2.

Third generation structures are represented by a spaced cleavage, S_3, a crenulation cleavage, S_{3c}, as well as a series of faults and fractures. Collectively these structures trend NNE-SSW to NNW-SSW and reflect dominantly E-W directed horizontal shortening. They are dominantly brittle in nature with some displaying significant lateral offset. Fourth generation structures are NE-SW and NW-SE trending kink bands. Finally, a late set of conjugate strike-slip faults transect all lithologies in the Mooshla area.

CHAPTER 5. GEOCHEMISTRY

5.1 Geochemistry of the Mooshla intrusion

5.1.1 Major elements

The preservation of primary textures and lack of quartz veining in altered rocks can be used as a basis for assuming isovolumetric alteration (e.g. Rivering and Hodgson, 1980). The hypidiomorphic units of the Mooshla intrusion are generally devoid of quartz veining and preserve many delicate primary textures which would suggests that constant volume was maintained during greenschist facies metamorphism. In contrast, the leucotonalites exhibit variable and intense fabric development, abundant evidence of grain size reduction (e.g. phyllonitic leucotonalite) and much recrystallization (e.g. porphyritic leucotonalite; see section 3.5). The destruction and overprinting of most primary textures would suggest that isovolumetric conditions did not prevail during alteration and deformation of the leucotonalites. Discretion should therefore be excercised when interpreting geochemical "trends" within this unit.

Variations of major elements within the Mooshla intrusion are plotted on Harker diagrams (recalculated to 100% volatile-free) as a function of SiO_2 (figure 18). Despite the obvious alteration, SiO_2 remains an important criteria in lithological classification and provides an effective index of differentiation. The gabbros, quartz diorites, tonalites and leucotonalites all display negative correlations of the elements Al_2O_3, MgO, CaO, FeO_T, TiO_2 and MnO with SiO_2. Na_2O and K_2O exhibit poor positive correlations with SiO_2. The overall correlation observed between the major oxides and SiO_2 is indicative of crystal-liquid fractionation. Note the Na_2O depletion within rocks of SiO_2 63.5 to 66.5

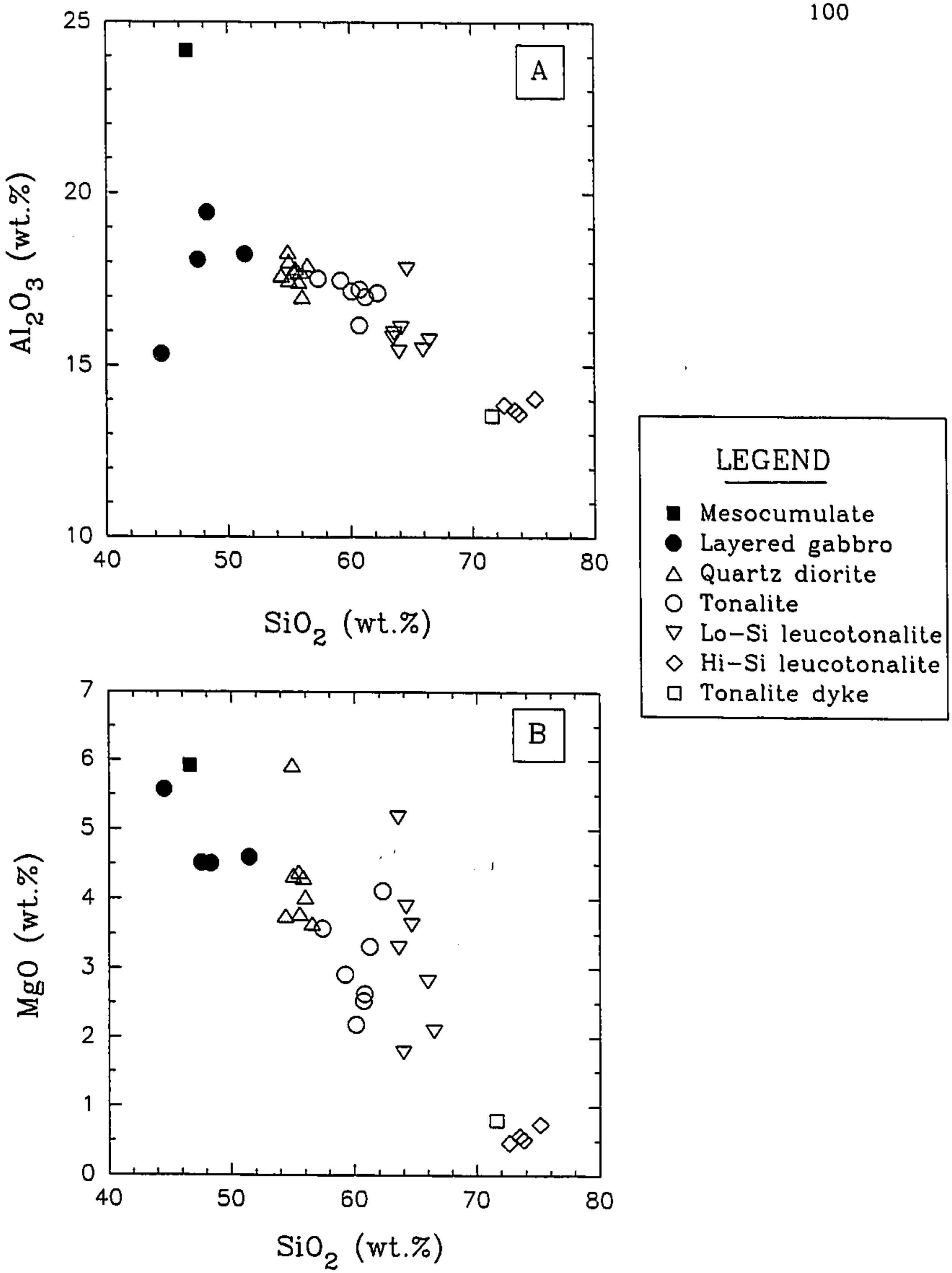

Figure 18 (A–H): Harker variation diagrams for the lithologies of the Mooshla intrusion. Lo–Si: low–silica, Hi–Si: high–silica.

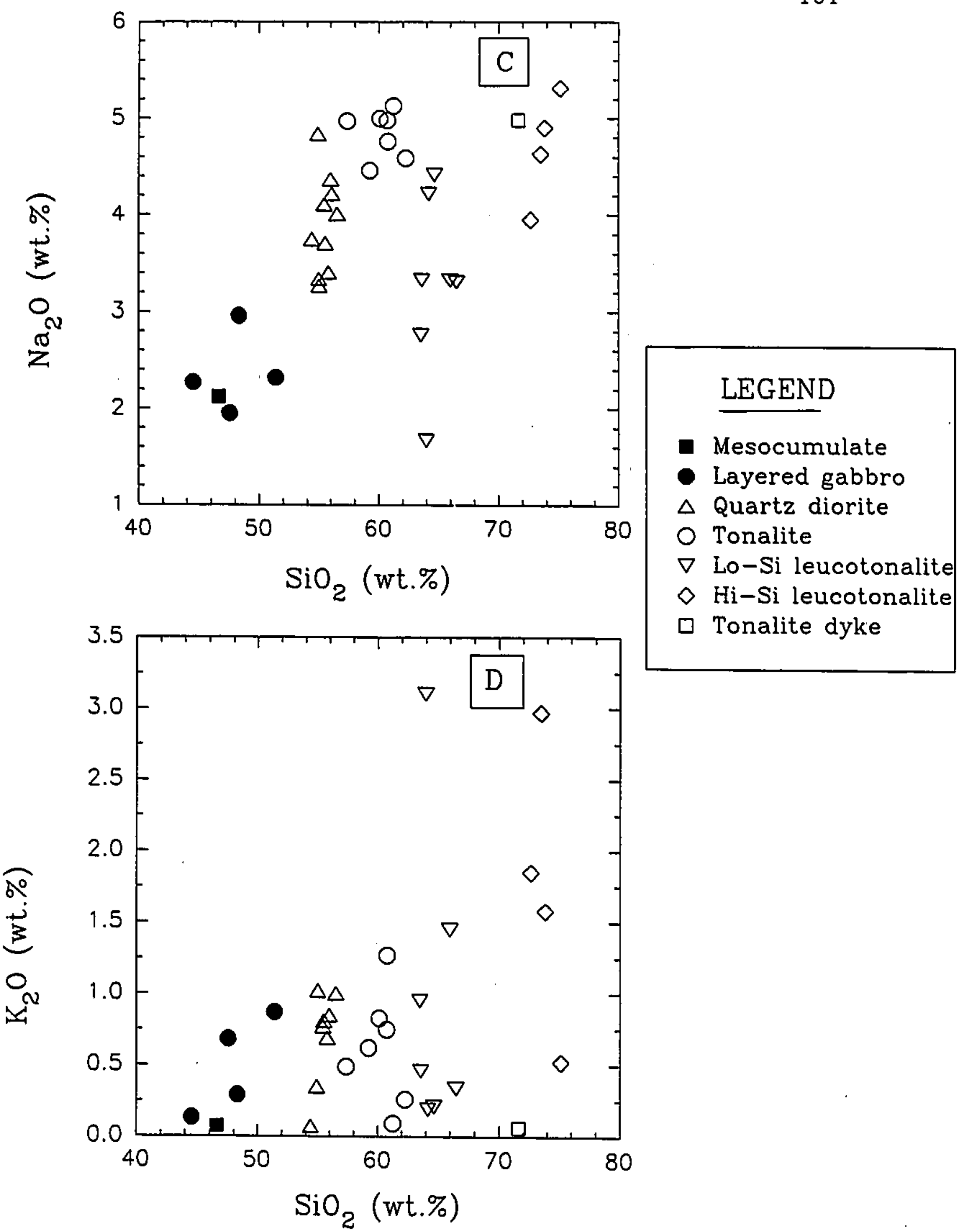

Figure 18 (A–H): Harker variation diagrams for the lithologies of the Mooshla intrusion. Lo–Si: low–silica, Hi–Si: high–silica.

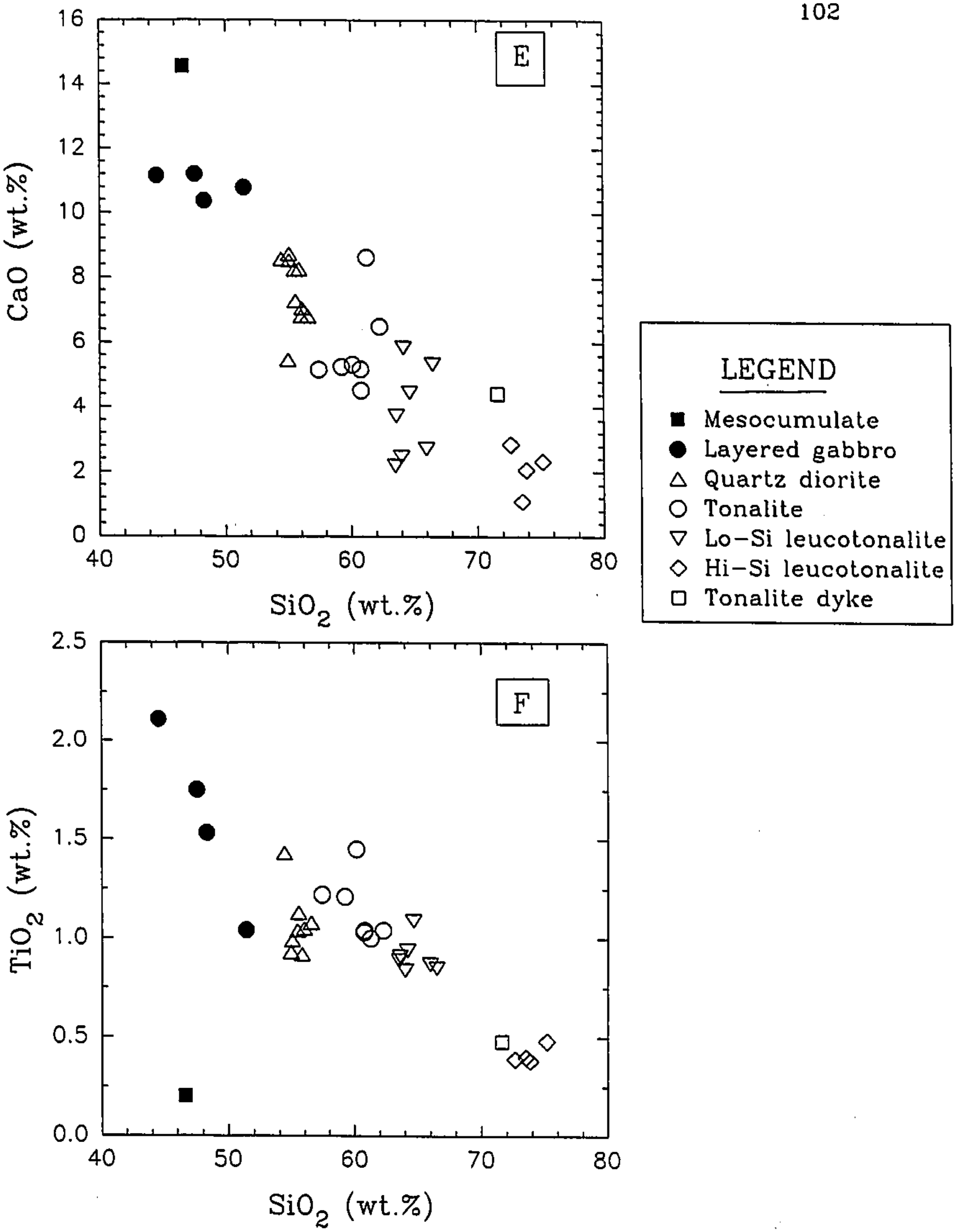

Figure 18 (A–H): Harker variation diagrams for the lithologies of the Mooshla intrusion. Lo–Si: low silica, Hi–Si: high–silica.

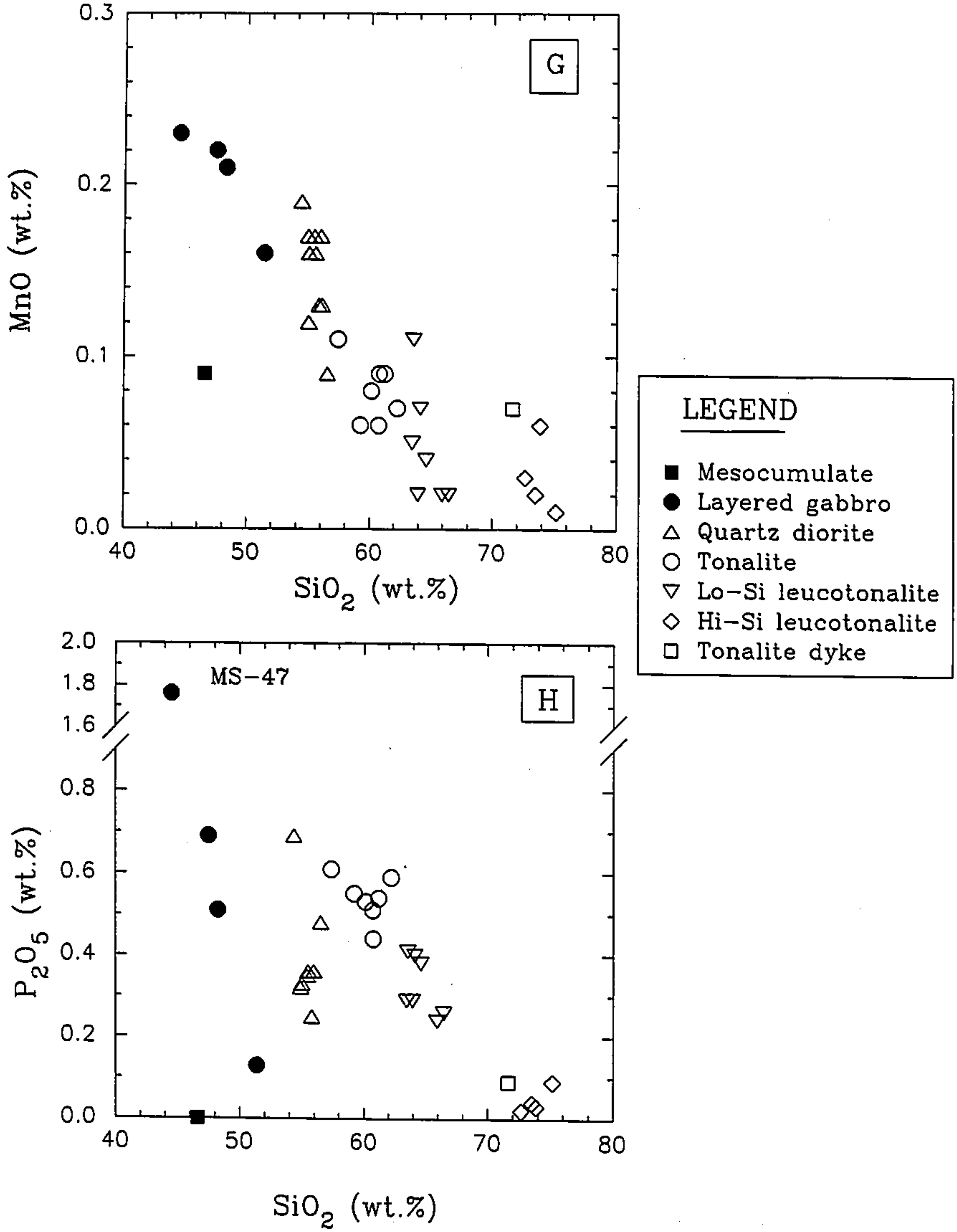

Figure 18 (A–H): Harker variation diagrams for the lithologies of the Mooshla intrusion. Lo–Si: low–silica, Hi–Si: high–silica.

wt.% (figure 18C) likely reflect alkali depletion during hydrothermal alteration (figure 18D). textural variations within the gabbro cumulates are reflected by chemical differences; note that the mesocumulate gabbro (sample MS-58) plots consistently apart from the layered gabbros on all diagrams. It is Al_2O_3, CaO and MgO rich, as well as FeO_t, TiO_2, MnO and P_2O_5 poor with respect to other samples (MS-31, MS-31a, MS-47 & MS-SQTR). The high Al_2O_3, CaO and low Na_2O contents reflect the plagioclase-rich, anorthositic character of the cumulates and is why the term gabbro is preferred over diorite for this unit. Furthermore, the average SiO_2 content of the cumulate gabbros (47.92 wt.%) is closer to that of common gabbros (50.14 wt.%) than it is to common diorites (57.48 wt.%; averages from Le Maitre, 1976).

The leucotonalite shows considerable scatter in all major oxide contents. Two populations are readily apparent on the basis of SiO_2 content; (1) SiO_2 = 60 to 64.6 wt.% and (2) SiO_2 = 73 to 76 wt.%. Samples of group 2 (MS-85, MS-87, MS-1054 & 622-22) display the highest degree of silicification, sericitization and carbonatization and as such are unlikely to have preserved primary chemical compositions. The remaining leucotonalite samples (group 1) are less altered, exhibit some preserved primary textures and have a higher percentage of porphyroclasts than group 2 samples. These compositions, although altered, are more likely to reflect primary values. It is therefore significant that these leucotonalites define a field which in part overlaps the tonalites.

The Al_2O_3 content of the gabbros, quartz diorites and tonalites are all > 17 wt.% whereas the leucotonalites (phyllonitic and porphyritic) are generally < 16 wt.%. The relatively unaltered portion of the Mooshla intrusion therefore resembles the high-Al_2O_3 type tonalite of Barker and Arth (1976). The quartz diorites are remarkable for their restricted range of SiO_2 and general tight clustering on most major element plots, with the notable exception of Na_2O. The P_2O_5 content of the lithologies is varied. The highest content is found in the layered gabbros (X= 0.76 wt.%), followed by the tonalites (X= 0.54 wt.%), the quartz diorites (X= 0.36 wt.%), the low-silica leucotonalites (X= 0.31 wt.%), the high-silica leucotonalites (X= 0.05 wt.%) and finally the mesocumulate gabbros (0.0 wt.%). A highly anomalous value of 1.78 wt.% P_2O_5 occurs within the massive gabbro which is transitional to the mesocumulates and layered gabbros (MS-47). The high content in the layered gabbros is interpreted as resulting from gravity settling of apatite.

The magma series (calc-alkaline or tholeiitic) to which the lithologies of the Mooshla intrusions belong are classified according to a Jensen cation plot (Jensen, 1976). This plot is preferred because its principal classification ratio ((Fe + Ti)/Mg) is relatively insensitive to alteration processes involving alkali element mobility (Jensen, 1976; Ujike and Goodwin, 1987). The lithologies of the Mooshla intrusion are of calc-alkaline affinity, but they do not define a classic calc-alkaline trend (figure 19).

5.1.2 Trace elements

Table 2 summarizes some of the trace element contents for each lithology within the Mooshla intrusion. The Zr, Y and Yb content for each lithology increases progressively with the degree of fractionation as expressed by the SiO_2 contents of the intrusive units (figures 20, 21, 22). The good correlation with SiO_2, in particular for Zr, suggests that these elements remained incompatible throughout the crystallization of the intrusion. In all three diagrams, the gabbro cumulates fall along the enrichment line and preserve the compositional gap observed in the major element plots. The high-silica leucotonalites plot as a distinct population that is displaced from the main Y and Yb trends. They have higher Zr (figure 20) and lower in Y and Yb (figures 21 & 22) contents compared to both

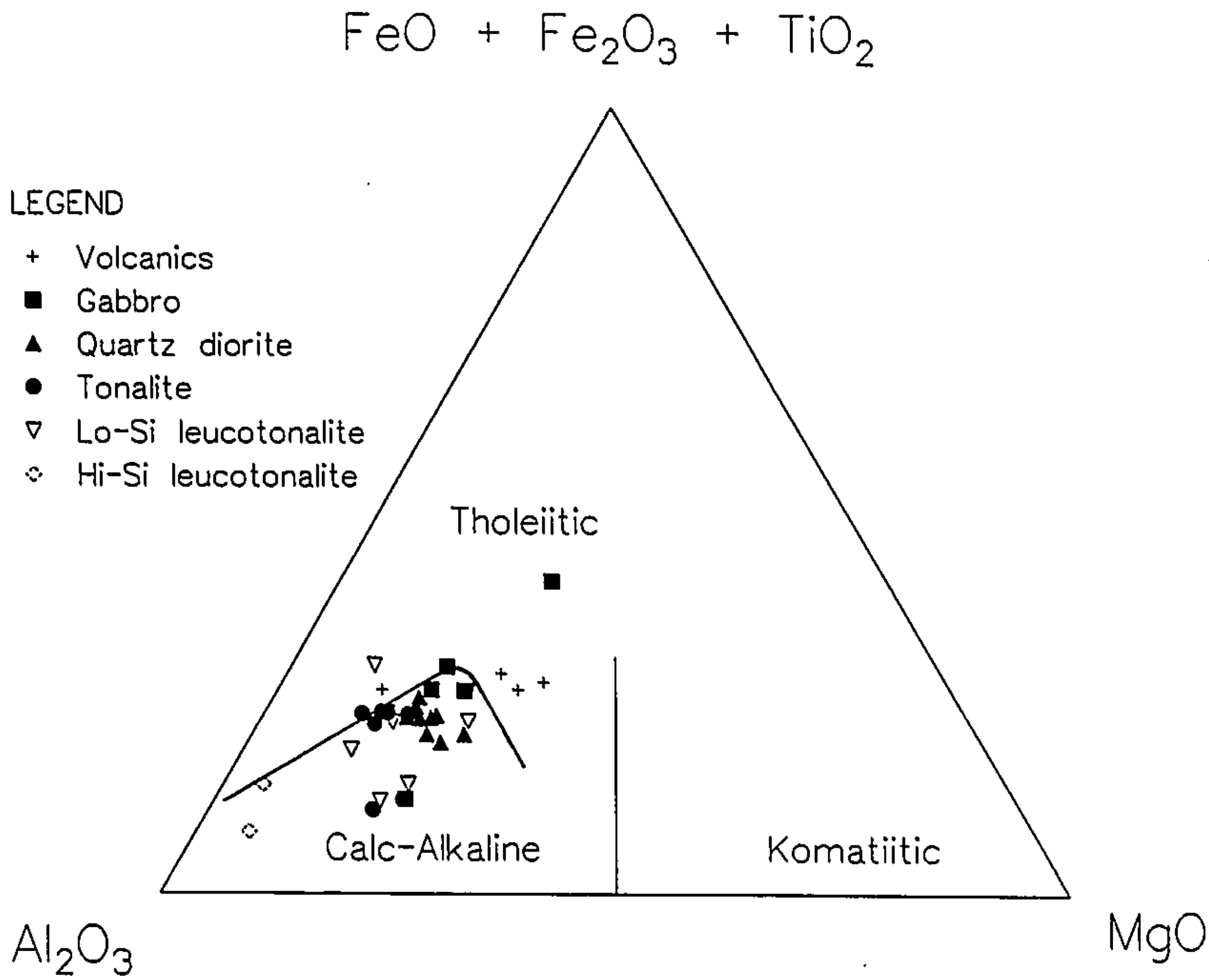

Figure 19: Jensen Cation Plot of the Mooshla intrusion and host volcanic rocks. Note scatter in plots of leucotonalites

(Jensen, 1976)

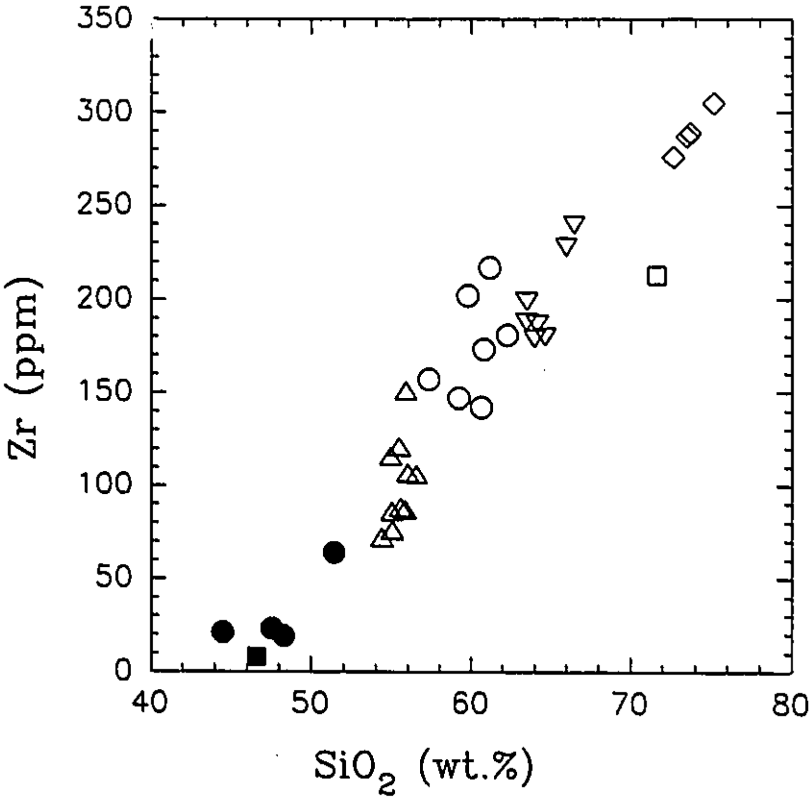

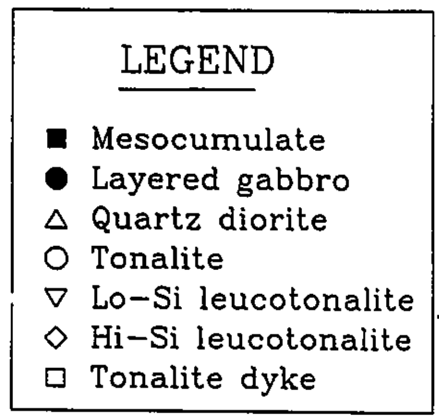

Figure 20: Zr versus SiO_2. Lo–Si: low–silica, Hi–Si: high–silica.

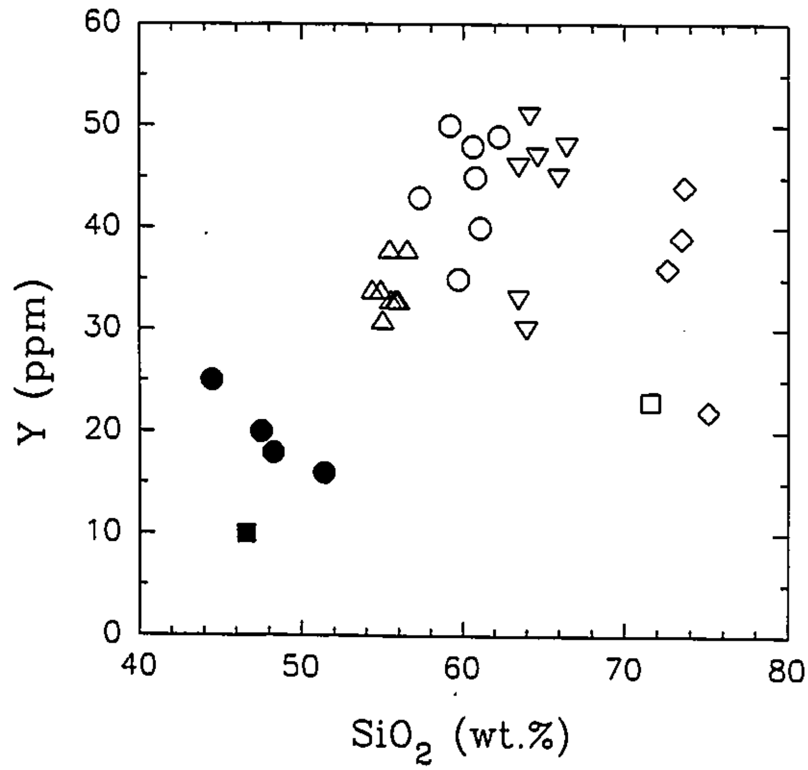

Figure 21: Y versus SiO_2. Lo–Si: low–silica, Hi–Si: high–silica.

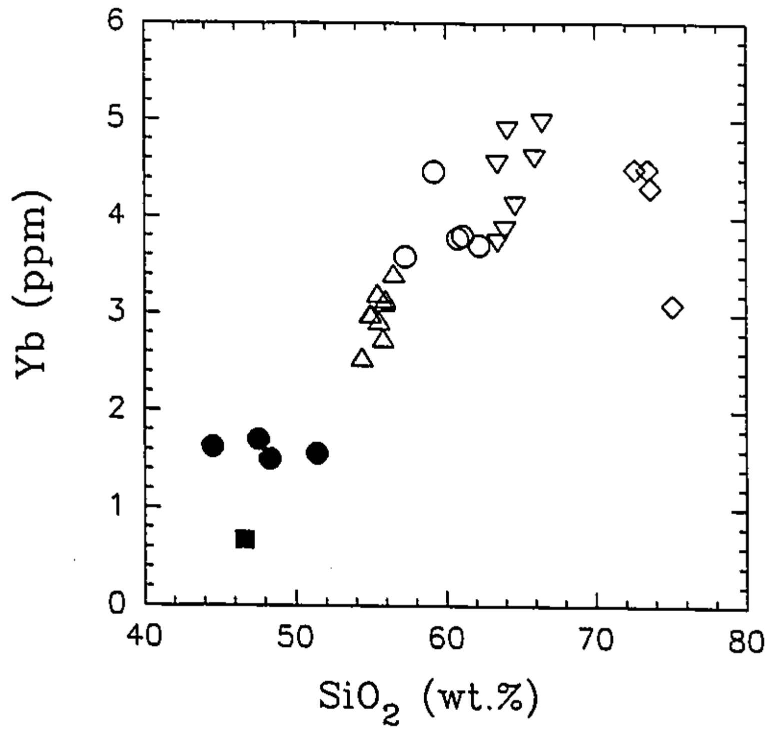

Figure 22: Yb versus SiO_2. Lo-Si: low-silica, Hi-Si: high-silica.

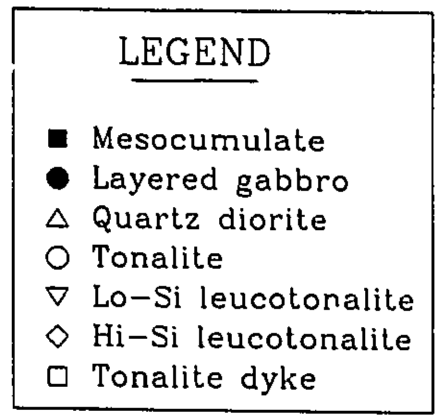

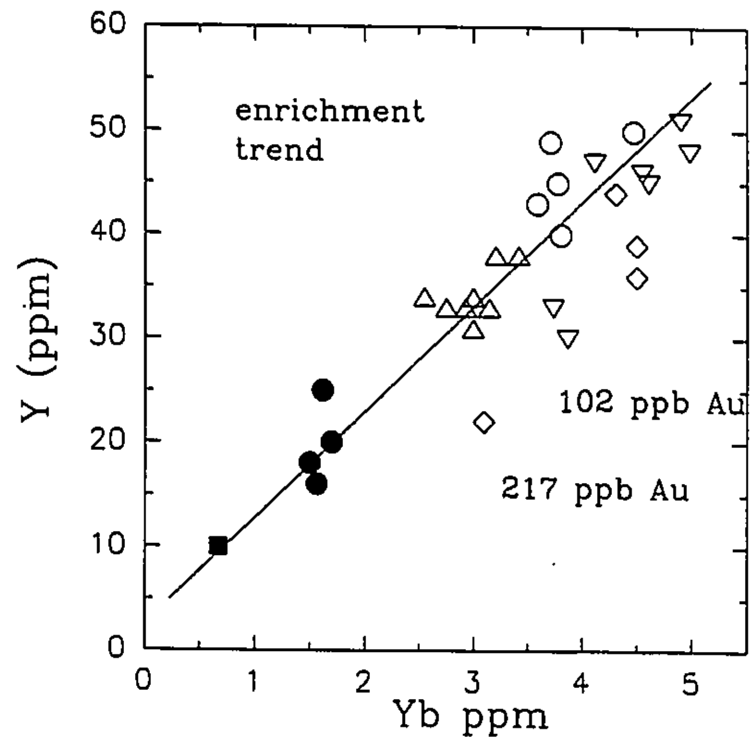

Figure 23: Y versus Yb. Note location of altered samples with respect to Y-Yb enrichment trend. Lo-Si: low-silica, Hi-Si: high-silica.

tonalites and low-silica leucotonalites. The low abundances of Y and Yb are well illustrated on a Y-Yb variation diagram (figure 23). Note the large gap between the cumulate gabbros and quartz diorites as well as the partial overlap in the low-silica leucotonalite and tonalite data. The hydrothermal alteration and/or volume change noted earlier which affected the high-silica leucotonalites may have produced the Zr enrichment and Y, Yb depletion.

TABLE 2: Trace element content (ppm) of the Mooshla intrusion lithologies. Results listed represent minimum, maximum and (mean). Analyses below detection limit reported as 0.

	GABBRO			QUARTZ DIORITE	
	Mesocumulate	Layered			
Zr	0	19 - 64	(31.8)	72 - 151	(101)
Y	10	16 - 25	(19.8)	31 - 38	(33.7)
Nb	0	0 - 0		0 - 15	(3.9)
Ta	0.41	0		0	
Th	0.56	1 - 2.03	(1.35)	3 - 4.7	(3.78)
Hf	0.31	0.71 - 1.73	(1.11)	2 - 5	(3.19)
Cr	100	15 - 27	(20.7)	37 - 80	(49.0)
Ni	45	10 - 48	(27.0)	15 - 61	(36.9)
V	107	321 - 498	(373)	178 - 254	(203.8)
Zr/Y	0.80	0.84 - 4.0	(1.61)	2.12 - 4.87	(3.00)
Y/Yb	14.93		(12.36)		(11.23)
Th/U	6.22	4.41 - 5.64	(5.03)	2.37 - 6.35	(4.20)
Mg#	68.12	38.1 - 44.2	(40.30)	38.3 - 54.6	(47.58)

	TONALITE		LEUCOTONALITE	
			Low-silica	High-silica
Zr	157 - 217	(179.5)	179 - 240 (200.1)	276 - 305 (289.3)
Y	35 - 50	(43.7)	30 - 51 (42.9)	22 - 44 (35.3)
Nb	0 - 10	(3.6)	0 - 11 (3.0)	0 - 14 (9.5)
Ta	0 - 1.78	(0.58)	0 - 1.1 (0.2)	0 - 1.75 (0.6)
Th	4.3 - 9.21	(6.19)	6 - 8.5 (7.41)	13 - 16.9 (14.63)
Hf	3.7 - 5.44	(4.53)	5 - 7 (5.90)	7.6 - 9 (8.2)
Cr	12 - 46	(26.25)	14 - 41 (28.0)	0 - 67 (40.5)
Ni	0 - 35	(22.8)	14 - 33 (23.0)	0 - 79 (39.3)
V	41 - 105	(73.3)	43 - 125 (78.3)	0 - 62 (21.3)
Zr/Y	2.94- 5.77	(4.11)	3.67- 6.03 (4.67)	7.63 - 13.86 (8.86)
Y/Yb		(11.75)	(9.7)	(8.49)
Th/U	4.96- 6.13	(5.72)	3.95- 11.57(5.66)	3.59 - 5.75 (4.73)
Mg#	35.02- 64.98	(44.58)		

Mg#= MgO/(MgO+FeO) wt.%

The gabbro cumulates have a substantially lower Zr/Y ratio compared to the other lithologies, whereas the Zr/Y ratios of the tonalites and low-silica leucotonalites are very similar. Other transition elements that exhibit incompatible element behavior are Th, Hf and U. They display a positive correlation for each lithology from gabbro mesocumulate through to the high-silica leucotonalite. The unit averaged Th/U ratios are similar for all lithologies, ranging from 4.20 to 5.72. Note, however, that the Th/U ratios of the layered gabbros and tonalites are slightly higher than that of the quartz diorite. Y/Yb ratios are very similar throughout the lithologic suite, and show only a slight decrease with increasing differentiation. Incompatible element ratios, such as Zr/Y, Th/U or Y/Yb, generally remain constant during ideal fractional crystallization. Variations in these interelement ratios are thought to reflect petrogenetic processes involving partial melting, magma mixing or host-rock assimilation (Cox *et al.*, 1979). Interestingly, Nb and Ta abundances are very low with virtually all samples having contents that are below dectection limits (Nb $<$ 10 ppm, Ta $<$ 1ppm). The highest value recorded is 15 ppm Nb in a quartz diorite. These are features characteristic of calc-alkaline affinity (Wilson, 1989).

Some incompatible elements show negative correlations, as observed for Sc and V. Note that the contents of these elements in both the low and high-silica leucotonalites are similar. A complex behavior is exhibited by Cr, Ni and Co. These elements are compatible and normally show progressive depletion with differentiation. It is therefore odd that the cumulate gabbros have noticeably lower abundances of incompatible elements relative to the other lithologies, in particular with respect to the quartz diorites. Note that the high-silica leucotonalites have remarkably high Cr and Ni contents.

5.1.3 Rare earth elements

Although the rare-earth elements share similar physical and chemical properties, they can be fractionated from each other by various petrological and mineralogical processes (Henderson, 1984). This phenomenom is a powerful tool when tracing the evolution of a suite of rocks and will be discussed later in petrogenesis.

Total rare earth element (REE_{TOT}) contents are elevated and increase sympathetically with SiO_2 (relative differentiation) and Zr (figure 24: A & B). The good clustering of these data suggests that significant fractionation of REE during crystallization of a mineral phase does not seem to have occurred. As in the major and trace element diagrams, a compositional gap seperates the cumulate gabbros from the remaining lithologies. Similarily, the high-silica leucotonalites retain their characteristic grouping. Note that their REE_{TOT} contents resemble those of both the low-silica leucotonalites and tonalites suggesting that silicification has not significantly modified their REE abundances.

The enrichment in REE with differentiation of the Mooshla intrusion is well illustrated in the chondrite normalized REE plots of each lithology (chondrite values from Anders and Grevesse, 1989). All units exhibit fractionated REE profiles (figures 25 to 28). With the exception of the cumulate gabbros, the $[La/Yb]_N$ ratio remains relatively unchanged throughout the differentiation suite despite a four fold increase (approximate) of the REE abundance. In contrast, the degree of light rare-earth element (LREE) enrichment, as expressed by the La_N/Sm_N ratio, displays a general increase from the gabbros ($La_N/Sm_N = 2.70$) through to the high-silica leucotonalites ($La_N/Sm_N = 5.04$).

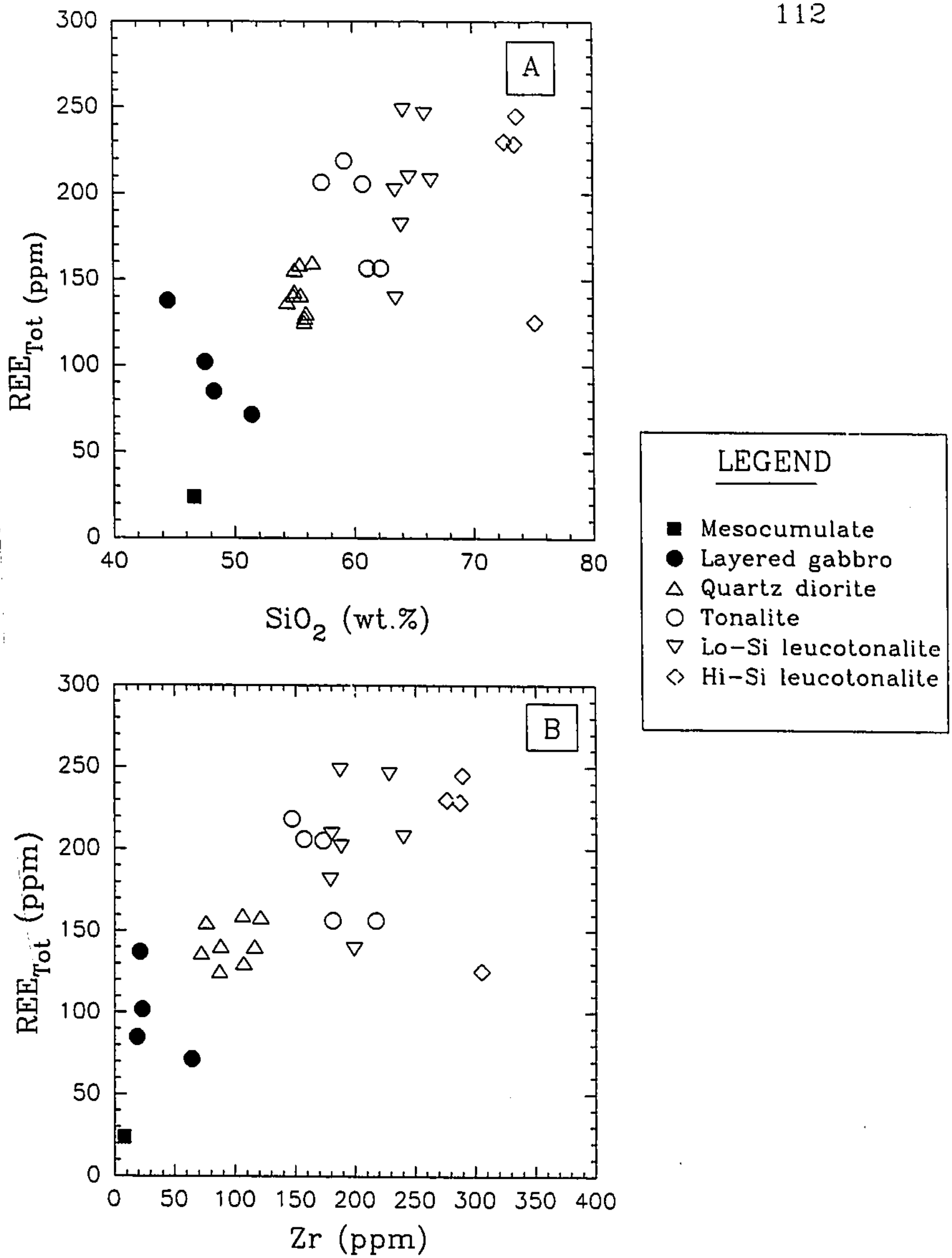

Figure 24: A) REE_{TOT} versus SiO_2
B) REE_{TOT} versus SiO_2. Lo-Si: low-silica, Hi-Si: high-silica.

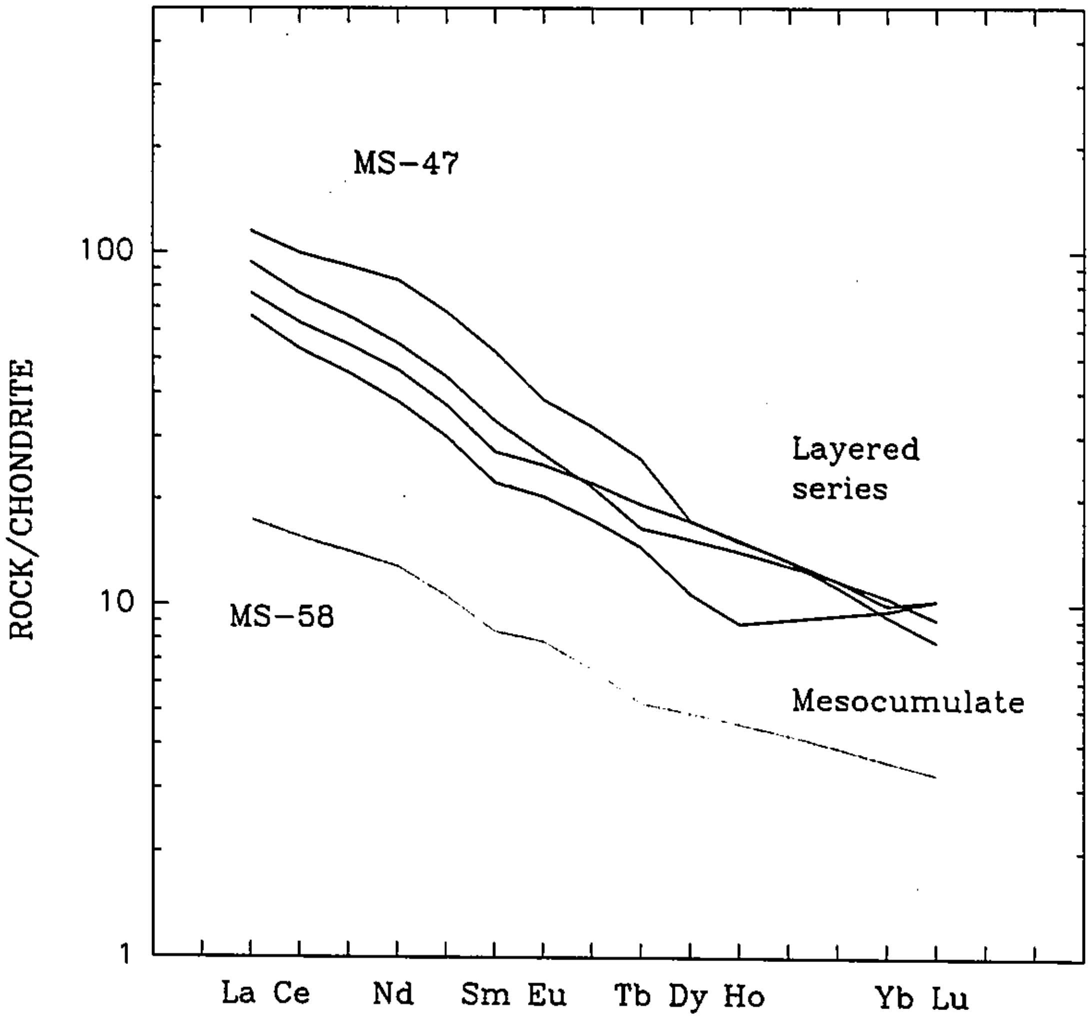

Figure 25: Chondrite normalized rare-earth element profiles for the cumulate gabbros of the Mooshla intrusion.

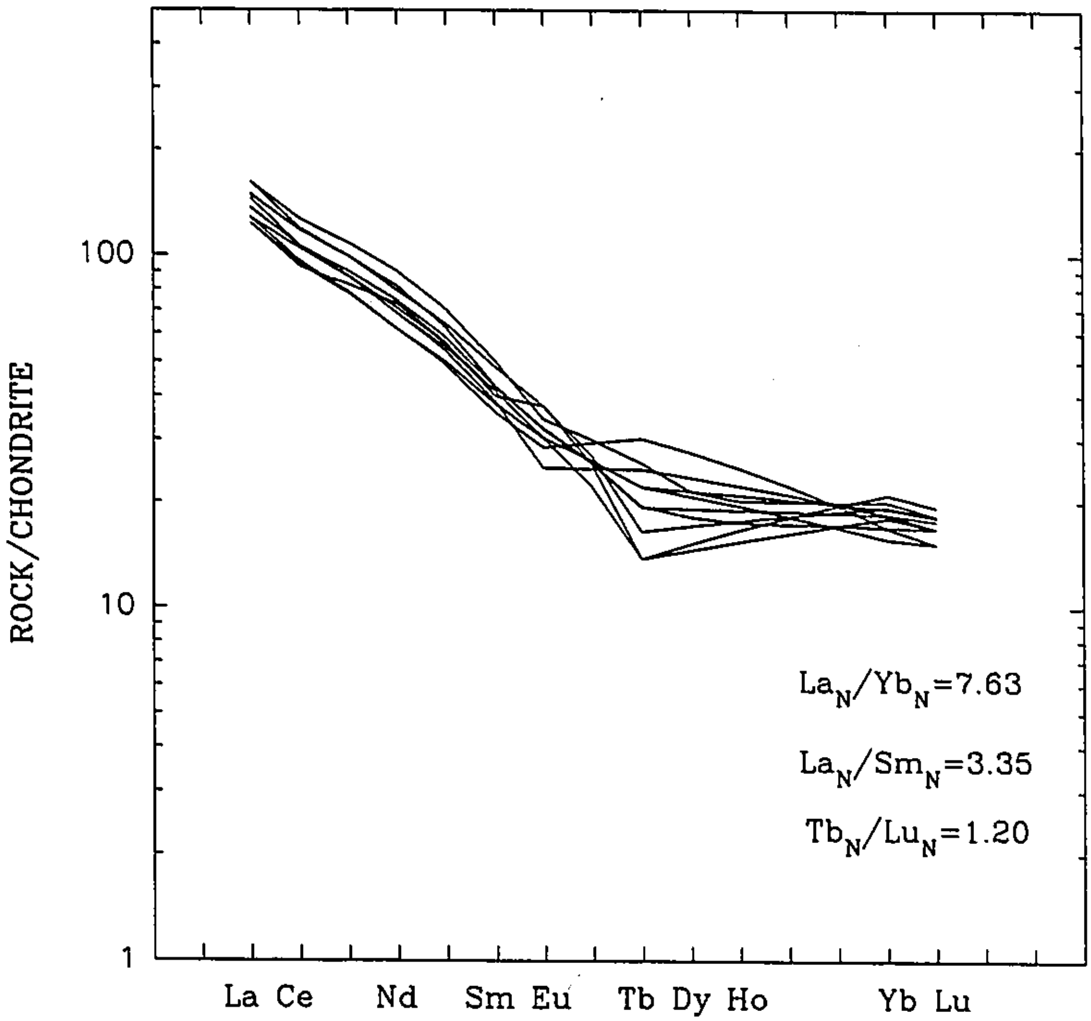

Figure 26: Chondrite normalized rare–earth element profiles for the quartz diorites of the Mooshla intrusion. Ratios are mean of 10 analyses.

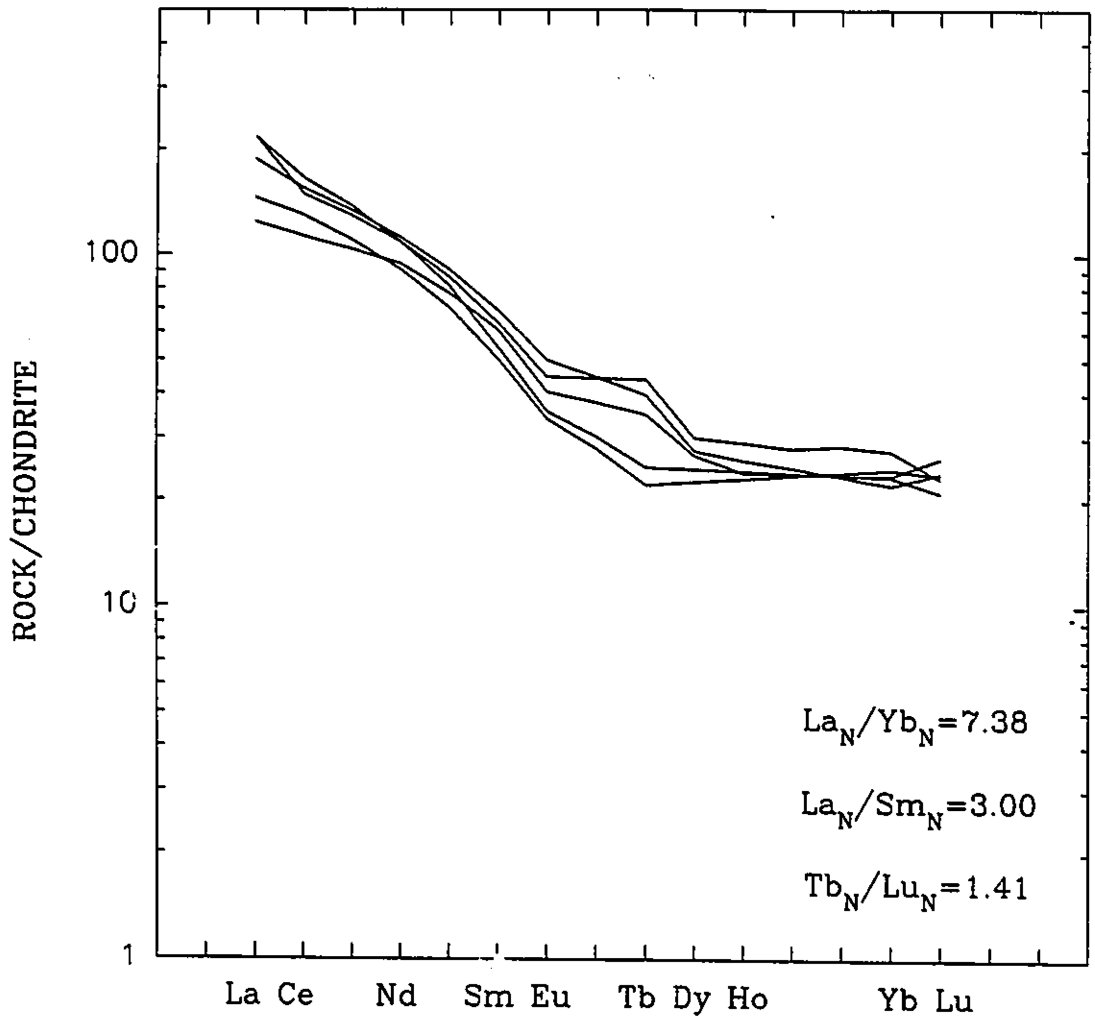

Figure 27: Chondrite normalized rare-earth element profiles for the tonalites of the Mooshla intrusion. Ratios are mean of 5 analyses.

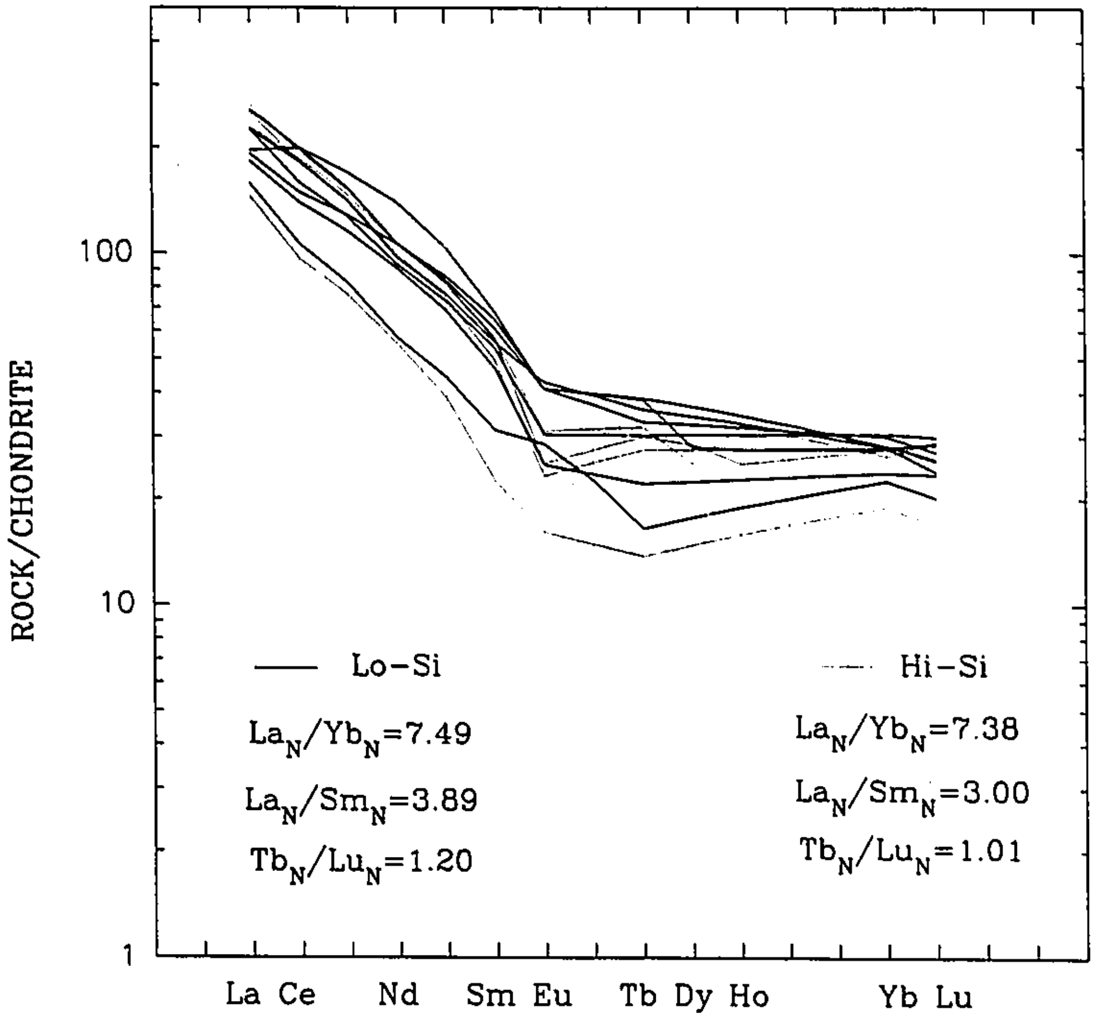

Figure 28: Chondrite normalized rare-earth element profiles for the Low and High-silica leucotonalites of the Mooshla intrusion. Ratios are mean of analyses Lo-Si leucotonalite=7, Hi-Si leucotonalite=4.

The textural and mineralogical variations of the cumulate gabbros are reflected in their REE profiles (figure 25). The layered gabbros exhibit strongly fractionated REE profiles ($[La/Yb]_N = 8.92$) and are significantly enriched in REE_N (8 to 115 x chondrite). By comparison, the mesocumulate gabbros display only moderate fractionation ($[La/Yb]_N = 4.89$) and have lower REE_N from 3.57 to 17.47 x chondrite. The differences in the REE characteristics between the mesocumulates and layered gabbros are largely due to apatite accessory-phase control. A characteristic feature of the layered-gabbros are layer-parallel concentrations of euhedral apatite crystals and high P_2O_5 contents. In contrast, the mesocumulates contain absolutly no P_2O_5 (figure 18H). Apatite control of REE is well evidenced by sample MS-47 which, despite having the lowest SiO_2 content of any gabbro analyzed, has both the highest REE_N abundances *and* the highest P_2O_5 contents (see figure 18H). Note that the slopes of the cumulate gabbro REE profiles are uniform; they lack the characteristic flat HREE profile of the other lithologies.

The quartz diorites are more enriched in LREE (124 to 162 x chondrite) and HREE (15 to 18 x chondrite) than the cumulate gabbros (figure 26). Their $[La/Yb]_N$ and Yb_N/Lu_N ratios ($X = 7.63$ and $X = 1.20$ respectively) are slightly lower relative to the cumulate gabbros, whereas their La_N/Sm_N ratios are higher (3.35). They plot within a fairly restricted range and define a smooth profile with no evidences of a europium anomaly.

The REE profiles of the tonalites, low-silica leucotonalites and high-silica leucotonalites overlap significantly (figures 27 & 28). In particular, their $HREE_N$ contents are very similar and do not display the enrichment observed from the gabbros to the quartz diorites. As mentioned previously, the La_N/Sm_N ratios increase from 3.00 (tonalites), to 3.89 (low-silica leucotonalites), to 5.09 (high-silica leucotonalites). This change in this ratio is the result of a selective decrease in Sm_N content coupled with an increase in La_N content and may reflect minor apatite fractionation (Henderson, 1982; p.94). A slight Eu anomaly ([Eu]/[Eu*] = 0.8 to 0.9) is present within the some of the leucotonalites. The overall geochemical similarity of these units is further evidence that the tonalite represents the leucotonalite protolith.

5.2 Overview of the geochemistry of the host rocks

5.2.1 Introduction

Host rocks were sampled within a 200 metre periphery of the intrusion. Analyses were performed only on samples that were aphyric, unaltered and not significantly tectonized. The major and trace element data presented in Table 3 are grouped into two classes on the basis of geographic location. Host rocks along the northern margin form part of the Northern Volcanic Series (NVS) whereas southern host rocks belong to the Southern Volcanic Series (SVS). Unfortunately, the pervasive alteration and deformation exhibited by the host rocks along the western end of the intrusion preclude their incorporation into the data set. No outcrops occur within 600 m of the eastern end of the intrusion.

The NVS and SVS belong to different magma series; the NVS are tholeiitic whereas the SVS are calc-alkaline (figure 19). They fall within the high-Fe to high-Mg tholeiitic basalts fields on figure 19. The lack of any trend is attributed to lack of stratigraphic and sampling diversity. The NVS have higher CaO, TiO_2, MnO and lower in Al_2O_3, Na_2O and P_2O_5 contents than the SVS. K_2O contents are very low for both (<0.34 wt.%). Significant differences exist in their trace element abundances. High Y, Cr, V, Sc and low Sr, Th, and U characterize the NVS relative to the SVS.

Note that the absolute abundances of Cr and Ni are high whereas Th, U, Zr and Y are low. Nb and Rb contents are below detection limits (10 ppm) for both series. The mean Zr/Y ratios are 3.56 and 2.2 for the SVS and NVS respectively.

TABLE 3: SiO_2, P_2O_5, TiO_2 (wt.%) and trace element contents (ppm) of the Northern Volcanic Series (NVS) compared with the Southern Volcanic Series (SVS).

	SVS		NVS	
	Range	Mean	Range	Mean
SiO_2	49.6 - 53.26	51.43	51.91 - 54.01	52.96
P_2O_5	0.12 - 0.14	13	0.07 - 0.10	0.09
TiO_2	0.85 - 1.03	0.92	1.08 - 1.12	1.10
Zr	69 - 87	75	70 - 100	85
Y	17 - 23	20	33 - 44	38.5
Sr	83 - 240	170.6	95 - 112	103.5
Th	0.6 - 0.66	0.62	0.43 - 0.52	0.47
U	0.5 - 1.55	0.97	0.12 - 0.15	0.13
Cr	176 - 202	184.7	229 - 236	232
Ni	89 - 124	109.7	88 - 106	97
V	213 - 282	252.7	376 - 377	376
Zr/Y		3.56		2.2
$(La/Yb)_N$		5.79		0.92

The differences in REE profiles for the two are striking (figure 29). The NVS exhibits flat profiles with negative Eu anomalies ([Eu]/[Eu*] = 0.72) and REE that range from 10 to 15 x chondrite. Profiles such as these are typical of modern-day mid-ocean ridge basalts (MORBS) (Wilson, 1989). The SVS have variable Eu anomalies ([Eu]/[Eu*] = 0.94 to 1.22), are LREE enriched and HREE depleted relative to the NVS. These REE profiles are typically associated with modern day oceanic arc basalts (OAB's; Gill, 1981). The average $[La/Yb]_N$ and La_N/Sm_N ratios of the SVS are 5.79 and 4.56 respectively, compared with $[La/Yb]_N = 0.92$ and $La_N/Sm_N = 0.90$ for the NVS. Ujike and Goodwin (1987) suggest that the upper boundary of the tholeiitic series relative to the calc-alkaline

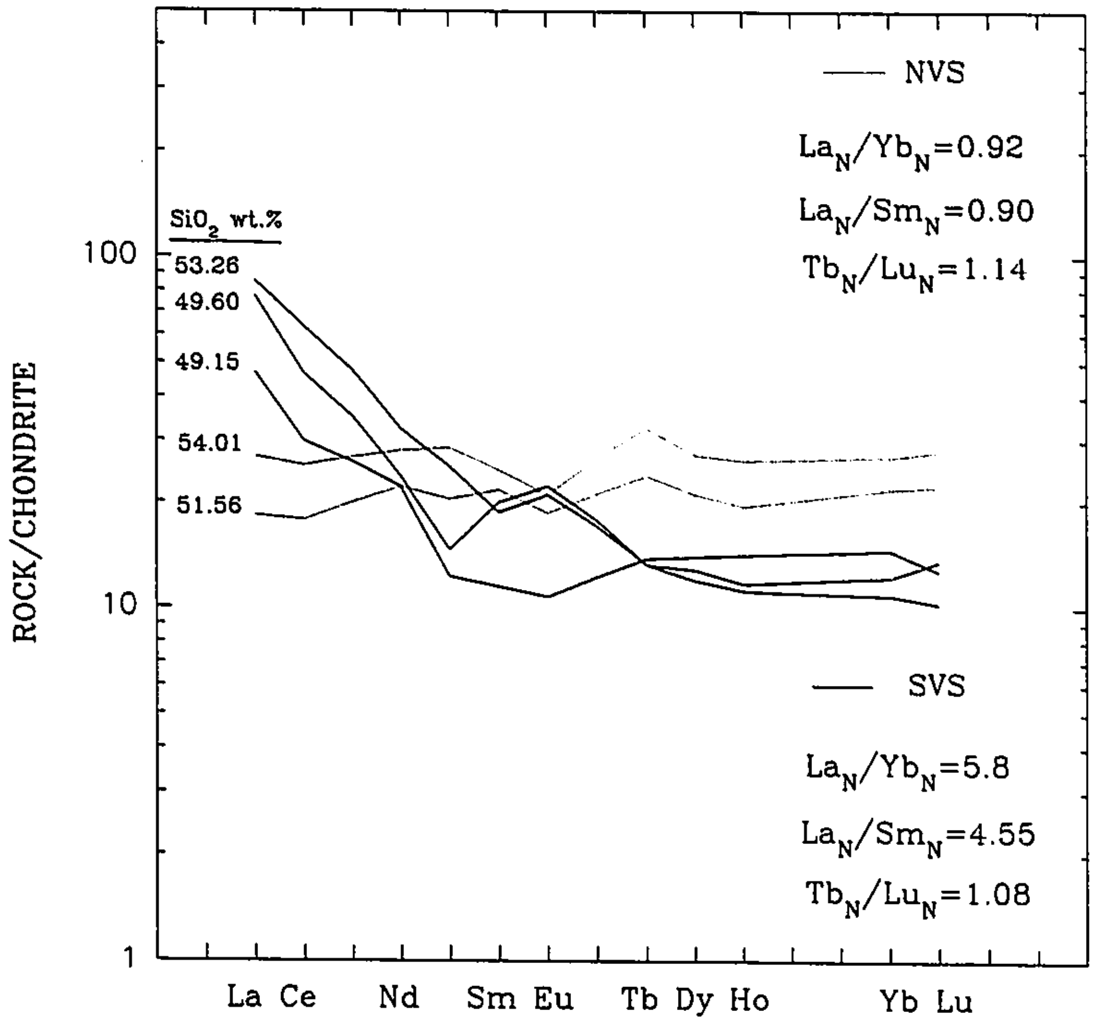

Figure 29: Chondrite normalized rare-earth element profiles for the Southern Volcanic Series (SVS) and the Northern Volcanic Series (NVS). Ratios are mean of analyses. SVS=3, NVS=2..

series be placed at $[La/Yb]_N = 2.2$. As in the plutonic differentiation suite, the total REE_N content increases with wt.% SiO_2 for both the NVS and SVS.

5.2.2 Stratigraphic correlation of the Northern Volcanic Series (NVS) and Southern Volcanic Series (SVS) with the Tholeiitic and Calc-Alkaline sequences of the Blake River Group.

To the west of the Davidson Creek fault, the Blake River Group is a bimodal volcanic sequence that is tholeiitic at its base and calc-alkaline at the top (Gélinas *et al.*, 1977, 1984). The stratigraphy of the tholeiitic sequence is well known and comprises (in ascending order) the Rouyn-Noranda, Pelletier, Tremoy, Destor and Dufresnoy units. These units display a geochemical evolution from the base to the top marked by a progressive increase in REE_{TOT}, Zr and Nb contents. REE profiles are typically flat and both La/Yb and Zr/Y are low (means of 2.9 respectively; Paradis *et al.*, 1988). The stratigraphy of the calc-alkaline sequence comprises the Dufault, Cléricy and Renault units. Aside from its calc-alkaline character, no systematic geochemical evolution has been defined within these units. Overall, they exhibit fractionated REE patterns with higher Zr/Y (3.9-6.8) and La/Yb (3.9-18.8) relative to the tholeiitic sequence (Gélinas, 1984; Paradis *et al.*, 1988).

Based on the major and trace element data, it is clear that the NVS basalts belong to the tholeiitic series whereas the SVS form part of the calc-alkaline series. To date, there has not been any systematic attempt to extend the Blake River stratigraphy east of the Davidson Creek fault. In a cursory comparison, Marquis *et al.*, (1990) and Stone (1988) demonstrated the geochemical similarities between the tholeiitic basalts of the Dumagami area and the Rouyn-Noranda, Pelletier and Tremoy units of the central Noranda area. The tholeiitic basalts of the Dumagami area (LTD1 of Marquis *et al.*, 1990) are the eastern equivalents of the NVS. Similarily, these units share many geochemical affinities with the NVS based on the results presented here. Due to the lack of systematic geochemical variation within the units of the calc-alkaline sequence, it is not feasible to attempt any stratigraphic correlation with the SVS.

5.3 The genetic relationship between extrusive rocks and the Mooshla intrusion.

5.3.1 Introduction

The Mooshla pluton is a sill-like intrusion within the Blake River Group that is located along the transition from tholeiitic to the calc-alkaline volcanism. This location at the transition from one magma series to another raises the question of what, if any, genetic relationship exists between the intrusion and host rocks; is the intrusion comagmatic and if so, to which magma series is it associated.

5.3.2 Comagmatism

The variations in major element geochemistry of the Mooshla intrusion are consistent with calc-alkaline fractionation trends with little or no iron enrichment and marked evolution towards more alkali-rich compositions. These trends resemble those found in the calc-alkaline (upper) sequence of the Blake River Group to which the SVS belong. The lack of a strong iron enrichement trend distinguishes the intrusion from the NVS tholeiites.

The calc-alkaline SVS and the intrusion exhibit very similar REE profiles (figures 24 - 29). Both are LREE enriched with similar $[La/Yb]_N$ ratios (SVS x=6.84; M.I. x=7.85), absolute REE abundances and exhibit a sympathetic increase in REE_{TOT} with SiO_2. The REE profiles of the SVS are almost identical to those of the quartz diorite. They differ significantly in that the volcanic rocks posses a Eu anomaly ([Eu]/[Eu*] = 0.82 to 1.59) that is not observed in the intrusive rocks.

The REE characteristics of a magma are set early during its crystallization history and reflect those of its source region (Gromet and Silver, 1983). Subsequent differentiation of the magma will cause the REE profiles to be raised or lowered but the slope remains relatively constant (Gromet and Silver, 1983; Jemielita *et al.*, 1988). Therefore, the REE profiles and $[La/Yb]_N$ ratios of the Mooshla intrusion, particularily the least evolved units (i.e. quartz diorites), should approximate those of its source magma. The extrusive rocks of the SVS display many obvious similarities in REE behaviour to the intrusion. These similarities are indicative of a shared parental magma. The Mooshla intrusion and the calc-alkaline rocks of the SVS must therefore be comagmatic.

Zirconium, Y, Nb and Yb abundances do not vary in a systematic fashion within the calc-alkaline sequence (Paradis *et al.*, 1988). In contrast, significant differences exist in the distribution of the transition elements Cr, Ni, Co, Th and U within the extrusive rocks of the SVS. The base of the sequence is enriched in Cr, Ni, Co and depleted in Th and U, whereas the top of the sequence is depleted in Cr, Ni, Co and enriched in Th and U relative to the intrusion. Their dissimilar transition element contents may result from a) fractionation of the intrusive magma with respect to the basal sequence lavas, or b) scavenging of Cr and Ni in one or more cumulate layers that are not exposed. In contrast, the intrusive magma is *less* fractionated than the lavas of the upper portion of the calc-alkaline sequence because it contains much more Cr, Ni and less Th, U. This relative fractionation possibly reflects the timing of emplacement; intrusion occurred subsequent to the basal sequence but prior to the extrusion of the upper portion of the Blake River Group calc-alkaline sequence.

Alternatively, it could simply reflect tapping of a zoned magma chamber at different levels by the extrusive and intrusive rocks (e.g. Hildreth, 1979).

5.4 Petrogenetic evolution of the Mooshla intrusion

5.4.1 Introduction

The petrogenetic evolution of the Mooshla intrusion is a two stage process. The first stage is pre-emplacement and involves the derivation of the parental melt that was eventually the source magma for the intrusive and extrusive rocks of the calc-alkaline Upper Blake River Group. The second stage is concerned with the emplacement, cooling and fractionation history of the intrusion. The following section discusses both these aspects and their respective influence on the petrogenesis of the Mooshla intrusion.

5.4.2. Petrogenesis of the Mooshla magma.

The geochemistry of the Mooshla intrusion is characterized by;

- LREE enrichment, $[La/Yb]_N$= 7.38 - 8.92,
- flat HREE profiles, $[Tb/Lu]_N$ = 1.01 to 2.04,
- low abundances of the high field strength (HFS) elements; Nb, Ta & Hf
- low abundances of the transition elements; Cr, Ni, Co
- low abundances of the large ion lithophile elements (LILE); K, Th, U, Rb, and Sr

Extended trace element abundance diagrams (spider diagrams) provide a simple means of visualizing the relative depletion and/or enrichment of trace elements with respect to a chondrite and/or primitive mantle reference. The Mooshla lithologies plotted on the spider diagram (figure 30) have been "double normalized"; first according to the chondrite values of Thompson *et al.*, (1984) and secondly by setting $Yb_N = 10$ so as to reduce the crossing of lines due to variable phase fractionation (Thompson *et al.*, 1982). A value equal to half the detection limit has been assigned for those elements whose abundances are below detection limits (e.g. Nb, Ta). The Mooshla spectra, or spidergrams, display a negative slope, a narrow trough at Nb, Ta and a broad trough at Zr, Hf and Ti (figure 30). They are enriched in Ba, Rb, Th, K and Sr (LILE) relative to Nb, Ta, Zr, Hf and Ti (HFS). Note that the cumulates give a small peak at Ti and P, a trough at Th and are not depleted in Sr relative to the more differentiated units.

5.4.2.1 Tectonic setting of the source area

It has become generally accepted over the course of the last decade that plate tectonics, or analogous mobilistic processes, were operative during the later part of the Archean (Bickle, 1978; Sleep and Windley, 1982; Windley, 1984; Hargraves, 1986; DeWit *et al.*, 1988; Devaney and Williams, 1989). This broad based concensus relies on geological, geochemical and geophysical considerations. The geological and geochemical similarities of many Archean granite-greenstone assemblages to modern day plate tectonic settings has prompted numerous comparisons to be made in the literature. The most frequently drawn analogies are with subduction zones (Blackburn, 1980; Dimroth *et al.*, 1982; Hodgson and Hamilton, 1989), back-arc spreading centres (Tarney *et al.*, 1976; Ludden and Hubert, 1986a & b) and ensialic rifts zones (Dimroth *et al.*, 1985; Picard and Piboule, 1986). As discussed by Thompson *et al.*, (1984), each of these tectonic setting can be characterized by their trace element

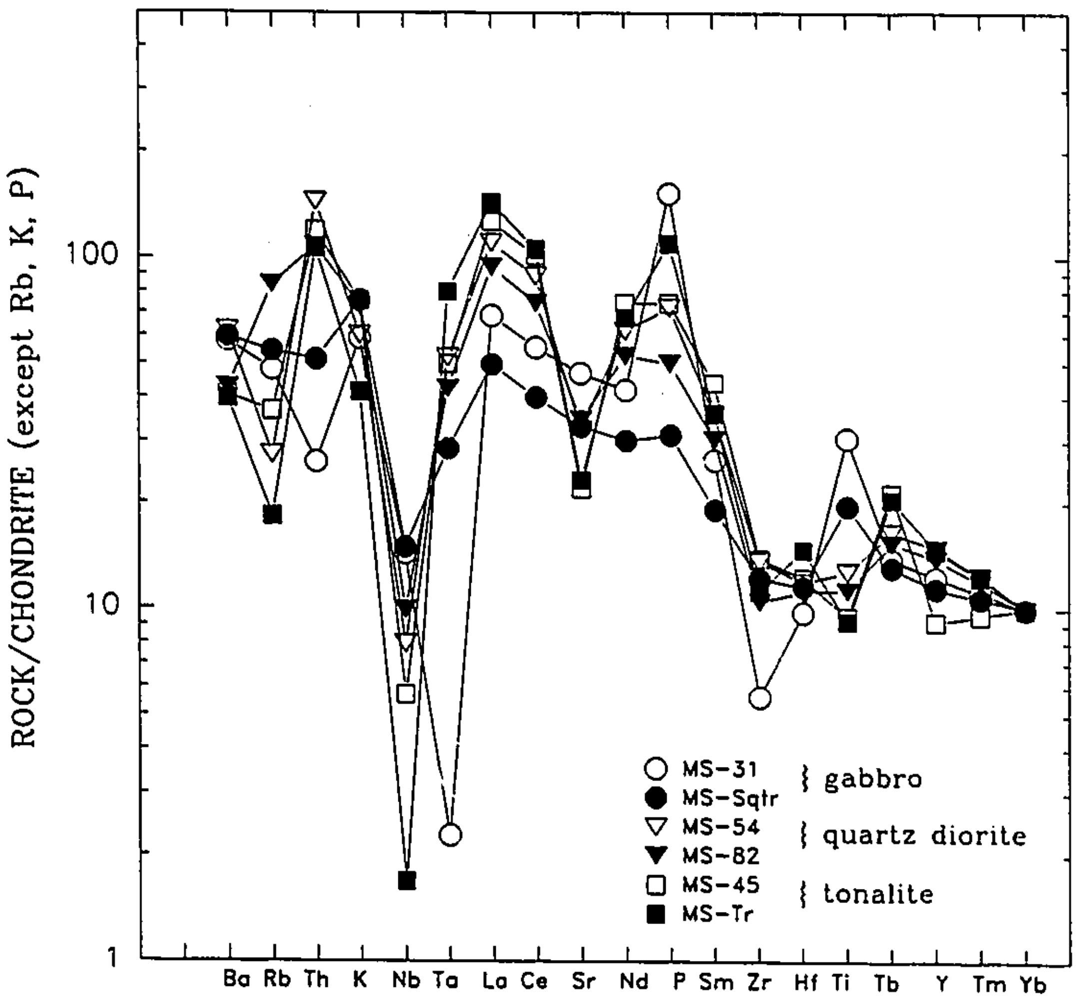

Figure 30: Chondrite normalised (except Rb, K and P, normalised tp estimated primitive mantle values) element profiles for the lithologies of the Mooshla intrusion. Normalising factors are from Thompson (1982).

contents and ratios. Assuming that data from modern tectonic settings is applicable to the Archean, it is possible to place constraints on the nature of the source area for the parental Mooshla magma through spidergram comparison.

Magma genesis in a subduction environment occurs within the mantle wedge which overlies the downgoing lithospheric plate. As the slab passes from greenschist through eclogite facies metamorphic fronts, fluids are released into an overlying mantle wedge that is composed of both depleted oceanic lithosphere (due to MORB extraction) and asthenospheric upper mantle. The hydration of the mantle wedge lowers its solidus and promotes partial melting. Direct partial melts of the slab will have a similar (mantle) solidus-lowering effect. Metasomatism of the mantle by both the slab-derived aqueous fluids and/or partial melts distinguishes magma generation in subduction-related environments from all others (Wilson, 1989). Regardless of the magma series to which they belong (tholeiitic, calc alkaline or shoshonitic) modern rocks produced in these environments are characterized by "spiked" spidergrams. In addition to their "spiked" nature, these spidergrams typically display troughs at Nb and Ta and an enrichment in LILE relative to HFS (Mueller and Wooden, 1988). Troughs at Zr and Hf are commonly observed for subduction-related basalts and may be associated with Th depletion (Thompson *et al.*, 1984).

The "spiked" form of the spidergrams may be due to the addition of a slab-derived component (possibly sedimentary) rich in LILE and LREE to the mantle wedge (Arculus and Powell, 1986). These elements, particularily K, Rb, Ba, Sr and Th, are of low ionic potential and are readily mobilized by a fluid phase (Wilson, 1989). Their enrichment is thought to reflect metasomatism of the mantle wedge from either a water-saturated silicate melt or by fluids released by the subducted dehydrating slab (Best, 1975; Hickey *et al.*, 1986; Arculus and Powell, 1986). It is unclear whether the depletion of HFS elements is; a) the result of their retention within minor residual phases (e.g. titanite, zircon, rutile, ilmenite) in the mantle source, or b) an inherent property of the source region related to remelting of an already depleted mantle source (Pearce, 1982).

The spidergrams of the Mooshla lithologies (figure 30) are very similar to those of modern subduction-related rocks (e.g. compare with Thompson *et al.*, 1984; Mueller and Wooden, 1988). These similarities include the characteristic Nb, Ta, Ti and Zr, Hf troughs as well as LILE enrichment relative to HFS elements. This strongly suggests a subduction process was involved in the genesis of the Mooshla parental magma.

Ridley and Kramers (1989) propose that a worldwide mafic magma or magma layer exhisted beneath the continents. Fractional crystallization of this magma layer then generated the Archean tonalites. Although plausible, this model would be expected to produce voluminous cumulates which have yet to be recognized in the Archean (Weaver and Tarney, 1981). In addition, it is not clear wether this model presupposes the existence of plate-tectonic processes.

5.4.3 Nature of the source material

Having reasonably established a subduction component to the source area during genesis of the Mooshla parental magma, it is possible to place constraints on the nature of the source material. The Mooshla intrusion is geochemically similar to a number of Archean tonalites (e.g. Arth *et al.*, 1978; Jahn *et al.*, 1981; Jemielita *et al.*, 1988). Archean tonalites are generally thought to be derived from partial melting of a mafic rather than a peridotitic rock (Taylor and Rudnick, 1987). A peridotitic source yields partial melts that have a higher Mg#, significantly higher Cr and Ni contents as well as lower LILE and HREE abundances (Shirey and Hanson, 1989). Three types of mafic materials have been proposed in the literature: 1) amphibolite (± garnet), 2) mafic garnet granulite and 3) eclogite (Martin, 1987; Rudnick and Taylor and references therein, 1987). Distinguishing between these three possible sources relies largely on REE data.

Following Gromet and Silver (1983), the REE characteristics of a melt will be determined very early on in its crystallization history. Magmas which are subsequently drawn off this source, assuming no appreciable crustal assimilation, will inherent its REE profile and be, in effect, "fingerprinted". Therefore, the similar REE profiles of the Mooshla intrusion reflect those of its parental magma. The quartz diorites have not undergone fractional crystallization and probably represent the initial bulk composition of the intrusion (see section 5.4.3.3). Their REE profiles should therefore approximate those of the source region. Accordingly, this parental magma was LREE enriched ($[La/Yb]_N$ 7.63) with a flat HREE profile ($\approx$ 15-20 x chondrite).

Archean tonalites and trondhjemites (ATT) typically exhibit significant LREE enrichment and HREE depletion (Taylor and McLennan, 1987). On a $[La/Yb]_N$ vs Yb_N plot, the ATT define a field distinguished by high $[La/Yb]_N$ ratios (5 to > 150) and low Yb_N ($0.3 < Yb_N < 8.5$) (figure 31) (Martin, 1986). In contrast, the lithologies of the Mooshla intrusion, with the exception of the mesocumulate gabbros, plot well outside the ATT field. The lower $[La/Yb]_N$ ratios of the Mooshla lithologies reflect in large part their much higher Yb_N. Garnet strongly fractionates HREE relative to LREE (Henderson, 1984). Its presence as a restite phase in the mantle during partial melting has frequently been invoked to account for the highly fractionated REE patterns of ATT (Martin, 1987; Rudnick and Taylor, 1987). The high Yb_N content, flat HREE pattern, $[Tb/Yb]_N$ ratio near unity and lower $[La/Yb]_N$ ratios of the non-cumulate Mooshla lithologies suggest that garnet was not prominent in the

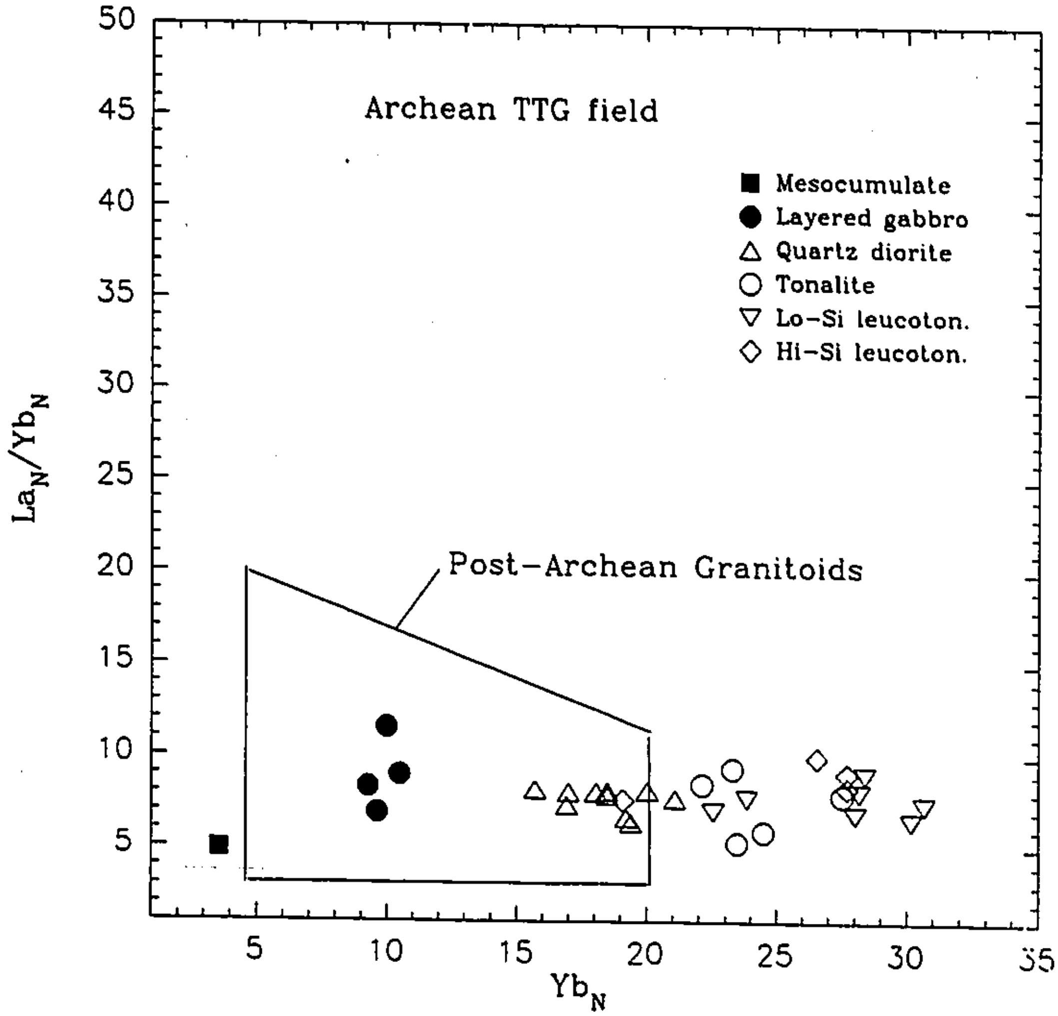

Figure 31: $(La/Yb)_N$ vs Yb_N diagram for the lithologies of the Mooshla intrusion. Limits of fields after Martin (1986) for Archean tonalite-trondhjemite and post-Archean granitoids.

source residue. Therefore garnet-bearing amphibolite, mafic garnet granulite and eclogite do not appear to represent the partial-melt source material. The REE characteristics of the Mooshla intrusion are more consistent with derivation from an garnet-free amphibolite source (e.g. Jahn *et al.*, 1981). Amphibole fractionates HREE relative to LREE but is unable to fractionate the HREE relative to one another (Henderson, 1984). Therefore partial melting of an amphibolite source will always produce characteristic flat HREE and enriched LREE patterns (Arth *et al.*, 1978; Henderson, 1984; Rudnick and Taylor, 1987).

The cumulate gabbros represent the residual phases formed during fractional crystallization of a quartz dioritic magma to produce the tonalites (section 5.4.3.3). Their sloped HREE profiles and low Yb_N content may indicate the presence of either; a) garnet in the the source residue, or b) clinopyroxene within the cumulate sequence itself. Due to the absence of a HREE (in particular Yb) depletion within the initial magma from which the cumulates precipitated (quartz dioritic in bulk composition), the latter explanation is likely more probable.

Martin (1987) and Rudnick and Taylor (1987) have modelled various degrees of partial melting for a tholeiite transformed into garnet-free amphibolite with chondritic REE values. Their models successfully reproduce the range in REE profiles exhibited by the the least fractionated intrusive and extrusive rocks (i.e. the quartz diorites and basal sequence volcanics). By way of example, 20% equilibrium partial melting of a garnet-free amphibolite composed of 34% plagioclase and 66% hornblende will produce REE patterns having $[La/Yb]_N = 6.6$ and $Tb_N/Yb_N = 1.0$. These ratios are in good agreement with those observed for the quartz diorites ($[La/Yb]_N = 7.63$; $[Tb/Yb]_N = 1.2$). The reader is referred to papers by Martin (1987) and Rudnick and Taylor (1987) for a thourough treatment and complete explanation of the modelling process.

5.4.4 Post emplacement evolution of the Mooshla intrusion

5.4.4.1 Introduction

The Mooshla intrusion is reversely zoned with a tonalitic rim and a quartz diorite core (section 2.8.1). This is interpreted as representing multiple pulses of magma (see below). The processes which governed the magmatic evolution of each magma pulse can be well constrained by geological, petrological and geochemical data. Differentiation of the first phase was largely through fractional crystallization whereas the dominant process operative during evolution of the second phase was equilibrium crystallization. The lack of structures associated with magma mixing suggests that little physical overturn occurred between the two magmas. The geochemical characteristics of the two pulses indicates that they were issued from the same magma that was undergoing fractionation through fractional crystallization. The following sections presents the detailed evolution of each pulse and discusses the nature of the mineralogical phases that governed fractionation.

5.4.4.2 The primary pulse: The tonalites and cumulate gabbros

The first magmatic pulse produced the rocks which border the intrusion. With some notable exceptions, these are tonalitic and gabbroic. The exceptions are; *a*) to the south where the tonalite has been uplifted, sheared and hydrothermally altered to form a leucotonalite and *b*) at the extreme western limit where there is a small window of quartz diorite.

Cumulates developed during periods of cooling from essentially stagnant melts are good evidence of closed system fractional crystallization (Sparks *et al.*, 1984). It is therefore important to establish their genetic relationship to the tonalites. The layered cumulates are *in situ* as evidenced by their well preserved fine-scale rhythmic banding and cyclic units. They are juxtaposed against the tonalites wherever outcrop control exists. These contacts are not significantly deformed which indicates that the relationships are primary. Their average Ni and Cr contents resemble those of the tonalites and are significantly lower than the Ni and Cr contents of the quartz diorites (Table 5.2). Similarily, the high P_2O_5 content of the cumulates are reflected in the tonalites and not the quartz diorites. These features strongly suggest that the layered cumulates and the tonalites are genetically related; they represent the solid phases extracted from the melt that produced the tonalites.

The linear trends that join the tonalites and cumulate gabbros on Harker and trace element diagrams are consistent with, among other processes, fractional crystallization (figures 18 through 24). A notable feature on these diagrams is the silica gap from SiO_2 51.5 to 57.5 wt.%. The initial bulk composition of the primary liquid fell within this gap. Fractionation and removal/crystal settling of the mafic phases during cumulate formation, drove the system towards a more silica-rich composition and enriched the melt in incompatible elements. Fractional crystallization is further suggested by the subparallel nature of the REE profiles for both the cumulates and the tonalites.

It is possible to place constraints on the nature of the fractionating phases that controlled REE distribution within the differentiating primary magmatic pulse. The tonalite REE profiles exhibit LREE enrichment ($[La/Yb]_N$ = 7.39), flat HREE profiles and lack of a well developed Eu anomaly. These profiles are typical of fractional crystallization dominated by removal of hornblende (Arth, 1979; Jahn *et al.*, 1981, Martin, 1987). This is consistent with the textural and chemical evidence which suggests that hornblende may be a primary cumulus phase in the layered gabbros (section 3.8). Cumulate rocks with a large hornblende component should show a HREE content similar to the primary magma and LREE contents that are lower than the magma (Arth *et al.*, 1978). The layered gabbros exhibit such patterns relative to a primary magma that was quartz dioritic in composition (see below). Note that the sloped nature of the HREE profiles in the cumulate gabbros suggest some degree of clinopyroxene fractionation occurred. In contrast, the flat HREE patterns of the tonalites indicates that clinopyroxene was no longer on the liquidus by the time of their crystallization. The much lower REE contents of the mesocumulate gabbros relative to the layered gabbros reflect the absence of cumulate apatite.

If hornblende was a primary liquidus phase, there are important implications as to the initial composition of the melt. Experimental studies of granitic systems indicate that for intermediate calc-alkaline rocks, the presence of hornblende may be an indicator of relatively high fH_2O of the primary magma (Naney, 1983). Specifically, in a granodiorite system at 2 kbar, hornblende requires a minimum of approximatly 4 wt.% H_2O, whereas in the same system at 8 kbar the H_2O minimum requirement decreases to 2.5 wt.% (Naney, 1983). While the initial bulk composition of the Mooshla intrusion was probably similar to a quartz diorite, it clearly achieved water saturation by the time tonalite crystallized as evidenced by the micrographic and vermicular textures in the tonalite (Coleman and Donato, 1979). Apatite is ubiquitous throughout the tonalite and occurs as bands within the layered cumulates. Its high concentration is further evidence of the water-rich nature of this phase. Tonalite (along with the low-silica leucotonalite) is the second most areally important unit of the intrusion at the present level of erosion. This indicates that a substantial portion of the magma was water saturated and implies that the primary magma was initially relatively hydrous.

5.4.4.3 Magma replenishment; The quartz dioritic pulse

Quartz diorite occupies the axial region of the pluton and breaches the tonalite rim along the western intrusive contact. These lithologic relationships clearly indicate the secondary nature of this pulse (Bourne and Danis, 1987). The quartz diorites are remarkable for their textural and geochemical homogeneity. They occur over a restricted silica range from 54.5 to 57.5 wt.% SiO_2 and plot generally as a tight to semi-tight cluster on all Harker variation diagrams (section 5.1.1). These features are consistent with equilibrium crystallization. If the quartz diorite pulse underwent fractional crystallization, the development of a cumulate sequence could be expected. In this regard, the possible genetic relationship between the mesocumulates and the quartz diorites should be evaluated. Although both have high Cr, Ni and low P_2O_5 contents, their contact relationship is very poorly constrained. The high transition metal and low P_2O_5 content of the mesocumulates does not preclude them being derived from the tonalites; it may simply reflect their primitive character. A genetic relationship between the mesocumulates and the quartz diorites is therefore speculative. However, this does not prevent the existence of a quartz diorite cumulate sequence at depth.

The REE profiles of the quartz diorites are characterized by LREE enrichement ($[La/Yb]_N$ = 7.63) and flat HREE ($[Tb/Lu]_N$ = 1.2). These are almost identical to the REE profiles of the tonalites and strongly suggests that both magmatic pulses are derived from the same parental magma. Based on the flat HREE profiles of both units, the parental magma may have undergone hornblende controlled fractional crystallization.

5.5 Discussion

5.5.1 Considerations for the multi-pulse model

The quartz diorites were emplaced after the first magma pulse differentiated to form tonalites and cumulate gabbros. The lack of magma mixing structures (section 2.8.1) suggests that this second pulse did not mix with the first. This may reflect the solidified to semi-solidified (?) nature of the primary pulse by the time of replenishment. It is therefore odd that no quartz diorite dykes or net vein structures reflecting the second pulse are observed within either the tonalites or cumulate gabbros. Furthermore, the temporal aspects of cooling and differentiation with respect to the magmatic pulses has not been evaluated. The time necessary to fractionate and solidify the primary pulse prior to replenishment implies that the source magma reservoir may have been very long.

5.5.2 La/Sm ratios

The increase in La_N/Sm_N ratio from the cumulate gabbros to the tonalites may be due to a combination of factors. As the silica content of a magma increases, the hornblende partition coefficient for Sm increases relative to that of La (Higuchi and Nagasawa, 1969; Arth *et al.*, 1978). This would cause progressive enrichment of La in the residual liquid thus increasing the La_N/Sm_N ratio. Alternatively, the K_D^{Sm} for apatite is marginally higher than that of La (Henderson, 1984; Irving and Frey, 1984). Therefore the increase in modal apatite with differentiation observed during petrographic study would have a similar effect on the La_N/Sm_N ratio.

5.5.3 Europium

The development of a negative Eu anomaly with increasing differentiation is commonly observed in plutonic and volcanic suites and is typically ascribed to early removal of Eu during plagioclase formation. When this is observed, there is usually a positive Eu anomaly within the more mafic equivalents. However, the mesocumulate and layered gabbros display virtually no evidence of a positive Eu anomaly, despite their plagioclase-rich nature. This is unusual, particularly given the clearly plagioclase-rich (originally anorthite) character of the mesocumulate gabbros. The lack of a Eu anomaly may be due to; a) high oxidation condition of the Mooshla magma causing Eu^{2+} to assume a Eu^{3+} valency hindering its ability to substitute in the Ca^{2+} site of plagioclase (Drake 1975), or b) liberation of Ca^{2+} during plagioclase sausseritization (formation of the metamorphic mineral assemblage albite+epidote+chlorite+quartz) causing loss of Eu^{2+}.

5.5.4 High-silica leucotonalites

The geochemical and petrological data indicate that the high-silica leucotonalite has undergone extensive hydrothermal alteration and deformation. The alteration is dominated by extensive introduction of silica, alkalies (K_2O and Na_2O) and S. The high field strength elements Zr, Y and Ti were mobile to varying degrees. Similarily, the abundances of the transition elements Cr, Ni and Co as well as LILE (Th, U, Hf) are high relative to the other lithologies. A note of caution is therefore warranted when interpreting the REE_N profiles of this sub-unit as even the REE were probably mobile to some extent. As such, although the REE_N data would suggest a common protolith to both the high and low-silica leucotonalites, these data are not conclusive. The location of this unit along the margin of the intrusion is consistent with a tonalite protolith.

5.6 Summary

The Mooshla intrusion is of calc-alkaline affinity and resembles the high-Al_2O_3 type continental tonalite trondhjemite of Barker and Arth (1976). Geological, petrological and geochemical observations are consistent with evolution through a two stage magma emplacement process. The first pulse fractionally crystallized to produce a tonalite and gabbroic cumulates. The second magma pulse was confined to the core of the intrusion and only locally breached the rim. It evolved primarily through equilibrium crystallization and produced the quartz diorites. The intrusion is therefore reversely zoned. Trace element and, to a lesser extent, major element data provides good evidence that the tonalite is the protolith of the low-silica leucotonalite. Intense alteration characterizes the high-silica leucotonalites and is reflected in the mobility of SiO_2, alkalies, HFS elements and transition elements.

The lithologies display increasing REE_N content with degree of differentiation. With one exception (mesocumulate gabbros), they are significantly LREE enriched (66 to 265 x chondrite) with unit averaged $[La/Yb]_N$ ratios ranging from 7.38 to 8.92. HREE are moderatly enriched at 9 to 30 x chondrite and exhibit relatively flat patterns with Tb/Lu ratios that range from 1.01 to 1.41 for the non-cumulate rocks. The cumulate gabbros, unlike all other lithologies, display a moderatly sloped HREE profile with $[Tb/Lu]_N$ ratios of ≈ 2. Fractional crystallization involving removal of hornblende and probably pyroxene is consistent with the REE_N profiles of the primary magmatic pulse. The presence of hornblende on the liquidus possibly from the onset of crystallization implies that the primary magma pulse was relatively hydrous. The lack of a Eu anomaly within any phase of the intrusion may indicate that the parental magma was oxidized.

The Mooshla intrusion is comagmatic with the host Upper Blake River Group calc-alkaline volcanic rocks. Trace element and REE data are consistent with parental magma derivation through partial melting of a tholeiite transformed into a garnet-free amphibolite in a subduction environment. Linear variations in major elements, selected trace elements and REE of both the intrusive and extrusive rocks indicate that evolution of their parental magma was dominated by fractional crystallization and may have led to the development of a zoned magma chamber.

CHAPTER 6: CONCLUSIONS AND FURTHER WORK

6.1 Conclusions

This study complements existing work in the Bousquet Mining Centre by contributing to the established geological database, and therefore furthering our understanding of an economically important area. Detailed information has been provided on the geographic distribution, lithologic relationships, petrography, and major, trace and rare-earth element chemistry of the mappable units as well as the tectonic setting, petrogenesis and strain fabrics for the Mooshla area and intrusion. The following are the principal conclusions of the thesis:

1) Geological mapping has established that the Mooshla intrusion is a reversely zoned, composite body comprised of four distinct units. These are 1) cumulate gabbros, 2) quartz diorites, 3) tonalites (micrographic) and 4) leucotonalites. The first three units are only weakly deformed and preserve many primary igneous fabrics. In contrast, the leucotonalite is significantly deformed and altered.

2) Field evidence suggests that the Mooshla was emplaced as a sub-concordant body from at least two pulses of magma. The lack of textural evidences typical of magma mixing implies that the primary pulse had, to some degree, solidified prior to magma replenishment

3) Textural and chemical evidences as well as geographic considerations strongly suggest that the leucotonalite is the hydrothermally altered and sheared equivalent of the tonalite. The leucotonalite is comprised of two sub-units; 1) phyllonitic leucotonalite which exhibits numerous strain fabrics and 2) "porphyritic" leucotonalite which is texturally heterogenous

with negligible strain fabrics.

4) The intrusion records four generations of deformation-related structures. S_1, related to D_1, is a shallowly southward dipping foliation localized in the core of the intrusion. It is not reported elsewhere within the BMC. The principal deformation event was D_2 expressed by a foliation, S_2. It represents the principal plane of flattening in the Mooshla area and therefore is the equivalent of the S_1 foliation described by Tourigny *et al.* (1988) for the central part of the BMC. D_3 structures include a spaced cleavage, S_3 and a crenulation cleavage, S_{3c}. S_3 trends north-south and is frequently host to sulphide bearing quartz veins (e.g. Doyon Mine west zone). D_4 structures are kink bands and record late, E-W directed layer-parallel shortening.

5) A wide zone of high strain, The Southern Mooshla Shear Zone (SMSZ) has been identified. The SMSZ is a first order shear which extends over the southern third of the intrusion (by area) and is hosted entirely within the leucotonalite. Ls-tectonites of the SMSZ record dominantly reverse-oblique movement. The intensity of hydrothermal alteration is heterogenous throughout the SMSZ and is characterized by mobility of SiO_2, alkalies, Cr and Ni as well as some HFS elements.

6) There is a structural asymmetry to the intrusion. Intense fabric development and alteration associated with the SMSZ characterize the southern margin. In contrast, the northern margin is characterized by a narrow, laterally discontinuous high strain zones that exhibit a restricted (<2m) chloritic alteration envelope. These narrow high strain zones are classified as second order shears. The core of the intrusion is noted for its lack of shears.

7) The second order shears along the northern intrusion margin record complex movement histories involving initially subvertical movement followed by a component of dextral shear. In many cases, the initial movement along the shears was normal dip-slip.

8) The Mooshla intrusion is of calc-alkaline affinity and is comagmatic with the host upper Blake River Group (BRG) volcanic and volcaniclastic rocks. It is located along the tholeiitic to calc-alkaline transition in the BRG. A comparison of trace element systematics between the intrusion and the host BRG suggests that they may have tapped different levels in a zoned parental magma chamber.

9) The lithologies exhibit highly fractionated REE profiles with high $[La/Yb]_N$ and generally flat HREE ($[Tb/Lu]_N \approx 1$-2). Zr/Y ratios tend to increase with differentiation whereas Th/U and Y/Yb remain essentially the same. Trace element geochemistry indicates that both pulses of magma were derived from a common source.

10) Extended trace element diagrams are consistent with a subduction related environment being the tectonic setting in which the parental Mooshla magma was generated. Rare-earth element data suggests that the source material for the intrusion was a garnet-free amphibolite.

11) The intrusion was formed through a two-stage process. The primary magmatic pulse differentiated through fractional crystallization and produced the tonalites with their associated cumulate gabbro sequence. A second magma pulse replenished the intrusion and apparently did not mix with the first. This second pulse remained in the axial region of the intrusion and underwent equilibrium crystallization to form the quartz diorite.

12) Significant gold mineralization interior to the intrusion (e.g. Mooshla A, Doyon West zone) is confined to the SMSZ and is typically associated with dilatant brittle structures that overprint the regional ductile deformation fabric (D_2). In contrast, gold mineralization in foliation-parallel second order shears located along the northern intrusion margin is generally of low grade and lenticular in form (e.g. Zone de Contact). This difference in mineralization scales probably reflects the much more permeable nature of the large SMSZ to auriferous fluids relative to the poorly interconnected (therefore less permeable) second order shears of the Zone de Contact.

6.2 Further Work

Having established during the course of this study the geological, structural and bulk geochemical framework of the Mooshla intrusion, the following is a list of additional work that may aid in further constraining the relationships of the intrusion to the host rocks, the sequence igneous events in the area and/or the timing and nature of the mineralization.

1) Age dating: Both the quartz diorite and in particular the tonalite contain large, subhedral zircon that appear amenable to U-Pb dating. In general, there is a paucity of high-quality age dates for intrusives along the southern marging of the Québec portion of the Abitibi greenstone belt. An age determination would provide important data as to the temporal development of the eastern limit of the BRG, as well as conclusively define the comagmatic relationship of the host rocks to the intrusion.

2) This study has shown that the tonalite probably represents the leucotonalite protolith. An

alteration study would therefore be warranted to document the nature of the hydrothermal fluids which permeated throughout the SMSZ. The leucotonalites have a high LILE content (in particular K) relative to the hypidiomorphic-granular units of the intrusion. This alteration signature may form part of the district wide pre-tectonometamorphic alteration documented by Marquis *et al.*, (1990). Alternatively, the alteration may be due to late-stage fluids associated with auriferous mineralization subsequent to cratonization (e.g. Fyon *et al.*, 1989).

REFERENCES

Abbey, S., 1983: Studies in "standard samples" of silicate rocks and minerals 1969-1982. Geological Survey of Canada Paper **83-15**, 114p.

Anders, E. and Grevess, N., 1989: Abundances of the elements: Meteoritic and solar. Geochimica et Cosmochimica Acta, **53**, pp. 197-214.

Arculus R.J. and Powell, R., 1986: Source component mixing in the regions of arc magma generation. Journal of Geophysical Research, **91**, No. B6, pp. 5913-5926.

Arth, J.G., 1979: Some trace elements in trondhjemites - their implications to magma genesis and paleotectonic setting. *In* Trondhjemites, dacites and related rocks. *Edited by* F. Barker. Elsevier, Amsterdam, The Netherlands, pp. 401-414.

---------, Barker, F., Peterman, Z.E. and Friedman, I., 1978: Geochemistry of the gabbro-diorite tonalite-trondhjemite suite of southwest Finland and its implications for the origin of tonalitic and trondhjemitc magmas. Journal of Petrology, **19** (2), pp. 299-316.

--------- and Barker, F., 1976: REE partitioning between hornblende and dacitic liquid and implications for the genesis of trondhjemitic-tonalitic magmas. Geology, **4**, pp. 534-536.

Barker, F. and Arth, J.G., 1976: Generation of trondhjemitic-tonalitic liquids and Archean bimodal trondhjemite-b asalt suites. Geology, **4**, pp. 596-600.

Best, M.G., 1975: Migration of hydrous fluids in the upper mantle and potassium variation in calc-alkaline rocks. Geology, **3**, pp. 429-432.

Bickle, M.J., 1978: Heat loss from the Earth: Constraints on Archean tectonics from the relationship between geothermal gradients and the rate of plate production. Earth and Planetary Science Letters, **40**, pp. 301-315.

Blackburn, C.E., 1980: Towards a mobilist tectonic model for part of the Archean of NW Ontario. Geoscience Canada, **7**, pp. 64-72.

Bourne, J. and Danis, D., 1987: A proposed model for the formation of reversely zoned plutons based on a study of the Lacorne Complex, Superior Province, Québec. Canadian Journal of Earth Sciences, **24**, pp. 2506-2520.

Burrows, D.R. and Spooner, E.T.C., 1989: Relationships between Archean gold quartz vein-shear zone mineralization and igneous intrusions in the Val d'Or and Timmins areas, Abitibi Subprovince, Canada. *in* The Geology of Gold Deposits: the Perspective in 1988, R. Keays, W.R.H. Ramsay and D. Groves eds. Economic Geology Monograph **6**, pp. 424-444.

Cameron, E.M. and Hattori, K., 1987: Archean gold mineralization and oxidized hydrothermal fluids. Economic Geology, **82**, pp. 1177-1191.

Card, K.D., and Ciesielski, A., 1986: Subdivisions of the Super.or Province of the Canadian Shield. Geoscience Canada, **13**, pp. 5-13.

Colvine, A.C. 1989: An empirical model for the formation of Archean gold deposits: Products of final cratonization of the Superior Province, Canada. *in* The Geology of Gold Deposits: the Perspective in 1988, R. Keays, W.R.H. Ramsay and D. Groves eds. Economic Geology Monograph **6**, pp. 37-53.

Cooke, D.L. and Moorhouse, W.W., 1969: Temiskaming volcanism in the Kirkland lake area, Ontario, Canada. Canadian Journal of Earth Science, **6**, pp. 117-132.

Cousineau, P. 1982: Campagne d'exploration été-automne 1981. Projet Mouska, 11-829, rapport interne, SOQUEM, 57 p.

Cox, K. G., Bell, J. D., and Pankhurst, R. J., 1979: The Interpretation of Igneous Rocks. George Allen and Unwin, London. 450p.

Davis, G. H., 1984: Structural Geology of Rocks and Regions. John Wiley and Sons, Inc. New York, New York. 492p.

Deer, W.A. Howie, R.A. and Zussman, J., 1966: An Introduction to the Rock Forming Minerals, Longman Group Limited, Harlow, 528p.

Devaney, J.R., and Williams, H.R., 1989: Evolution of an Archean subprovince boundary: A sedimentological and structural study of part of the Wabigoon-Quetico boundary in northern Ontario. Canadian Journal of Earth Sciences, **26**, pp. 1013-1026.

Dewit, M.J., Armstrong, R., Hart, R.J., and Wilson, A.H., 1987: Felsic igneous rocks within the 3.3 to 3.5 Ga Barberton Greenstone Belt: High crustal level equivalents of the surrounding tonalite-trondhjemite terrain, emplaced during thrusting. Tectonics, **6**, pp. 529-549.

Dimroth, E., Cousineau, P., Leduc, M., and Sanschagrin, Y., 1979: Flow Mechanisms of Archean Subaqueous Basalt and Rhyolite Flows; p. 207-211 *in* Current Research, Part A., Geological Survey of Canada Paper 79-1A.

----------, Imreh, L., Rocheleau, M. and Goulet, N. 1982: Evolution of the south-central part of the Archean Abitibi Belt, Quebec. Part I: Stratigraphy and paleogeographic model. Canadian Journal of Earth Sciences, **19**, pp. 1729-1758.

----------, Imreh, L., Goulet, N. and Rocheleau, M., 1983: Evolution of the south-central segment of the Abitibi Belt, Quebec. Part III: Plutonic and metamorphic evolution and geotectonic model. Canadian Journal of Earth Sciences, **20**, pp. 1374-1388.

----------, Rocheleau, M., Mueller, W., Archer, P., Brisson, H., Fortin, G., Jutras, M., Lefebvre, C., Piché, M., Pilote, P., and Simoneau, P., 1985: Paleogeographic and paleotectonic response to magmatic process: a case history from the Archean sequence in the Chibougamau area, Québec. Geologische Rundschua, **74/1**, pp. 11-32.

Drake, M.J., 1975: The oxidation state of europium as an indicator of oxygen fugacity. Geochemica et Cosmochimica Acta, **39**, pp. 55-64.

Fyon, J.A., Troop, D.G., Marmont, S. and Macdonald, A.J., 1989: Introduction of gold in Archean crust, Superior Province, Ontario - Coupling between mantle-initiated magmatism and lower crustal thermal maturation. *in* The Geology of Gold Deposits: the Perspective in 1988, R. Keays, W.R.H. Ramsay and D. Groves eds. Economic Geology Monograph **6**, pp. 479-490.

Gaudreau, R., 1986: Intrusion Syn-Volcanique et Minéralisations Aurifères. Exemple du Pluton de Mooshla, Canton de Bousquet, Abitibi. Thèse de Maitrise, non-publiée, Université de Laval, Québec, Québec (unpubl).

Gélinas, L., Brooks, C., Perrault, G., Carrigan, J., Trudel, P. and Grasso, G., 1977: Chemostratigraphic divisions within the Abitibi volcanic belt, Rouyn Noranda district, Quebec. *in* Volcanic regimes in Canada, W.R.T. Baragar, L.C. Coleman and J. M Hall, eds. Geological Association of Canada, Special Paper 16, pp. 265-295.

---------, Trudel, P., and Hubert, C., 1984: Chemostratigraphic division of the Blake River Group, Rouyn-Noranda area, Abitibi, Quebec. Canadian Journal of Earth Sciences, **21**, pp. 220-231.

Giachino, D.M., 1936: Summary reports; Mooshla Gold Mines Co. Ltd., internal report.

Gill, J.B., 1981: Orogenic Andesites and Plate Tectonics. Springer-Verlag, Berlin. 358 p.

Goldie, R., 1978: Magma mixing in the Flavrian pluton, Noranda area, Quebec. Canadian Journal of Earth Sciences, **15**, pp. 132-144.

Gorman, B.E. 1986: The Bousquet-Cadillac district, *in* J. Pirie and M.J. Downes eds., Excursion Guidebook: Gold'86, Toronto. pp.78-90.

Gromet, L.P. and Silver, L.T., 1983: Rare earth element distributions among minerals in a granodiorite and their petrogenetic implications. Geochimica and Cosmochimica Acta, **47**, pp. 925-939.

Guha, J., Gauthier, A., Vallée, M., Descarreaux, J., and Lange-Bard, F., 1982: Gold mineralization patterns at the Doyon Mine (Silverstack), Bousquet, Québec, *in* R.W. Hodder and W. Petruk, eds: Geology of Canadian Gold Deposits. Canadian Institute of Mining and Metallurgy Special Volume No. 24, pp 50-57.

Gunning, H.C., 1941: Bousquet-Joannes area, Quebec. Geological Survey of Canada Memoir 231, 110p.

Haggerty, R., 1976: Oxidation of opaque mineral oxides in basalts. *in* Oxide Minerals, D. Rumble III ed. Mineralogical Society of America, Reviews in Mineralogy, **3**, pp. Hg1-Hg100.

Hargraves, R.B., 1986: Faster spreading or greater ridge length in the Archean? Geology, **14**, pp. 750-752.

Helz, R.T., 1973: Phase relations of basalts in their melting range at P_{H_2O}=5 kb as a function of oxygen fugacity. Part I; Mafic phases. Journal of Petrology, 14, pp. 249-302.

Henderson, P., 1982: Inorganic Geochemistry, Pergamon Press, Oxford. 353p.

------------, 1984: General geochemical properties and abundances of the rare earth elements. *In* Developments in Geochemistry part 2: Rare earth element geochemistry. *Edited by* Paul Henderson. Elsevier, Amsterdam, The Netherlands. pp. 1-32.

Hickey, R.L., Frey, F.A., Gerlach, D.C. and Lopez-Escobar, L., 1986: Multiple sources for basaltic arc rocks from the southern volcanic zone of the Andes (34°-41°S): Trace element and isotipic evidence for contributions from subducted oceanic crust, mantle and continental crust. Journal of Geophysical Research, 91, No. B6, pp. 5963-5983.

Higuchi, H., and Nagasawa, H., 1969: Partition of trace elements between rock forming minerals and the host volcanic rocks. Earth and Planetary Science Letters, 7, pp.281-287.

Hobbs, B.E., Means, W.D. and Williams, P.E., 1976: An Outline of Structural Geology. John Wiley and Sons, New York. 577 p.

Hodgson, C.J. and MacGeehan, P.J., 1982: A review of the geological characteristic of "gold only" deposits in the Superior province of the Canadian shield: Canadian Institute of Mining and Metallurgy Special Volume 24, pp. 211-228.

Hodgson, C.J., 1989: Patterns of Mineralization, *in* Bursnall, J.T. ed., Mineralization and Shear Zones: GAC Short Course Notes, Volume 6, pp. 51-88.

------------, and Hamilton, J.V., 1989: Gold mineralization in the Abitibi greenstone belt: End-stage result of Archean collisional tectonics? *in* Reid R. Keays, W.R.H. Ramsay and David I. Groves, eds., The Geology of Gold Deposits: The Perspective in 1988. Economic Geology Monograph 6, pp. 86-100.

Hubert, C. and Marquis, P., 1989: Structural framework of the Abitibi greenstone belt of Quebec and its implications for mineral exploration. *in* Bursnall, J.T. ed., Mineralization and Shear Zones: GAC Short Course Notes, Volume 6, pp. 219-225.

Huddleston, P.J., Schultz-Ela, D., and Southwick, D.L., 1988: Transpression in an Archean greenstone belt, northern Minnesota. Canadian Journal of Earth Sciences, 25, pp. 1060-1068.

Hyde, R.S., 1980: Sedimentary facies in the Archean Timiskaming Group, and their tectonic implications, Abitibit greenstone belt, north-eastern Ontario, Canada. Precambrian Research, 12, pp. 161-196.

Imreh, L., 1984: Sillon de LaMotte-Vassan et son avant-pays méridional: synthèse volcanologique, litho-stratigraphique et gîtologique. Ministère de l'énergie et des ressources, Québec, MM 82-04, 72 p.

Irving, A.J. and Frey, F.A., 1984. Trace element abundances in megacrysts and their host basalts: Constraints on partition coefficients and megacryst genesis. Geochimica et Cosmochimica Acta, **48**, pp. 1201-1221.

Jackson, E.D., 1967: Ultramafic cumulates in the Stillwater, Great Dyke and Bushveld Intrusions. *In* Ultramafic and related rocks, P.J. Wyllie, ed.. John Wiley, New York.

Jahn, B., Glikson, A.Y., Peucat, J.J. and Hickman, A.H., 1981: REE geochemistry and isotopic data of Archean silicic volcanics and granitoids from the Pilbara Block, Western Australia: implications for the early crustal evolution. Geochimica et Cosmochimica Acta, **45**, pp. 1633-1652.

Jemielita, R.A., Callan, N.J. and Spooner, E.T.C., 1988: Petrogenesis of Archean trondhjemite-tonalite-granodiorite (TTG) intrusions and their relationships to gold mineralization, Renabie and Magino areas, Wawa. Ontario Geological Survey Miscellaneous Paper, **140**, pp. 78-93.

Jensen, L.S., 1976: A new cation plot for classifying subalkalic volcanic rocks. Ontario Geological Survey, Miscellaneous Paper, No. 66, 22p.

Jolly, W.T. 1978: Metamorphic history of the Archean Abtibi belt. *in* I.A. Fraser and W.W. Heywood, eds. Metamorphism of the Canadian Shield. Geological Survey of Canada, Paper 78-10, pp. 63-78.

Leake, B.E., 1978: Nomenclature of amphiboles. Canadian Mineralogist, **16**, pp. 501-520.

Kerrich, R. 1989: Geochemical evidence on the sources of fluids and solutes for shear zone hosted mesothermal Au deposits. *in* Bursnall, J.T. ed., Mineralization and Shear Zones: GAC Short Course Notes, Volume 6, pp. 129-197.

Le Maitre, R.W., 1976: The chemical variability of some common igneous rocks. Journal of Petrology, **17**, pp. 589-637.

Ludden, N.J. and Hubert, C., 1986a: The tectonic evolution of the Abitibi greenstone belt of Canada. Geological Magazine, **123** (2), pp. 153-166.

----------, and ---------, 1986b: Geologic evolution of the late Archean Abitibi greenstone belt of Canada. Geology, **14**, pp. 707-711.

MacFie, R. 1989: The Petrology and Mineralogy of the Clinton-Colden gabbro anorthosite intrusion, Slave Province, N.W.T. Unpublished M.Sc. Thesis, University of Ottawa, Ottawa, Ontario. 126p.

Marquis, P., Hubert, C, Brown, A.C. and Rigg, D.M., 1990: An evaluation of genetic models for gold deposits of the Bousquet district, Québec, based on their mineralogic, geochemical and structural characteristics, *in* The Northwestern Quebec Polymetallic Belt. *Edited by* M.Rive, P Verpaelst, Y. Gagnon, J.M. Lulin, G. Riverin and A. Simard. The Canadian Institute of Mining and Metallurgy, Special volume **43**, pp. 383-400.

----------, 1990: Metallogénie des gisements archéens d'Au-Ag-Cu de la mine Donald J. LaRonde (Dumagami), Cadillac, Abitibi, Québec. Thèse de doctorat, publiée, Université de Montréal, Montréal (Québec). 139p.+ appendices

---------- and Hubert, C., 1989: Part II: The Dumagami Structural Zone: its evolution and features for the Doyon, Bousquet nos. 1 and 2, and Donald J. LaRonde gold mines of southwestern Abitibi, Quebec. *in* Bursnall, J.T. ed., Mineralization and Shear Zones: GAC Short Course Notes, Volume 6, pp. 226-238.

Martin, H., 1987: Petrogenesis of Archean trondhjemites, tonalites and granodiorites from eastern Finland: Major and trace element geochemistry. Journal of Petrology, 28, pp. 921-953.

---------- 1986: Effect of steeper Archean geothermal gradient on geochemistry of subduction-zone magmas. Geology, 14, pp. 753-756.

Midra, R., 1987: Rapport de la cartographie détaillée, Projét Mouska (117), Eté 1987. Rapport interne, Cambior Ltée, 34p.

Mills, J.W. 1948: Mic-Mac mine, *in* Structural Geology of Canadian ore deposits; a symposium. Canadian Institute of Mining 50th anniversary Jubilee volume. pp. 803-808.

Mueller P.A. and Wooden, J.L., 1988: Evidence for Archean subduction and crustal recycling, Wyoming province. Geology, 16, pp. 871-874.

Naney, M.T., 1983: Phase equilibria of rock-forming ferrogmagnesian silicates in granitic systems. American Journal of Science, 283, pp.993-1033.

Paradis, S., Ludden, J. and Gelinas, L., 1988: Evidence for contrasting compositional spectra in comagmatic intrusive and extrusive rocks of the late Archean Blake River Group, Abitibi, Quebec. Canadian Journal of Earth Sciences, 25, pp. 134-144.

Parsons, I., 1979: The Klokken gabbro-syenite complex, South Greenland: Cryptic variation and origin of inversely graded layering. Journal of Petrology, 20, pp. 653-694.

Passchier, C.W. and Simpson, C., 1986: Porphyroclast systems as kinematic indicators. Journal of Structural Geology, 8, pp. 831-843.

Pearce, J.A., 1982: Trace element characteristics of lavas from destructive plate boundaries. *In* Andesites: orogenic andesites and related rocks, R.S. Thorpe, ed. Wiley, Chichester, pp. 525-548.

Picard, C., et Piboule, M., 1986: Petrologie des roches volcaniques du sillon de roches vertes archéenes de Matagami - Chibougamau a l'ouest de Chapais (Abitibi est, Québec). 2: Le groupe hautement potassique d'Opémiska. Canadian Journal of Earth Sciences, 23, pp. 1169-1189.

Poulsen, K.H., and Robert, F., 1989: Shear Zones and Gold: Practical Examples from the Southern Canadian Shield. *in* Bursnall, J.T. ed., Mineralization and Shear Zones: GAC Short Course

Notes, **6**, pp. 239-236

Ramsey, J.G., and Huber, M.I., 1987: The techniques of modern structural geology. Volume 2: Folds and Fractures, Academic Press Inc., London, 700p.

Ridley, J.R. and Kramers, J.D. 1989: The evolution and tectonic consequences of a tonalitic magma layer within Archean continents. Canadian Journal of Earth Sciences, **27**, pp. 219-228.

Riverin, G. and Hodgson, C.J., 1980: Wall-rock alteration at the Millenbach Cu-Zn Mine, Noranda, Québec. Economic Geology, **75**, pp.424-444.

Robert, F. 1989: Internal structure of the Cadillac tectonic zone southeast of Val d'Or, Abitibi greenstone belt, Quebec. Canadian Journal of Earth Sciences, **26**, pp. 2661-2675.

Rosen-Spence (de), A.F., 1976: Stratigraphy, volcanic history and chemistry of Archean volcanic rocks in the Noranda area, Quebec. Unpublished Ph.D. thesis, University of Toronto.

Rudnick, R.L. and Taylor, S.R., 1987: Geochemical constraints on the origin of Archaean tonalitic trondhjemitic rocks and implications for lower crustal composition. *in* The Nature of the Lower Continental Crust, J.B. Dawson, D.A. Carswell, J. Hall and K.H. Wedepohl eds. Geological Society Special Publication No. 24, pp. 179-191.

Sanderson , D.J. and Marchini, W.R.D. 1984: Transpression. Journal of Structural Geology, **6**, pp. 449-458.

Savoie, A., Sauve, P., Trudel, P. and Lao, K., (in press): Geologie de la mine Doyon, Cadillac Quebec: Ministère de l'Energie et des Ressources du Quebec.

Savoie, A., Perrault, G., and Filion, G., 1986: Geological setting of the Doyon gold deposits, Bousquet Township, Abitibi, Quebec, Canada, *in*, Macdonald, A.J., ed., Gold '86: Konsult International, Toronto, pp. 97-107.

Shirey, S.B., and Hanson, G.N., 1989: Petrogenesis of mantle-derived, LILE enriched Archean monzodiorites and trachyandesites (sanukitoids) in the southwestern Superior province. Canadian Journal of Earth Sciences, **26**, pp. 1688-1712.

Sibson, R.H., 1977: Fault rocks and fault mechanisms: Journal of the Geological Society of London, **133**, pp. 191-213.

Sibson, R.H., Robert, F., and Poulsen, H., 1988: High angle faults, fluid pressure cycling and mesothermal gold-quartz deposits: Geology, **16**, pp. 551-555.

Sleep, N.H. and Windley, B.F. 1982: Archean plate tectonics: constraints and inferences. Journal of Geology, **90**, pp. 363-379.

Sparks, R.S.J., Huppert, H.E. and Turner, J.S., 1984: The fluid dynamics of evolving magma chambers. Philosophical Transactions of the Royal Society of London, Series A, **310**, pp. 511-534.

Stone, W.E., 1988: Nature and significance of metamorphism in gold concentration, Bousquet township, Abitibi greenstone, belt, northwest Quebec. Unpublished Ph.D. Thesis, University of Western Ontario, London, Ontario. 441p.

----------, 1990: Archean volcanism and sedimentation in the Bousquet gold district, Abitibi greenstone belt, Quebec: Implications for stratigraphy and gold concentration. Geological Society of America Bulletin, **102**, No.1, pp.147-158.

Streckeisen, A., 1976: To each plutonic rock its proper name: Earth Science Reviews, **12**, pp. 1-33.

Sutcliffe, R.H., 1989: Magma mixing in late Archean tonalitic and mafic rocks of the Lac des Iles area, western Superior province. Precambrian Research, **44**, pp. 81-101.

Tarney, J., Dalziel, I.W.D. and De Wit, M.J., 1976: Marginal basin 'Rocas Verdes' complex from S Chile: a model for Archean greenstone belt formation. *In* The Eartly History of the Earth, B.F. Windley ed. Wiley-Interscience, London, pp. 131-146.

Taylor, S.R. and Hallberg, J.A., 1977: Rare-earth elements in the Marda calc-alkaline suite: an Archaean geochemical analogue of Andean-type volcanism. Geochimica et Cosmochimica Acta, **41**, pp. 1125-1129.

----------, and McLennan, S.M., 1985: The Continental Crust: Its Composition and Evolution. Blackwell Scientific, Oxford. 312p.

-----------, & -----------, 1987: The chemical composition of the Archean crust. *in* The Nature of the Lower Continental Crust, J.B. Dawson, D.A. Carswell, J. Hall and K.H. Wedepohl eds. Geological Society Special Publication No. 24, pp. 173-179.

Thompson, R.N., Dickin, A.P., Gibson, I.L. and Morrison, M.A., 1982: Elemental fingerprints of isotopic contamination of Hebridean Palaeocene mantle-derived magmas by Archaean sial. Contributions to Mineralogy and Petrology, **79**, pp. 159-168.

------------, Morrison, M.A., Hendry, G.L., and Parry, S.J., 1984: an assessment of the relative roles of crust and mantle in magma genesis: An elemental approach: Royal Society of London, Philosophical Transactions, **A 310**, pp.549-590.

Toogood, D. J., and Hodgson, C.J. 1985: Structural investigation between Kirkland Lake and Larder Lake gold camps. Ontario Geological Survey, Miscellaneous Paper 127, pp. 200-205

------, 1986: Relationship between gold deposits and tectonic framework of the Abitibi greenstone belt in the Kirklan Lake - Larder Lake area. Ontario Geological Survey, Miscellaneous Paper 130, pp. 79-86.

Tourigny, G., Hubert, C., Brown, A.C. and Crepeau, R., 1988: Structural Geology of the Blake River Group at the Bousquet mine, Abitibi, Quebec; Canadian Journal of Earth Sciences, **25**, pp. 581-592.

-------, 1989: Structural control of gold mineralization at the Bousquet mine, Abitibi, Quebec;

Canadian Journal of Earth Sciences, 26, pp. 157-175

Ujike, O. and Goodwin, A.M., 1987: Geochemistry and origin of Archean felsic metavolcanic rocks, central Noranda area, Quebec, Canada. Canadian Journal of Earth Sciences, 24, pp. 2551-2567.

Valliant, R.I., 1981: The Geologly, stratigraphic relationships and genesis of the Bousquet gold deposit, northwest Québec. Unpublished Ph.D. Thesis, University of Western Ontario, London, Ontario, 323 p.

--------------- and Hutchinson, R.W., 1982: Stratigraphic distribution and genesis of gold deposits, Bousquet region, Northwestern Quebec. *in* Geology of Canadian Gold deposits, R.W. Hodder and W. Petruk, eds. Canadian Institute of Mining and Metallurgy, Special Volume 24. pp. 27-40.

Wager, L.R., and Brown, G. M., 1968: Layered Igneous Rocks. Oliver and Boyd, London. 588p.

Weaver, B.L. and Tarney, J., 1981: Lewisian gneiss geochemistry and Archean crustal development models. Earth and Planetary Science Letters, 55, pp. 171-180.

Wilson, A.D., 1960: A modified scheme for the determination of ferrous iron in rocks. Analyst, 85, pp. 823-827

Wilson, M., 1989: Igneous Petrogenesis. Unwin Hyman, London. 466 p.

Windley, B.F., 1984: The Evolving Continents. 2nd ed. Wiley, Chichester. 399 p.

APPENDIX A: WHOLE ROCK GEOCHEMISTRY

A.1 Sample preparation

Forty-seven whole-rock samples were prepared at the University of Ottawa. Weathered crusts were slabbed-off and a minimum of 3 kg of sample was reduced to chips < 1 cm large in a steel plate jaw crusher. The chips were homogenized and systematically split (homogenization between each split) to arrive at a sample fraction suitable for powdering. The chips were pulverized down to -200 mesh in a tungsten-carbide shatter box. Care was taken at all steps to minimize contamination; samples of same lithologic suite were processed in batches and rock chips were used to pre-contaminate the tungsten-carbide shatter box between each sample. The tungsten-carbide shatter box was run for a minimum of 4 minutes to maximize uniformity of grain size and homogeneity of the sample.

A.2 X-Ray fluorescence spectroscopy

All prepared samples were analyzed for major elements and selected trace elements (Cr, Ni, V, Zn, Nb, Y, Zr, Rb, Sr and Ba) by X-Ray fluorescence spectroscopy (XRF) at the University of Ottawa. A mixture of 1.5 gm of sample + 0.433 gm Li_2CO_3 + 3.9 gm $Li_2B_4O_7$ was first fused for 20 minutes in a platinum crucible. The fused sample was then analyzed on a Philips model PW1410-80 XRF. Calibration curves based on a number of standards were corrected following the LaChance-Traill procedure (LaChance and Traill, 1966).

The analytical precision for the range of major element values in this study are the following: $SiO_2 \pm 1.02\%$; $TiO_2 \pm 1.9\%$; $Al_2O_3 \pm 1.8\%$; $MgO \pm 8.0\%$; $CaO \pm 1.1\%$; $Na_2O \pm 7.9\%$; $K_2O \pm 1.2\%$;

P_2O_5±18%; MnO±0.0%; Fe_2O_3±2.5%. The detection limits for the trace elements Cr, Ni, V, Zn, Nb, Y, Zr, Rb, Sr and Ba were 10 ppm. Values less than 10 ppm are reported as zero. With the exception of Ba, the error is ± 50% for values between 10 and 30 ppm, and ± 10% for values >30 ppm. For Ba, the error is ± 50% for values between 10 and 50 ppm, whereas it is ± 10% for values >50 ppm. Total iron was calculated as Fe_2O_3.

The international standard, DR-N (1), a diorite, was used to test the accuracy of the analytical technique. The following table lists the average of 8 analyses of DR-N (including the first standard deviation), the values for DR-N from Abbey (1983) and the accuracy (in % error (B-A)/B*100).

	A		B	
	DR-N (1); (n=8)		DR-N; Abbey (1983)	% error
	Avg wt.%	Std. Dev.	Avg (wt.%)	(B-A)/B*100
SiO_2	53.20	±0.27	52.98	0.42
Al_2O_3	17.59	±0.16	17.56	0.18
Fe_2O_{3T}	9.66	±0.12	9.72	0.63
MgO	4.25	±0.17	4.41	3.71
CaO	7.02	±0.04	7.07	0.65
Na_2O	3.02	±0.12	3.00	0.67
K_2O	1.71	±0.01	1.70	0.44
MnO	0.22	-----	0.22	0.00
TiO_2	1.05	±0.01	1.09	3.90
P_2O_5	0.22	±0.02	0.25	3.50
	ppm		ppm	
Ba	422	±82.9	390	8.21
Cr	47.75	± 4.12	42	13.69
Ni	22.13	± 4.96	16	38.28
V	222.6	±13.8	230	3.21
Zn	137.8	± 4.92	145	5.00

A.3 Instrumental Neutron Activation Analysis

Instrumental neutron activation analysis (INAA) was completed on 37 samples to determine their rare-earth element La, Ce, Nd, Sm, Eu, Tb, Ho, Dy, Yb and Lu contents. In addition, the following trace elements were analyzed; Th, Hf, U, Co, Ta, Au, Ag and As. Twenty-eight analyses were completed at Activation Laboratories Ltd. of Ancaster Ontario. These samples were irradiated for 20 minutes at a flux of 7 x 10^{12} neutron/cm^2 x sec at the nuclear reactor facility of Michigan University. After one week, samples were counted using a high-purity Ge detector with a resolution of 1.73 KeV (cobalt 60 as standard). The detection limits for the elements are as follows (in ppm): La 0.5; Ce 3.0; Nd 5.0; Sm 0.1; Eu 0.2; Tb 0.5; Yb 0.2; Lu 0.05; Th 0.5; Hf 0.5; U 0.5; Co 1.0; Ta 1.0; Au 5.0; & Ag 5.0.

Nine samples were analyzed for the rare-earth elements La, Ce, Nd, Sm, Eu, Tb, Dy, Ho, Yb and Lu as well as the trace elements Sc, Rb, Ba, Hf, Ta, Th and U at the Ecole Polytechnique (Université de Montréal). Samples were placed in a polyethylene capsule and irradiated for 2 hours under a flux of 10^{12} neutrons/cm^2 x sec in the Slowpoke II reactor of the Université de Montréal. Irradiated samples were counted 5 times over a period of 30 days.

The following table lists the percent error for interlab analyses of the same sample. A.L = Activation Laboratories, E.P. = Ecole Polytechnique.

	MS-54 (ppm)			MS-82 (ppm)		
	A.L. A	E.P. B	% error (B-A)/B*100	A.L A	E.P. B	%error (B-A)/B*100
La	38	38	0	33	32	3.0
Ce	73	80	8.75	64	66	3.03
Nd	40	41.5	3.61	34	34.4	1.16
Sm	6.6	8.06	18.11	6.1	6.58	7.29
Eu	1.9	2.15	11.62	1.7	1.93	11.91
Tb	0.8	1.07	25.23	0.5	0.91	45.05
Dy		5.2	----		4.4	-----
Ho		1.12	----		0.97	-----
Yb	3.23	3.10	4.19	3.0	2.67	12.23
Lu	0.43	0.46	6.52	0.38	0.43	11.62
Th	5.15	6.21	17.06	3.9	4.6	15.22
U	0.9	0.74	21.16	1.1	0.82	34.15
Hf	3.0	3.21	6.25	3.0	2.66	12.78
Sc	25	25	0.00	25	25	0.00

A.4 Ferrous iron determinations

Ferrous iron contents were determined by titration following the procedures outlined by Wilson (1960). Titrations were completed for nearly all the samples of quartz diorites, tonalites and gabbros. Due to persistent problems with decomposing the pyrite in the leucotonalites (3-6 vol.% pyrite), only a few samples of this unit were titrated. To a mixture of 0.2 grams of powdered sample in 5 ml of ammonium vanadate solution were added 10$\pm$1 ml of 40% cold HF acid. After decomposing overnight, ferrous iron is completely oxidized by the ammonium vanadate. To this solution is added 10 ml of ferrous ammonium sulphate solution and 2 ml of barium diphenylamine sulphonate (indicator). Standard potassium dichromate solution was then titrated against the excess pentavalent vanadium for each mixture. The standard SY-3 was used to check the accuracy of the results.

A.5 Loss on ignition (LOI)

Approximately 1 gm of powdered sample was weighed into a fired empty crucible of known weight. This was heated to 120°C for 2 hrs, allowed to cool and then weighed. The difference in the weight of the sample+crucible subsequent to firing relative to pre-firing is the value known as hydroscopic or absorbed water (H_2O^-). The crucible is returned to the oven and heated at 1050°C for 2 hrs and then allowed to cool in a desiccator overnight. The fired sample+crucible is then weighed. The difference relative to the pre-firing weight is know as LOI. The LOI is generally the sum of many factors, some of which are: 1) loss of essential water (H_2O^+), and 2) loss of elements, etc. (e.g. alkali metals, CO_2, fluorine and sulphur oxides). A gain in weight may be observed when ferrous iron is oxidized.

A.6 ANALYSES

The following pages present the whole rock analyses of Mooshla intrusion lithologies and host volcanic rocks. Samples are grouped according to lithology. Major elements in wt.%; trace elements in ppm. The 89 & 90 series of samples were collected by A. Langshur during the course of this study. The m622 series were collected by K. Hattori during a visit to the Doyon mine (22-06-87). Trace element data less than 10 ppm reported as < 10. All Fe is reported as Fe_2O_3 for analyses of both the phyllonitic and porphyritic leucotonalites (see A.4 Fe titrations) and some volcanic rocks. Sample locations on the geological map (see back pocket), are listed without the prefix 89 or 90.

MG= Mesocumulate gabbro; LG= Layered gabbro; QD= Quartz diorite; TON= Tonalite; PHYL= Phyllonitic leucotonalite; PORL= Porphyritic leucotonalite; QPAD= Quartz-phyric aplite dyke; NS= North sector basalts; WS= West sector Basalts; SS= South sector basalts; indicates not analyzed.

Element	89-58 MG	89-31 LG	89-31a LG	89-47 LG	89-SQ LG	89-13 QD	89-15 QD	89-35 QD	89-41 QD	89-42 QD	89-48 QD
SiO_2	45.15	46.82	45.48	43.26	50.48	53.86	52.22	53.84	54.08	54.66	53.08
Al_2O_3	23.38	18.86	17.30	14.87	17.87	17.12	16.93	16.82	17.15	17.34	17.70
Fe_2O_3	3.39	5.45	6.34	8.13	5.11	4.64	3.46	3.44	4.03	2.46	3.49
FeO	2.69	6.09	7.09	9.09	5.71	4.03	5.68	5.03	4.29	5.68	4.99
MgO	5.65	4.37	4.32	5.41	4.51	4.25	3.61	4.16	3.94	3.52	5.73
CaO	14.06	10.07	10.72	10.82	10.59	8.36	8.24	7.98	6.58	6.62	5.27
Na_2O	3.98	2.87	1.87	2.20	2.25	3.20	3.60	3.29	4.05	3.87	4.68
K_2O	0.07	0.28	0.65	0.13	0.86	1.00	0.07	0.67	0.82	0.97	0.34
Ti_2O	0.19	1.48	1.67	2.05	1.02	0.97	1.37	0.89	1.01	1.04	0.90
P_2O_5	0.00	0.49	0.66	1.71	0.13	0.32	0.66	0.24	0.36	0.46	0.31
MnO	0.09	0.20	0.21	0.22	0.15	0.16	0.18	0.13	0.16	0.09	0.16
S	0.01	0.01	0.02	0.01	0.02	0.01	0.01	0.00	0.01	0.06	0.01
LOI	3.90	2.93	4.46	3.08	2.70	2.51	3.46	3.15	3.75	2.58	2.99
TOTAL	102.56	100.01	100.79	100.98	101.4	99.57	99.63	100.02	100.11	99.49	99.81
Ba	85	164	384	40	391	342	56	208	454	288	186
Cr	100	15	27	17	26	39	29	80	57	21	71
Zr	< 10	19	23	21	63	76	72	87	107	106	116
Sr	331	474	526	307	355	436	550	449	323	395	251
Rb	< 10	< 10	16	< 10	16	27	< 10	17	15	29	< 10
Y	< 10	18	20	25	17	31	34	33	33	38	34
Nb	< 10	< 10	< 10	< 10	< 10	< 10	< 10	12	12	15	< 10
Zn	19	75	64	73	43	53	39	40	41	29	55
Ni	60	10	48	15	23	25	45	61	42	15	165
Co	31	33	--	--	--	33	19	27	26	27	31
Sc	16.9	29	35	37.7	27.4	27	21	25	26	21	26
V	96	321	373	498	429	212	178	254	182	172	218
Hf	0.31	1	1	0.71	1.73	2	2	4	3	5	3
Th	0.56	1	1.28	1.28	2.03	3.7	3.2	4.5	3	3.8	4.3
U	0.09	0	0	0.29	0.36	1	0	1.9	0	1	0
Ta	0.41	< 1	< 1	0.55	0.51	1	< 1	< 1	1	< 1	< 1
Au	<5	5	<5	---	---	32	<5	<5	23	<5	6
Ag	<5	<5	<5	---	---	<5	<5	<5	<5	<5	<5
La	4.1	18	22	27	15.5	35	30	29	29	38	34
Ce	9.4	38	46	60	32	71	63	57	56	72	64
Nd	5.8	21	25	37.7	17.1	37	32	28	33	36	31
Sm	1.23	4.0	4.9	7.68	3.27	6.3	6.1	5.3	5.9	7.1	5.7
Eu	0.44	1.4	1.5	2.14	1.14	1.8	1.7	1.6	2.1	2.1	1.4
Tb	0.19	0.7	0.6	0.94	0.53	0.7	0.8	1.1	0.6	<0.5	0.9
Dy	0.94	---	---	4.2	2.6	---	---	---	---	---	---
Ho	0.19	---	---	0.84	0.49	---	---	---	---	---	---
Yb	0.58	1.5	1.70	1.62	1.56	3.0	2.55	2.75	3.15	3.42	3.0
Lu	0.08	0.19	0.22	0.25	0.25	0.41	0.37	0.37	0.44	0.47	0.43

Element	89-52 QD	89-54a QD	89-82 QD	89-90 QD	89-30 TON	89-45 TON	89-50 TON	89-56 TON	89-TR TON	m662-06 TON
SiO_2	54.34	54.22	53.91	54.52	59.01	56.72	60.30	61.00	57.31	58.46
Al_2O_3	17.45	17.29	17.68	16.80	15.17	17.33	16.57	16.86	16.91	16.91
Fe_2O_3	4.98	4.03	3.47	3.46	2.31	4.46	1.20	1.46	4.20	3.28
FeO	4.23	3.57	4.15	5.12	4.74	4.99	2.15	1.63	3.78	3.84
MgO	3.71	4.34	4.94	4.24	2.55	3.54	3.99	3.32	2.82	2.13
CaO	7.13	8.09	8.57	6.91	4.39	5.10	6.30	8.58	5.08	5.17
Na_2O	3.63	3.82	3.27	4.43	4.62	4.91	4.45	5.19	4.32	4.86
K_2O	0.79	0.75	0.88	0.96	1.23	0.48	0.25	0.08	0.60	0.81
TiO_2	1.11	1.02	0.81	0.96	1.01	1.21	1.01	1.00	1.17	1.41
P_2O_5	0.35	0.35	0.24	0.37	0.43	0.60	0.57	0.62	0.53	0.52
MnO	0.16	0.17	0.12	0.13	0.09	0.11	0.07	0.09	0.06	0.08
S	0.00	0.01	0.00	0.00	0.01	0.01	0.02	0.05	0.00	0.05
LOI	2.27	1.71	1.94	2.34	4.65	3.12	2.40	1.68	2.27	1.30
TOTAL	100.29	99.72	99.98	100.17	99.57	102.58	99.38	101.56	99.14	99.13
Ba	287	453	309	343	445	237	144	140	345	407
Cr	37	52	55	48	17	21	30	42	12	22
Zr	88	122	86	136	173	157	181	218	147	202
Sr	370	433	433	337	337	350	366	457	395	408
Rb	19	11	25	36	39	12	< 10	< 10	10	19
Y	33	37	32	32	45	43	49	42	50	35
Nb	< 10	< 10	< 10	< 10	10	< 10	< 10	< 10	< 10	12
Zn	40	33	28	28	17	41	14	17	< 10	14
Ni	26	34	40	22	35	17	19	32	< 10	< 10
Co	38	26	33	25	31	--	23	--	18	--
Sc	25	25	25	27	18	21.8	20	20.6	23	--
V	200	200	210	226	98	102	41	65	105	28
Hf	3	3.2	2.66	4	4	3.71	4.5	5.44	5	---
Th	3	6.21	4.60	3.7	4.3	5.26	7.3	9.21	4.9	---
U	0	0.74	0.82	0	0	1.06	1.2	0.55	0.8	---
Ta	< 1	1.12	0.89	< 1	1	1.12	< 1	1.78	2	---
Au	< 5	5.8	19	< 5	< 5	---	< 5	---	< 5	---
Ag	< 5	< 5	< 5	< 5	< 5	---	< 5	---	< 5	---
La	34	38	32	30	90	44	34	29	51	---
Ce	64	80	66	58	49	93	78	68	100	---
Nd	31	41.6	34.4	28	8.0	50.6	42	42.5	49	---
Sm	6.1	8.06	6.58	5.6	2.0	10.2	7.4	8.98	9.4	---
Eu	1.7	2.15	1.93	1.7	0.9	2.80	1.9	2.27	2.5	---
Tb	< 0.5	1.07	0.91	0.8	3.78	1.44	0.8	1.27	1.6	---
Dy	---	5.2	4.4	---	---	6.7	---	6.5	---	---
Ho	---	1.12	0.97	---	---	1.44	---	1.33	---	---
Yb	2.93	3.10	2.67	3.12	3.78	3.59	3.98	3.81	4.47	---
Lu	0.41	0.46	0.43	0.44	0.51	0.58	0.57	0.64	0.56	---

Element	90-02 TON	89-27 PHYL	89-72 PHYL	89-73 PHYL	89-74 PHYL	89-85 PHYL	89-87 PHYL	89-1039 PORL	89-1042 PORL
SiO_2	59.58	60.47	60.76	62.16	61.36	70.67	72.18	61.08	57.04
Al_2O_3	15.86	15.17	16.73	15.59	15.29	13.18	13.30	14.31	13.78
Fe_2O_3	7.92	3.94	4.05	8.04	3.48	2.97	2.97	6.86	9.31
FeO	---	---	---	---	4.62	---	---	---	---
MgO	2.49	3.67	3.41	3.23	5.00	0.55	0.51	2.60	1.63
CaO	5.07	5.51	4.19	3.66	2.12	1.04	2.01	2.53	2.21
Na_2O	4.88	3.98	4.15	3.26	2.67	4.45	4.79	3.08	1.63
K_2O	0.74	0.18	0.20	0.45	0.92	2.86	1.54	1.34	2.77
TiO_2	1.01	0.89	1.02	0.89	0.86	0.38	0.37	0.81	0.75
P_2O_5	0.50	.038	0.36	0.40	0.28	0.04	0.03	0.22	0.28
MnO	0.06	0.07	0.04	0.11	0.05	0.02	0.06	0.02	0.02
S	0.05	0.21	0.20	0.03	0.04	0.46	0.07	1.37	1.81
LOI	---	4.65	---	2.47	3.80	1.61	2.71	4.64	6.84
TOTAL	98.16	99.23	95.11	100.38	100.3	98.41	100.68	98.99	98.23
Ba	382	105	94	168	313	993	505	428	938
Cr	24	22	14	30	32	32	63	27	30
Zr	142	187	180	203	199	287	289	228	179
Sr	317	231	265	188	117	86	64	111	70
Rb	22	< 10	< 10	< 10	19	62	51	26	70
Y	48	51	47	46	33	39	44	45	30
Nb	< 10	< 10	< 10	< 10	< 10	13	14	10	< 10
Zn	18	< 10	12	34	< 10	< 10	32	< 10	< 10
Ni	13	30	14	19	27	79	113	12	26
Co	---	24	24	---	22	27	---	31	46
Sc	---	19	23	19	17	9.4	8.6	18	17
V	46	125	121	62	84	< 10	< 10	66	43
Hf	---	6	5	5.28	6	8	7.59	7	6
Th	---	8.1	6.6	8.49	6	13	16.9	8.3	7
U	---	0.7	1.6	1.69	1.4	3.1	2.94	2.1	1.4
Ta	---	1	< 1	1.10	1	2	1.75	1	1
Au	---	< 5	6	---	6	102	---	25	25
Ag	---	< 5	< 5	---	< 5	< 5	---	< 5	< 5
La	---	46	53	45	37	59	62	60	43
Ce	---	120	110	90	64	110	118	120	84
Nd	---	63	44	48.1	26	45	48.6	48	41
Sm	---	10	8.2	9.57	4.6	7.3	8.42	9.0	6.9
Eu	---	2.3	2.5	2.31	2.0	1.3	1.74	2.3	1.4
Tb	---	1.2	1.4	1.39	0.5	1.0	1.16	1.4	0.8
Dy	---	---	---	6.8	---	---	6.1	---	---
Ho	---	---	---	1.54	---	---	1.80	---	---
Yb	---	1.2	4.55	4.55	3.7	4.5	4.31	4.61	3.87
Lu	---	0.66	0.58	0.70	0.5	0.6	0.71	0.63	0.57

Element	89-1052 PORL	89-1064 PORL	m622-31 PORL	89-55 PHYL	90-04 QPAD	89-75 NS	89-78 NS	89-57 WS
SiO_2	72.66	64.15	69.11	56.13	70.03	53.31	50.52	50.42
Al_2O_3	13.58	15.19	13.18	15.53	13.24	14.40	14.42	17.77
Fe_2O_3	1.45	5.37	3.44	2.70	3.84	11.12	12.52	2.30
FeO	----	----	----	----	----	----	----	5.73
MgO	0.72	2.02	0.45	3.10	0.79	6.26	7.31	9.17
CaO	2.24	5.15	2.71	7.05	4.30	9.52	9.10	8.71
Na_2O	5.14	3.19	3.76	4.55	4.90	2.43	1.93	2.48
K_2O	0.50	0.33	1.76	0.90	0.06	0.12	0.05	0.08
TiO_2	0.46	0.82	0.37	0.88	0.47	1.09	1.12	0.67
P_2O_5	0.09	0.25	0.02	0.46	0.09	0.10	0.07	0.01
MnO	0.01	0.02	0.03	0.07	0.06	0.17	0.20	0.17
S	0.07	0.22	0.14	0.02	0.07	0.02	0.00	0.00
LOI	1.04	2.56	2.61	7.78	-----	2.23	2.71	3.53
TOTAL	98.06	99.39	97.58	99.31	97.70	100.93	100.09	101.04
Ba	195	127	1012	272	27	42	< 10	91
Cr	67	41	< 10	26	25	236	229	218
Zr	305	240	276	246	213	100	70	20
Sr	147	354	101	306	281	95	112	187
Rb	14	< 10	43	13	< 10	< 10	< 10	---
Y	22	48	36	46	23	44	33	13
Nb	< 10	11	11	< 10	< 10	< 10	< 10	---
Zn	< 10	< 10	16	< 10	11	66	71	62
Ni	59	33	< 10	25	13	88	106	129
Co	39	35	---	12	---	---	---	---
Sc	7.6	17	---	---	---	---	---	---
V	23	47	< 10	24	10	377	382	242
Hf	9	6	---	6	---	3.00	2.23	---
Th	14	7.4	14.7	5.0	---	0.52	0.43	---
U	2.6	0	4.1	<5	---	0.15	0.12	---
Ta	2	< 1	---	< 1	---	0.69	0.50	---
Au	<5	10	---	<5	---	---	---	---
Ag	<5	<5	---	<5	---	---	---	---
La	34	53	54	23	---	6.3	4.3	---
Ce	58	96	112	52	---	15.3	10.7	---
Nd	25	42	48	28	---	12.7	10.0	---
Sm	3.3	7.9	8.4	6.4	---	4.18	3.18	---
Eu	0.9	1.7	1.41	1.4	---	1.17	1.04	---
Tb	<0.5	1.1	1.09	0.8	---	1.18	0.86	---
Dy	---	---	6.9	---	---	6.6	5.1	---
Ho	---	---	1.4	---	---	1.46	1.08	---
Yb	3.10	4.98	4.5	3.75	---	4.39	3.55	---
Lu	0.41	0.73	0.69	0.49	---	0.68	0.54	---

Element	89-57a WS	89-59 SS	89-70 SS	90-01 SS	89-68 QD
SiO_2	50.52	47.63	48.75	52.43	56.10
Al_2O_3	16.38	19.07	17.86	18.70	14.55
Fe_2O_3	2.59	3.44	13.26	11.32	1.97
FeO	5.73	11.43	----	----	4.44
MgO	9.40	7.19	5.68	2.68	1.93
CaO	9.10	2.53	7.44	6.32	5.64
Na_2O	2.37	3.81	4.02	5.48	5.34
K_2O	0.18	0.19	0.07	0.33	0.73
TiO_2	0.63	1.04	0.88	0.82	0.94
P_2O_5	0.06	0.14	0.12	0.13	0.38
MnO	0.17	0.13	0.09	0.10	0.08
S	0.01	0.00	0.01	0.02	----
LOI	3.22	3.89	3.34	3.66	----
TOTAL	100.35	100.29	101.63	102.11	92.10
Ba	78	31	55	148	202
Cr	282	204	176	176	17
Zr	64	88	69	69	124
Sr	190	84	188	240	192
Rb	< 10	< 10	< 10	< 10	15
Y	24	23	23	17	36
Nb	< 10	< 10	< 10	< 10	< 10
Zn	44	38	22	12	39
Ni	265	124	89	116	19
Co	---	---	---	---	---
Sc	---	---	---	---	---
V	232	256	213	282	95
Hf	---	3	1.96	1.67	---
Th	---	0.6	0.62	0.66	---
U	---	<0.5	1.55	0.88	---
Ta	---	< 1	0.51	0.61	---
Au	---	<5	<5	---	---
Ag	---	<5	<5	---	---
La	---	11	18.1	20	---
Ce	---	18	28	38	---
Nd	---	10	10.7	14.6	---
SM	---	1.8	2.15	2.75	---
Eu	---	0.6	1.24	1.17	---
Tb	---	<0.5	0.48	0.48	---
Dy	---	---	3.1	2.9	---
Ho	---	---	0.65	0.62	---
Yb	---	2.37	1.99	1.76	---
Lu	---	0.31	0.33	0.25	---

APPENDIX B: ELECTRON MICROPROBE ANALYSES

B.1 Operating conditions

Microprobe analyses of selected samples were completed using the CAMECA electron microprobe (model MB1) of the McGill University microprobe laboratory. Four spectrometer wavelength dispersive analysis of carbon-coated polished thin sections were performed under the following operating conditions; 15 kv accelerating voltage, sample current of 8 nA and a counting time of 25 seconds. The calibration standards were; ANDR= andradite, MnTi= $MnTiO_3$, ALBI= albite, DIOPS= diopside, and ORTH= orthoclase; Kα lines were used for all elements. Accuracy of $\pm 1\%$ relative to standard and totals are within $\pm 1\%$. Data reduction was carried out using the ONQUANT resident software of CAMECA.

Assignement of elements to sites in the amphibole and plagioclase structures were accomplished following the methods of Deer *et al.*, (1966) and assisted by the computer program MINFILE by A.M. Afifi and E.J. Essene of the University of Michigan.

B.2 Amphiboles

Microprobe analyses of selected amphiboles from the Mooshla intrusion classified according to sample and grain number. Recalculated on the basis of 22 oxygens, OH+Cl+F=2.

	31-1	31-2	31-3	31-4	31-5	31-11	50-9	50-20a	50-20b	54-2
SiO2	49.33	49.50	49.13	48.25	50.14	50.33	55.91	51.18	51.66	53.69
TiO2	1.29	1.13	1.29	1.86	0.82	0.58	0.05	1.03	0.42	0.60
Al2O3	6.34	6.04	6.30	7.00	5.13	5.11	1.17	5.91	4.63	2.80
Fe2O3	3.28	3.26	3.36	3.15	3.25	3.47	2.27	2.26	2.10	2.73
FeO	11.79	11.74	12.10	11.36	11.70	12.48	8.18	8.14	7.54	9.31
MnO	0.24	0.32	0.33	0.30	0.36	0.41	0.20	0.23	0.33	0.38
MgO	14.20	14.30	13.86	13.83	14.89	13.66	18.05	16.38	19.13	15.30
CaO	10.94	10.92	11.03	11.38	11.02	10.96	12.63	12.12	10.83	11.62
Na2O	1.15	1.16	1.23	1.02	0.92	1.00	0.18	0.62	0.43	0.43
K2O	0.48	0.48	0.51	0.54	0.50	0.45	0.06	0.29	0.16	0.20
H2O	2.08	2.08	2.08	2.07	2.08	2.07	2.14	2.11	2.11	2.10
Total	101.12	100.93	101.22	100.76	100.81	100.52	100.84	100.27	99.34	99.86
#Si IV	7.10	7.13	7.08	6.97	7.23	7.30	7.83	7.26	7.35	7.68
#Al IV	0.90	0.87	0.92	1.03	0.77	0.70	0.17	0.74	0.65	0.32
#Fe +3	-	-	-	-	-	-	-	-	-	-
#Ti IV	-	-	-	-	-	-	-	-	-	-
T site	8.00	8.00	8.00	8.00	8.00	8.00	8.00	8.00	8.00	8.00
#Al VI	0.17	0.16	0.15	0.17	0.10	0.17	0.03	0.25	0.12	0.15
#Fe +3	0.36	0.35	0.36	0.34	0.35	0.38	0.24	0.24	0.22	0.29
#Ti	0.14	0.12	0.14	0.20	0.09	0.06	0.01	0.11	0.04	0.06
#Mg	3.05	3.07	2.98	2.98	3.20	2.95	3.77	3.46	4.06	3.26
#Fe +2	1.29	1.29	1.36	1.31	1.26	1.43	0.96	0.93	0.55	1.17
#Mn	-	-	-	-	-	-	0.00	-	-	0.06
#Ca	-	-	-	-	-	-	-	-	-	-
M1,2,3	5.00	5.00	5.00	5.00	5.00	5.00	5.00	5.00	5.00	5.00
#Mg	-	-	-	-	-	-	-	-	-	-
#Fe +2	0.13	0.12	0.10	0.06	0.15	0.08	-	0.03	0.34	-
#Mn	0.03	0.04	0.04	0.04	0.04	0.05	0.02	0.03	0.04	0.02
#Ca	1.69	1.69	1.70	1.76	1.70	1.70	1.90	1.84	1.62	1.78
#Na	0.16	0.15	0.16	0.14	0.10	0.17	0.05	0.10	-	0.12
M4 site	2.00	2.00	2.00	2.00	2.00	2.00	1.97	2.00	2.00	1.91
#Ca	-	-	-	-	-	-	-	-	0.03	-
#Na	0.17	0.17	0.18	0.15	0.15	0.11	-	0.07	0.12	-
#K	0.09	0.09	0.09	0.10	0.09	0.08	0.01	0.05	0.03	0.04
A site	0.25	0.26	0.28	0.25	0.25	0.20	0.01	0.13	0.18	0.04
#O	22.00	22.00	22.00	22.00	22.00	22.00	22.00	22.00	22.00	22.00
#OH	2.00	2.00	2.00	2.00	2.00	2.00	2.00	2.00	2.00	2.00

Explanations

31-1: Hornblende; layered gabbro
31-2: Hornblende; layered gabbro
31-3: Hornblende; layered gabbro
31-4: Hornblende; layered gabbro
31-5: Hornblende; layered gabbro
31-11: Act-hornblende; layered gabbro
50-9: Actinolite; tonalite
50-20a: Act-hornblende, rim of grain; tonalite
50-20b: Act-hornblende, core of grain; tonalite
54-2: Actinolite, margin; quartz diorite

Amphiboles, cont'd

	54-5a	54-5b	54-8	54-9	54-12	58-3a	58-3b	58-5	82-1	90-4	90-52
SiO2	52.60	51.44	50.72	54.36	48.70	56.25	51.48	57.15	50.14	50.84	51.70
TiO2	0.70	1.04	1.02	0.46	0.07	-	-	-	1.25	0.84	0.69
Al2O3	3.50	4.30	5.10	2.45	7.40	1.42	5.99	1.19	5.47	4.54	4.70
Fe2O3	2.71	2.59	2.75	2.41	3.13	2.03	1.99	1.59	2.87	3.00	3.09
FeO	9.76	9.31	9.90	8.88	11.28	7.31	7.17	5.48	10.33	10.81	11.13
MnO	0.60	0.31	0.33	0.61	0.36	0.13	0.20	0.26	0.31	0.43	0.41
MgO	15.40	15.81	16.12	16.46	16.96	17.97	17.17	19.47	14.54	15.02	14.92
CaO	11.37	11.32	11.31	11.59	9.18	12.56	11.77	12.23	10.94	11.22	10.85
Na2O	0.50	0.69	0.80	0.41	0.30	0.08	0.95	0.21	0.92	0.78	0.86
K2O	0.30	0.42	0.56	0.19	0.13	0.03	0.29	0.06	0.52	0.41	0.44
H2O	2.09	2.08	2.10	2.11	2.08	2.14	2.10	2.16	2.07	2.08	2.10
Total	99.53	99.31	100.71	99.93	99.59	99.92	99.11	99.80	99.36	99.97	100.89
#Si IV	7.56	7.41	7.25	7.72	7.03	7.90	7.34	7.95	7.27	7.35	7.39
#Al IV	0.44	0.59	0.75	0.28	0.97	0.10	0.66	0.05	0.73	0.65	0.61
#Fe +3	-	-	-	-	-	-	-	-	-	-	-
#Ti IV	-	-	-	-	-	-	-	-	-	-	-
T site	8.00	8.00	8.00	8.00	8.00	8.00	8.00	8.00	8.00	8.00	8.00
#Al VI	0.15	0.14	0.11	0.13	0.29	0.13	0.35	0.14	0.21	0.12	0.18
#Fe +3	0.29	0.28	0.30	0.26	0.34	0.21	0.21	0.17	0.31	0.33	0.33
#Ti	0.08	0.11	0.11	0.05	0.01	-	-	-	0.14	0.09	0.07
#Mg	3.30	3.40	3.43	3.49	3.65	3.76	3.65	4.04	3.14	3.24	3.18
#Fe +2	1.17	1.07	1.05	1.06	0.72	0.86	0.79	0.64	1.20	1.23	1.23
#Mn	0.00	-	-	0.02	-	0.02	-	0.02	-	-	-
#Ca	-	-	-	-	-	0.02	-	-	-	-	-
M1,2,3	5.00	5.00	5.00	5.00	5.00	5.00	5.00	5.00	5.00	5.00	5.00
#Mg	-	-	-	-	-	-	-	-	-	-	-
#Fe +2	-	0.05	0.13	-	0.65	-	0.07	-	0.05	0.08	0.10
#Mn	0.07	0.04	0.04	0.06	0.04	-	0.02	0.01	0.04	0.05	0.05
#Ca	1.75	1.75	1.73	1.76	1.31	1.89	1.80	1.82	1.70	1.74	1.66
#Na	0.14	0.16	0.10	0.11	-	0.02	0.11	0.06	0.21	0.13	0.19
M4 site	1.96	2.00	2.00	1.93	2.00	1.91	2.00	1.89	2.00	2.00	2.00
#Ca	-	-	-	-	0.11	-2E-02	-	-	-	-	-
#Na	-	0.03	0.12	-	0.08	-	0.15	-	0.05	0.09	0.05
#K	0.06	0.08	0.10	0.03	0.02	0.01	0.05	0.01	0.10	0.08	0.08
A site	0.06	0.11	0.23	0.03	0.22	-2E-02	0.21	0.01	0.15	0.16	0.13
#O	22.00	22.00	22.00	22.00	22.00	22.00	22.00	22.00	22.00	22.00	22.00
#OH	2.00	2.00	2.00	2.00	2.00	2.00	2.00	2.00	2.00	2.00	2.00

Explanations

54-5a: Actinolite, core of grain; quartz diorite
54-5b: Actinolitic-hornblende, rim of grain; quartz diorite
54-12: Hornblende; quartz diorite
90-4: Actinolitic-hornblende, rim; quartz-diorite
90-5: Actinolitic-hornblende, core; quartzdiorite
58-3a; Actinolite, core of grain; mesocumulate gabbro
58-3b; Actinolitic-hornblende, rim of grain; mesocumulate gabbro

58-5: Actinolite; mesocumulate gabbro
82-1: Actinolitic-hornblende; quartz diorite
54-8: Hornblende; quartz diorite
54-9: Actinolite; quartz diorite

B.3 Plagioclase

Microprobe analyses of plagioclase, classified according to sample and grain number. Recalculated on the basis of 32 oxygen, all Fe expressed as FeO.

	50-2a	50-2b	50-2c	50-10	50-13	50-14	50-15	TR-1	TR-4	TR-5
SiO2	64.28	68.38	65.27	67.69	66.04	64.70	65.20	58.51	67.31	69.78
Al2O3	22.12	20.06	21.49	20.36	21.89	22.24	21.74	23.11	19.87	18.98
FeO	-	0.12	0.05	-	0.02	0.27	0.16	0.45	0.04	-
CaO	3.97	1.52	3.35	1.25	2.90	3.74	3.61	7.74	1.32	0.52
Na2O	9.05	10.30	9.44	10.89	10.02	9.27	9.22	6.96	9.78	10.89
K2O	0.07	0.07	0.07	0.06	0.07	0.08	0.10	0.14	0.08	0.03
Total	99.49	100.45	99.67	100.25	100.94	100.30	100.03	96.91	98.40	100.20
#Si+4	11.38	11.89	11.52	11.82	11.51	11.38	11.47	10.80	11.92	12.12
#Al+3	4.62	4.11	4.47	4.19	4.50	4.61	4.51	5.03	4.15	3.89
#Fe+2	-	0.02	0.01	-	0.00	0.04	0.02	0.07	0.01	-
#Ca+2	0.75	0.28	0.63	0.23	0.54	0.70	0.68	1.53	0.25	0.10
#Na+1	3.11	3.47	3.23	3.69	3.38	3.16	3.15	2.49	3.36	3.67
#K+1	0.02	0.02	0.02	0.01	0.02	0.02	0.02	0.03	0.02	0.01
#TOTAL	19.87	19.80	19.87	19.94	19.95	19.91	19.86	19.95	19.70	19.77
#O-2	32.00	32.00	32.00	32.00	32.00	32.00	32.00	32.00	32.00	32.00
Ab	0.80	0.92	0.83	0.94	0.86	0.81	0.81	0.61	0.92	0.97
Or	-	-	-	-	-	-	0.01	0.01	0.01	-
An	0.20	0.08	0.17	0.06	0.14	0.19	0.18	0.38	0.07	0.03

Comments:

Single grain analyses:
50-2a: Outer rim of zoned plagioclase; tonalite
50-2b: Inner rim of zoned plagioclase; tonalite
50-2c: Core of zoned plagioclase; tonalite

Individual analyses:
50-10: Rim of twinned plagioclase proximal to quartz grain; tonalite
50-13: Margin of twinned plagioclase; tonalite
50-14: Margin of twinned plagioclase; tonalite
50-15: Relict core of twinned plagioclase; tonalite
Tr-1: Fresh, unaltered twinned plagioclase; tonalite
Tr-4: Plagioclase in mymerkitic intergrowth with quartz; tonalite
Tr-5: Plagioclase in mymerkitic intergrowth with quartz; tonalite

Plagioclase, cont'd.

	TR-6	30-2	30-3	30-1	90-1	90-2	72-1	72-2	72-3
SiO2	58.61	67.68	67.79	68.29	67.69	61.35	64.30	67.08	65.53
Al2O3	25.76	19.67	19.43	19.57	19.86	22.91	21.35	19.61	21.78
FeO	0.38	-	-	0.05	0.12	0.05	-	0.01	0.06
CaO	7.95	0.58	0.51	1.12	0.98	5.51	3.38	1.59	2.80
Na2O	6.85	10.94	10.97	10.81	10.81	8.57	9.98	10.97	9.71
K2O	0.04	0.10	0.08	0.08	0.04	0.06	0.04	0.02	0.25
Total	99.59	98.97	98.78	99.92	99.50	98.45	99.05	99.28	100.13
#Si+4	10.52	11.94	11.97	11.94	11.89	11.06	11.45	11.85	11.51
#Al+3	5.45	4.09	4.04	4.03	4.11	4.87	4.48	4.08	4.51
#Fe+2	0.06	-	-	0.01	0.02	0.01	-	0.00	0.01
#Ca+2	1.53	0.11	0.10	0.21	0.18	1.06	0.64	0.30	0.53
#Na+1	2.38	3.74	3.76	3.67	3.68	3.00	3.45	3.76	3.31
#K+1	0.01	0.02	0.02	0.02	0.01	0.01	0.01	0.00	0.06
#TOTAL	19.95	19.90	19.89	19.88	19.90	20.01	20.03	19.99	19.92
#O-2	32.00	32.00	32.00	32.00	32.00	32.00	32.00	32.00	32.00
Ab	0.61	0.96	0.97	0.94	0.95	0.74	0.84	0.93	0.85
Or	-	0.01	-	-	-	-	-	-	0.01
An	0.39	0.03	0.03	0.06	0.05	0.26	0.16	0.07	0.14

Comments:

Tr-6: Fresh, unaltered and twinned plagioclase; tonalite
30-2: Plagioclase in mymerkitic intergrowth with quartz; tonalite
30-3: Plagioclase in mymerkitic intergrowth with quartz; tonalite
30-1: Plagioclase in mymerkitic intergrowth with quartz; tonalite
90-1: Plagioclase in mesostasis proximal to mymerkitic intergrowth;quartz diorite
90-2: Well twinned, relatively fresh plagioclase proximal to quartz grain; quartz diorite
72-1: Core of twinned, well preserved plagioclase porphyroclast; leucotonalite
72-2: Anhedral, groundmass plagioclase; leucotonalite
72-3: Margin of twinned, plagioclase porphyroclast; leucotonalite

B.4 Ilmenite

Microprobe analyses of rutile, classified according to sample number and grain number in each sample. Recalculated on the basis of 6 oxygen. MS-54= quartz diorite; MS-31= layered gabbro.

	MS-54 1	MS-54 2	MS-54 3	MS-54 4	MS-31 4	MS-31 5
FeO	45.50	46.14	46.62	44.59	44.70	45.32
TiO_2	49.54	48.99	49.56	49.37	48.93	47.91
MnO	2.20	2.49	2.29	3.01	3.75	4.01
Total	97.24	97.62	98.47	96.97	97.38	97.24
Fe^{+3}	0.151	0.199	0.187	0.141	0.195	0.273
Ti	1.925	1.901	1.906	1.929	1.903	1.864
Fe^{+2}	1.815	1.792	1.807	1.797	1.738	1.688
Mn	0.109	0.109	0.096	0.133	0.164	0.176

B.5 Biotite

Microprobe analyses of biotite, classified according to sample number and grain number in each sample.

	50-1a	50-1b	50-23	31-1	31-3	31-5	30-2	30-3	30-4	90-3	13-1	13-2	13-3
SiO_2	39.83	40.01	39.32	36.63	35.56	36.69	36.71	35.77	36.30	37.47	37.60	37.19	37.99
Al_2O_3	15.85	15.65	15.56	16.51	16.04	16.28	16.35	15.04	16.34	15.69	15.85	16.42	16.35
FeO	11.95	11.50	11.57	22.50	21.79	21.92	20.39	18.72	19.92	19.07	17.15	17.07	16.90
MgO	16.65	17.61	16.93	10.15	10.34	9.73	10.80	9.48	9.93	11.77	12.53	10.27	13.03
CaO	0.05	0.11	0.09	0.10	0.02	0.00	0.01	0.13	0.03	0.03	0.03	0.02	0.08
Na_2O	0.09	0.09	0.09	0.08	0.06	0.06	0.07	0.29	0.15	0.05	0.07	0.04	0.02
K_2O	10.52	9.92	10.11	9.40	9.45	9.95	10.29	8.94	9.74	10.43	10.26	10.27	10.23
TiO_2	0.99	0.96	0.98	1.94	1.78	1.79	1.68	1.82	1.88	1.44	1.17	1.48	1.19
MnO	0.13	0.07	0.11	0.12	0.22	0.17	0.12	0.13	0.06	0.22	0.20	0.17	0.20
Total	96.06	95.93	94.76	97.50	95.26	96.60	96.41	90.33	94.33	96.17	95.16	95.27	96.02

Explanations:

50-1a: Phlogopite, central portion of basal section; tonalite.
50-1b: Phlogopite, edge of basal section near apatite inclusion; tonalite.
50-23: Phlogopite, near contact with hornblende grain; tonalite.
31-1: Biotite, overprinting chlorite; layered gabbro.
31-3: Biotite, overprinting chlorite; layered gabbro.
31-5: Biotite, overprinting chlorite; layered gabbro.
30-2: Biotite; tonalite from northern margin.
30-3: Biotite; tonalite from northern margin.
30-4: Biotite; tonalite from northern margin.
90-3: Biotite; quartz diorite.
13-1: Biotite; quartz diorite.
13-2: Biotite; quartz diorite.
13-3: Biotite; quartz diorite.

APPENDIX C: MODAL ANALYSES

Modal mineralogy (vol.%) of the units of the Mooshla intrusion, based on >600 counts per thin section, in conjunction with visual estimations for some of the more coarse grained samples.

ROCK UNIT Mineral	Mesocumulate gabbro n=1	Layered gabbro n=4	Quartz diorite n=7	Tonalite n=4
Plagioclase	80	54 - 62	55 - 65	55 - 66
Amphibole	10	5 - 20	2 - 6	0 - 5
Quartz	6	3 - 5	8 - 16	16 - 20
Chlorite	4	10 - 15	10 - 15	5 - 10
Biotite	0	2 - 7	2 - 7	2 - 6
Sericite	0	0 - 5	tr - 2	0 - 2
Calcite	0	0 - 3	0 - 2	< 1
Apatite	0	2 - 3	< 1	0.5- 2
Titanite	0	tr	tr	1 - 3
Zircon	0	0	tr	< 1
Magnetite	0	<1	tr	tr
Ilmenite	0	1 - 4	0 - 2	0 - 2
Fe-Sulphides	0	tr	tr	tr

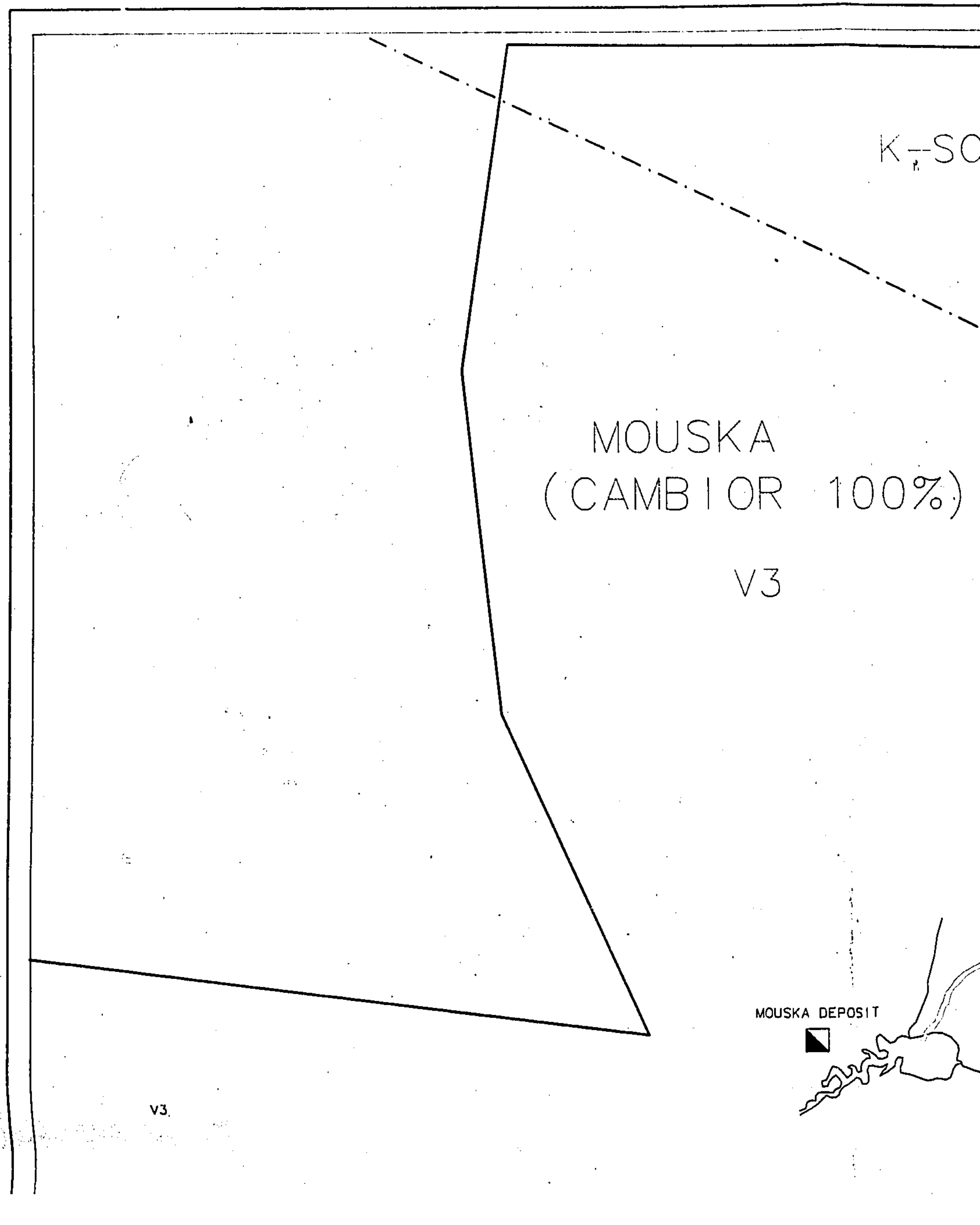
K-SC
MOUSKA
(CAMBIOR 100%)
V3
MOUSKA DEPOSIT
V3

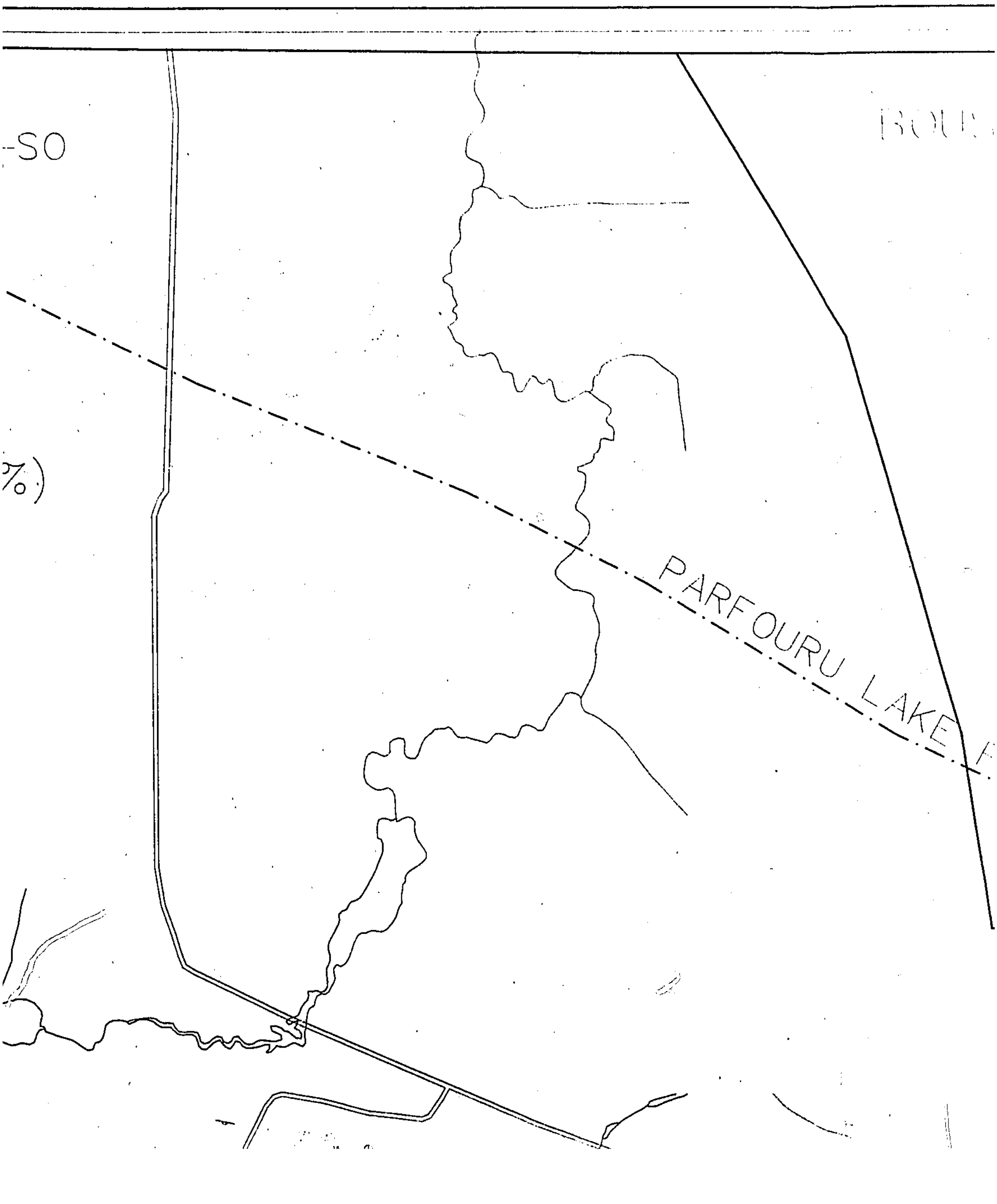

-SO
%)
PARFOURU LAKE

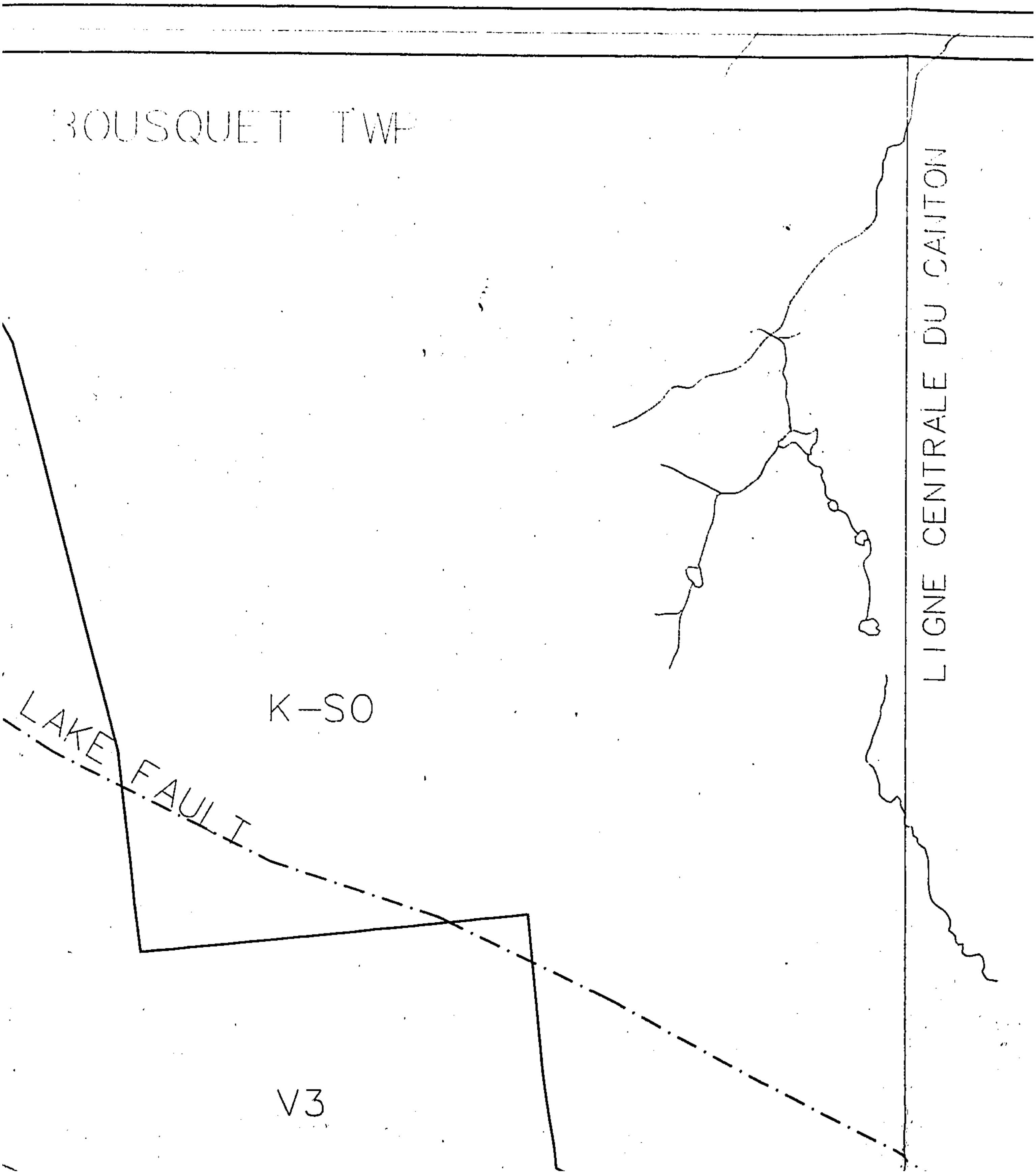
BOUSQUET TWP
LIGNE CENTRALE DU CANTON
K-SO
LAKE FAULT
V3

LEGEN

PROTEROZ

Diabase

ARCHEA

CADILLAC GROUP

C-SG Undifferentiated sediments

BLAKE RIVER GROUP

V2 Calc-alkaline volcanics & volcaniclastics

V3 Tholeitic volcanics (+/- volcaniclastics)

KEWAGAMA GROUP

K-SG Undifferentiated sediments

SYMBOL

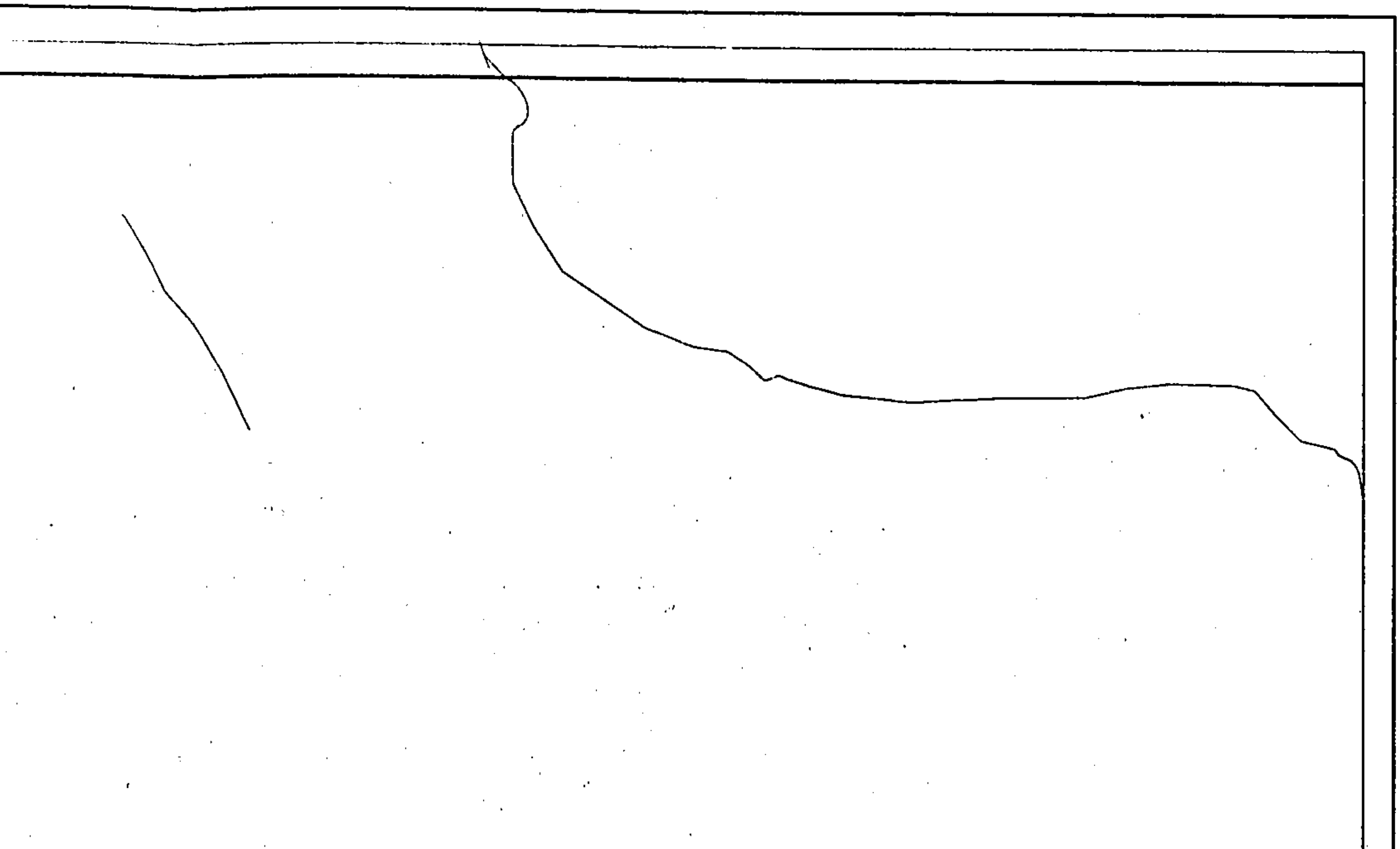

LEGEND

PROTEROZOIC

ARCHEAN

volcaniclastics

MOOSHLA INTRUSION

- Gabbro : mc= mesocumulate
  ls=layered series
- Quartz diorite
- Tonalite
- Leucotonalite
- Porphyritic leucotonalite
- ▲ Xenolith lense

SYMBOLS

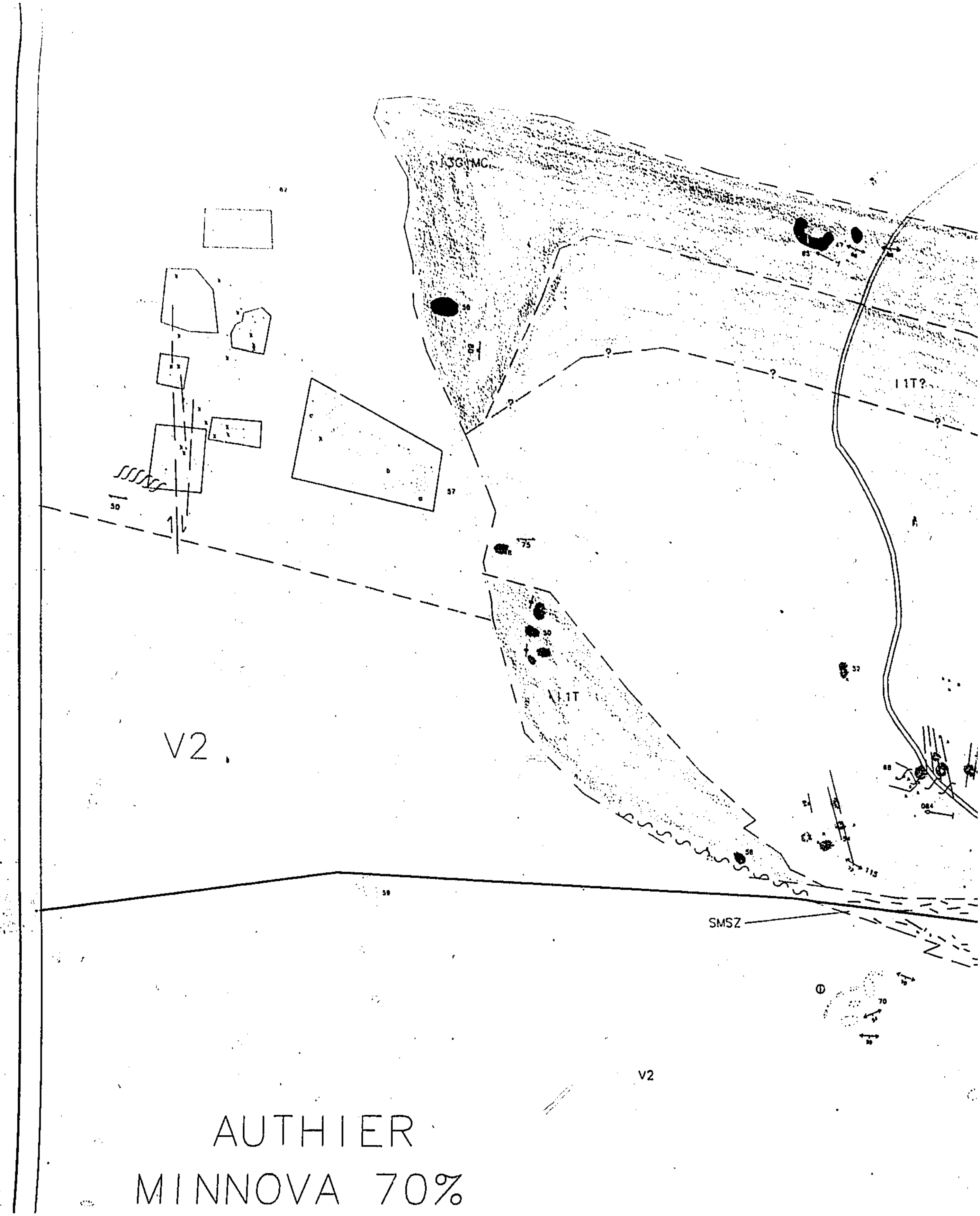

I3G MC
I1T?
I1T
V2
SMSZ
V2
AUTHIER
MINNOVA 70%

MIC MAC MINE
13G;L.S.
11T?
13G;L.S.
12J
90-04
90-01


11T
12J
trenched area
89-Tr

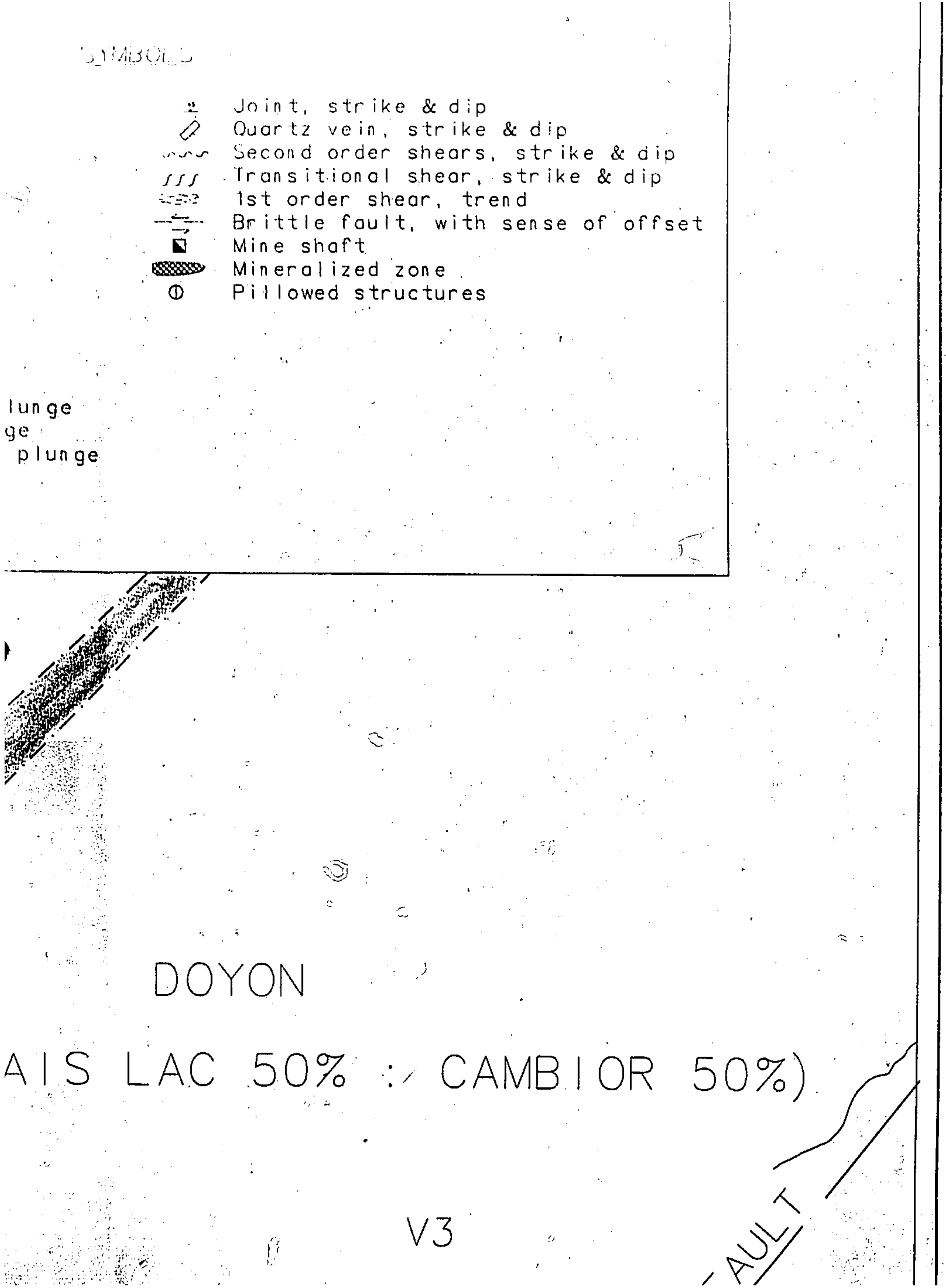

SYMBOLS
Joint, strike & dip
Quartz vein, strike & dip
Second order shears, strike & dip
Transitional shear, strike & dip
1st order shear, trend
Brittle fault, with sense of offset
Mine shaft
Mineralized zone
Pillowed structures
lunge
ge
plunge
DOYON
AIS LAC 50% :/ CAMBIOR 50%)
V3
AULT

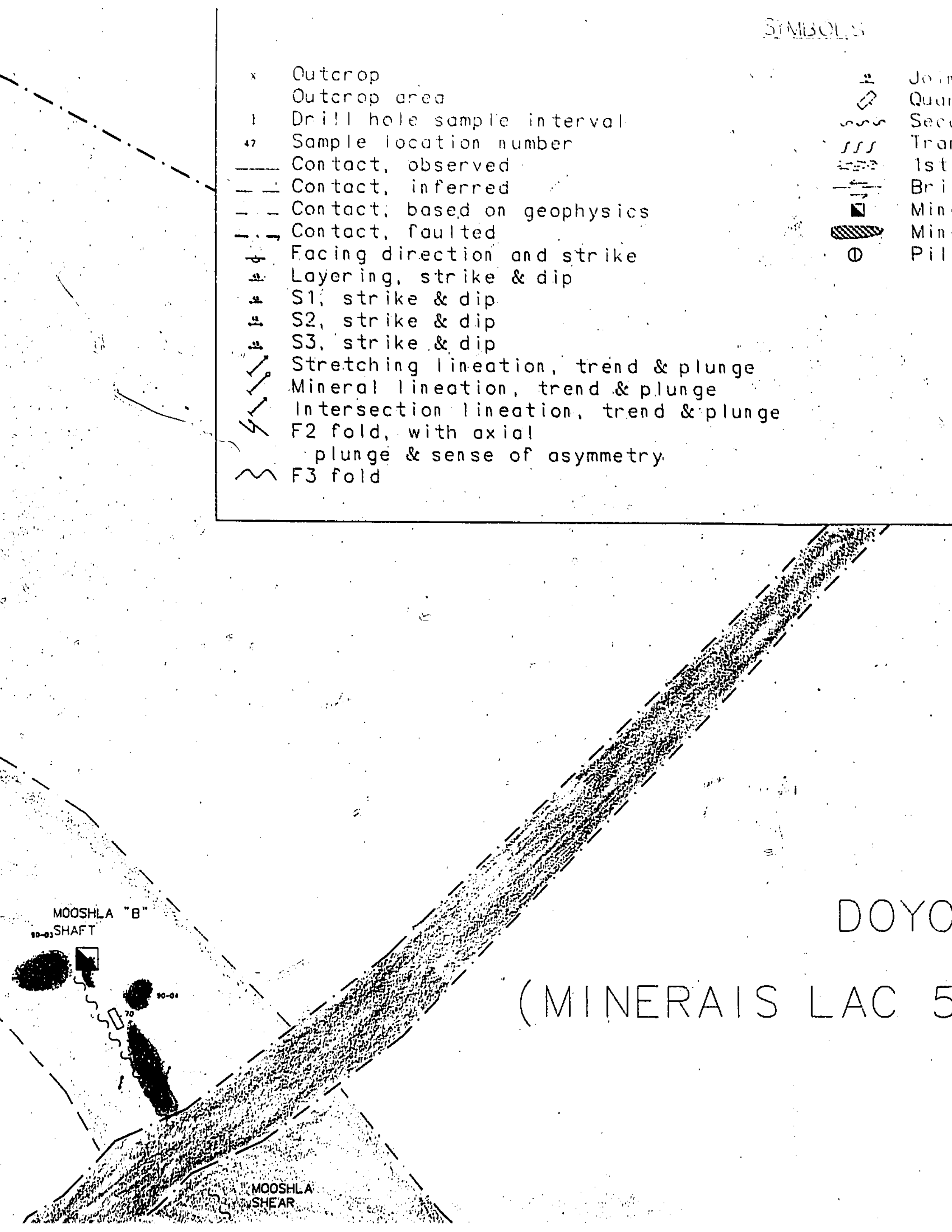
SYMBOLS
Outcrop
Outcrop area
Drill hole sample interval
Sample location number
Contact, observed
Contact, inferred
Contact, based on geophysics
Contact, faulted
Facing direction and strike
Layering, strike & dip
S1, strike & dip
S2, strike & dip
S3, strike & dip
Stretching lineation, trend & plunge
Mineral lineation, trend & plunge
Intersection lineation, trend & plunge
F2 fold, with axial plunge & sense of asymmetry
F3 fold
DOYO
(MINERAIS LAC 5
MOOSHLA "B" SHAFT
90-03
90-04
70
MOOSHLA SHEAR

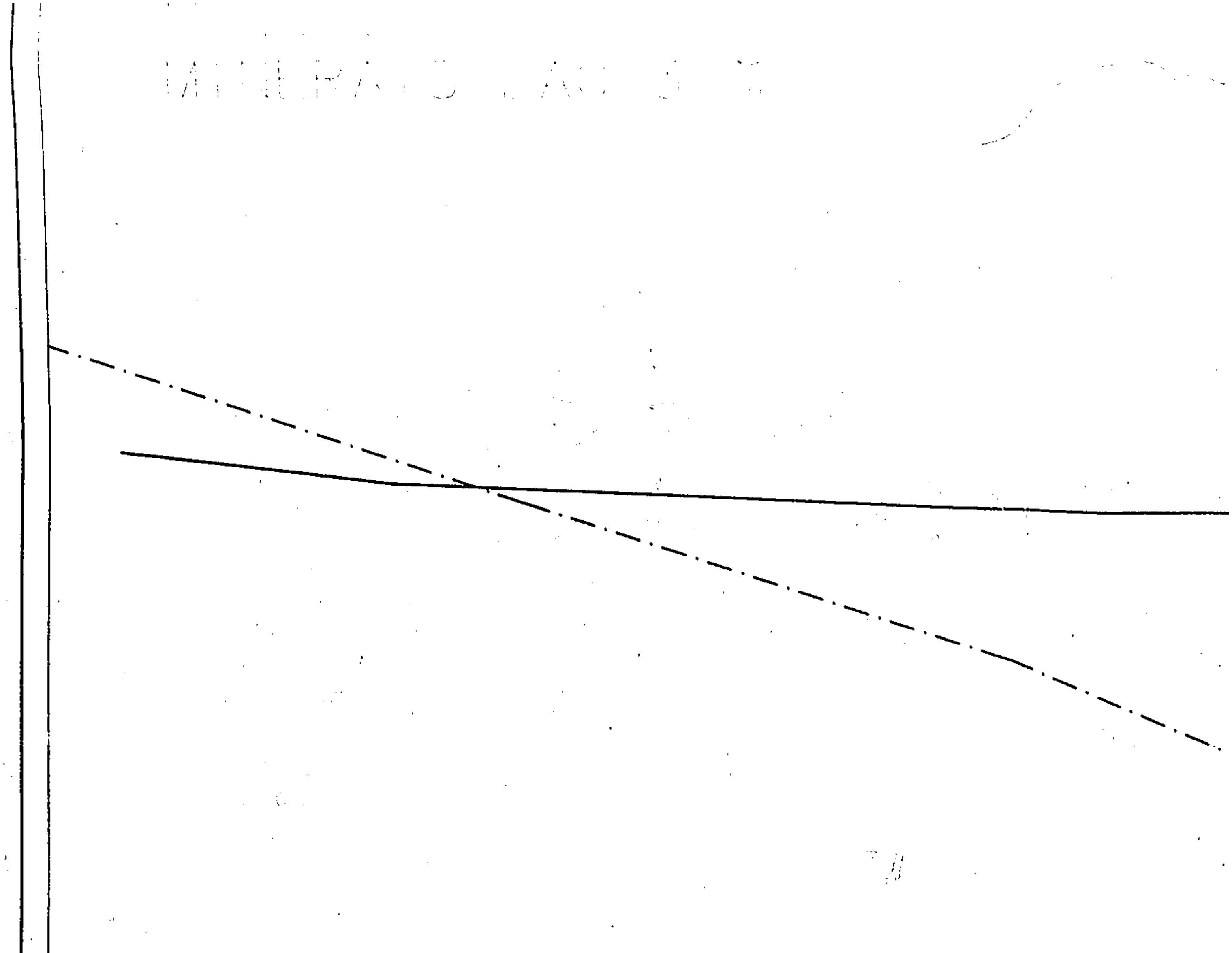

LAC

UNIVERSITE D'OTTAWA

GEOLOGY OF THE MOOSHLA INTRUSION

DESSINE PAR		DATE
GEOLOGIE PAR	ALEXANDRE LANGSHUR	09/1989
PLAN No:	APPROUVE PAR	

ECHELLE

1 : 5000

0 50 100 200 300

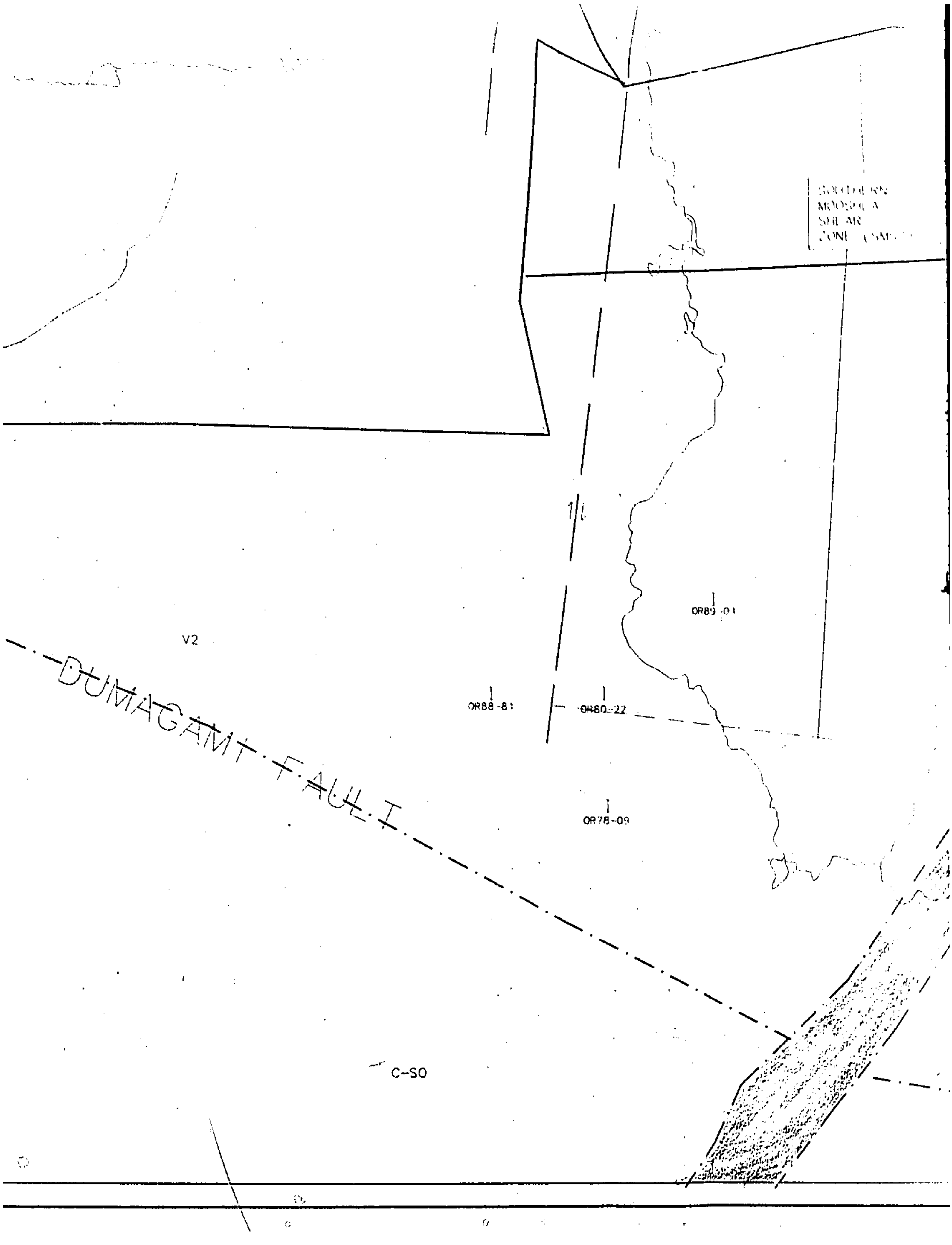
V2
DUMAGAMI FAULT
OR89-01
OR88-81
OR80-22
OR78-09
C-SO

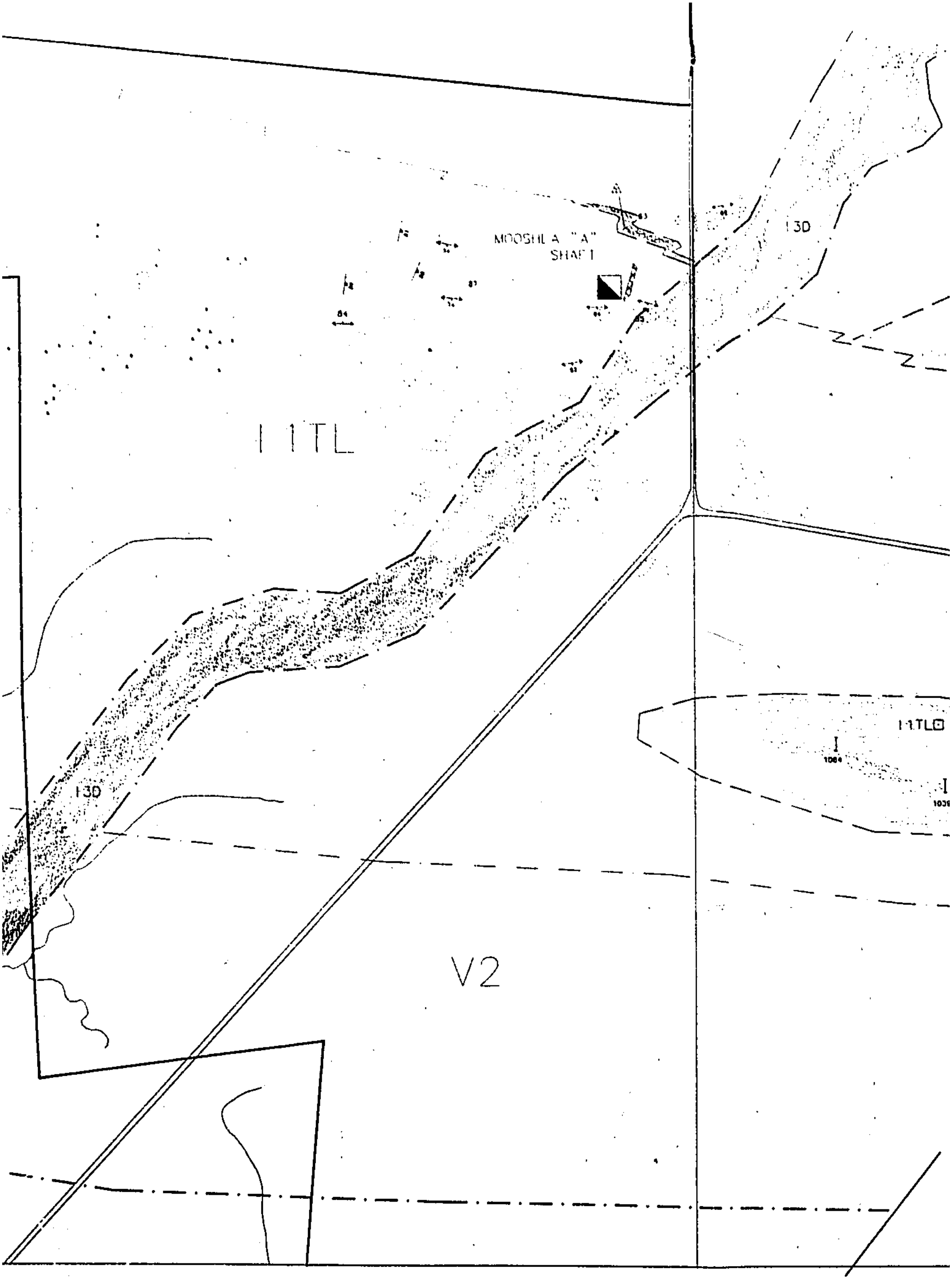

MOOSHLA "A"
SHAFT
I 1TL
I 3D
I 3D
I 1TL
V2

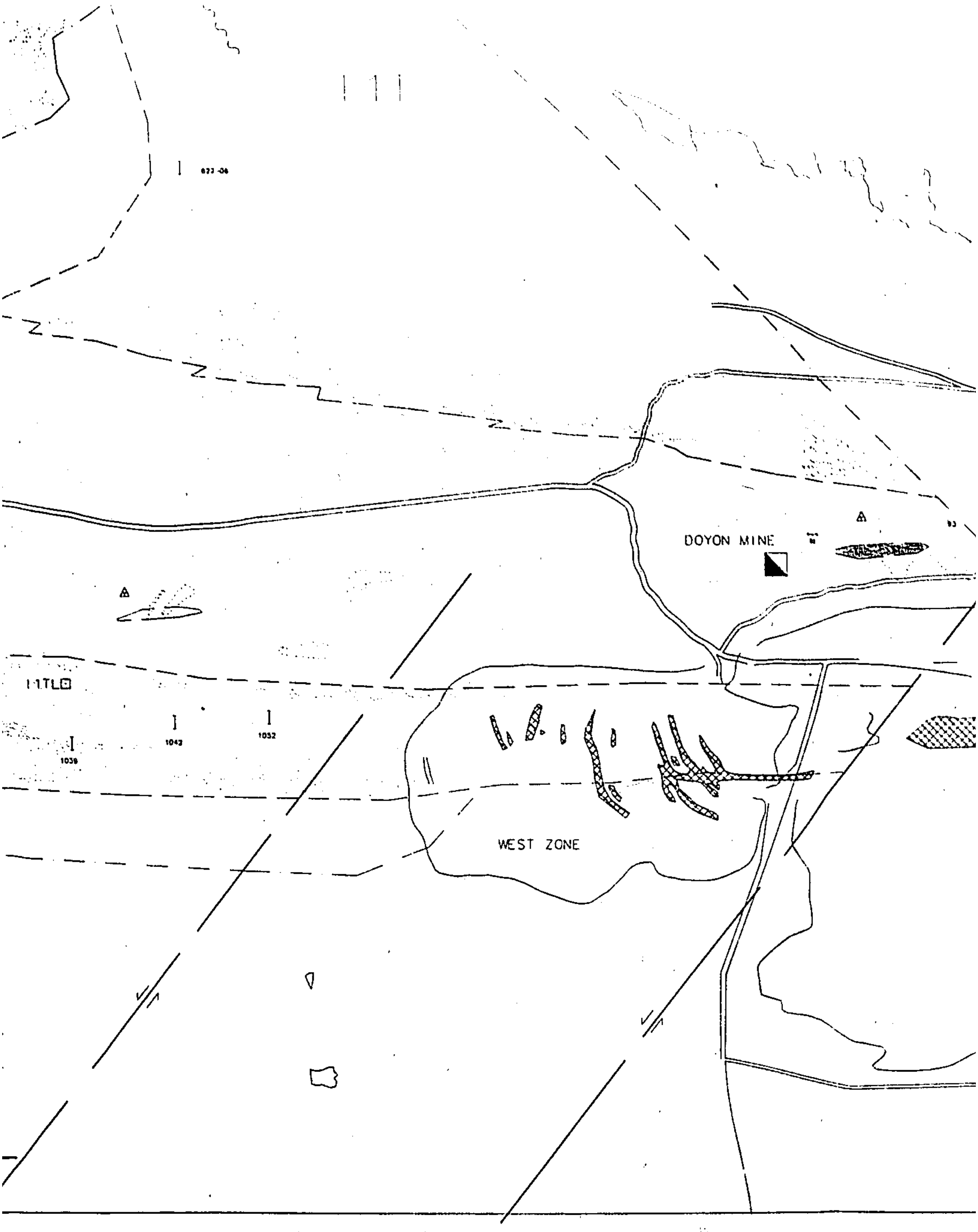
DOYON MINE
WEST ZONE
1032
1039

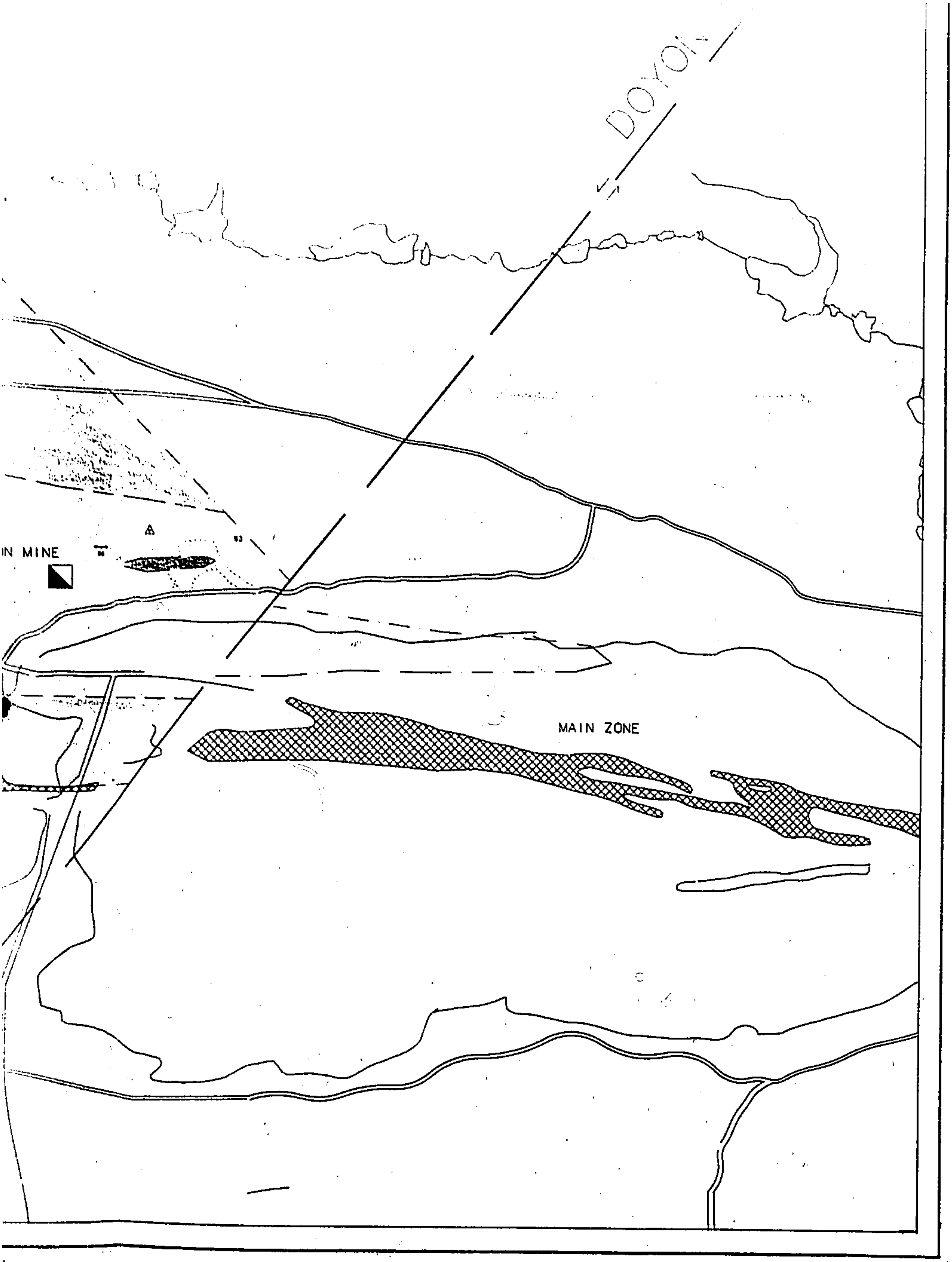
DOYON
N MINE
MAIN ZONE